ADDIS ABABA UNIVERSITY

ADDIS ABABA INSTITUTE OF TECHNOLOGY

SCHOOL OF CIVIL AND ENVIRONMENTAL ENGINEERING

Enhancement of the Flexural Behavior of CFRP Strengthened RC Beams in Medium and Low Grade Concrete

A Thesis in Structural Engineering

By: Abenezer Negussie

24/10/2018

Addis Ababa

In partial fulfillment of the requirement for Master of Science in Structural Engineering

ADDIS ABABA UNIVERSITY

ADDIS ABABA INSTITUTE OF TECHNOLOGY

SCHOOL OF CIVIL AND ENVIRONMENTAL ENGINEERING

"Enhancement of the Flexural Behavior of CFRP Strengthened RC Beams in Medium and Low Grade Concrete"

BY

Abenezer Negussie

Dr.-Ing. Girma Zerayohannes		
Advisor	**Signature**	**Date**
Internal Examiner	**Signature**	**Date**
External Examiner	**Signature**	**Date**
Chair Person	**Signature**	**Date**

Declaration

I, the undersigned, declare that this thesis is my original work and has not been presented for a degree in any other university and that all sources of material used for the thesis have been duly acknowledged.

Candidate

Name: Abenezer Negussie

Signature:_____

Faculty of Technology

Addis Ababa Institute of Technology

Date of submission: October 2018

Acknowledgement

It is because of the unyielding aid and provision of the almighty lord that the crumbly being manages to achieve even the slightest success in life. But this one is fairly great, and for his merciful kindness, I praise the lord.

Then, my immense gratitude goes to my advisor Dr.-Ing. Girma Zerayohannes for his positive attitude and guidance since the commencement of this research work. His constant encouragement also up kept the momentum of this work till the end. Wasihun Nimassie, Structural Engineer and Marketing Manager of SIKA-Ethiopia, played a great role that left me short of words. He has been so kind and dedicated to provide every help needed from allowing the use of Sikadur design software up to sponsoring experiment materials. I would also like to thank his colleague Mr. Fitsum Negussie for his key role as a contact person for all linkages from AAiT.

Dr.-Ing Adil Zekaria has been overviewing the progress of this research; he has given me so many critical comments that shaped this research this way. His availability and commitment has taught me so many lessons and he is a great model to look up for all academicians. Dr. Esayas G/Youhannes have given me some intellectual insights I had to consider, his research oriented lecture in class and friendly approach outside elevates every student's understanding to the level the science demands.

Hawassa University granted me a study leave that stayed till the end of the master's program. Thus, I like pay my respect to all staff members and the head of School of Water Resources and Irrigation Engineering of Hawassa University, Mr. Ayele. Samuel Tilahun and Girma Kebede made me smile on the worst days.

I am also thankful to all AAiT Material Laboratory staff members, Biniyam F., Wubet A, Demis and Fikru B. Their cooperation and help during the experimental program was really far beyond their responsibility takes them. And to my family, I have nothing to say except to remain in debt I cannot be able to repay even if I serve them till their last day on earth.

Table of content

List of Figures

List of Tables

List of Symbols

b_c= Concrete width

b_f =CFRP plate width

C_c=Compression force in concrete

^{0}c=Degree Centigrade

d= Damage parameter

d_c= Compression damage parameter

d_t= Tension damage parameter

Δ= Deflection, Displacement

E_{cm}= Secant Modulus of Elasticity

E_f = Elastic modulus of FRP

E_{fib} = Elastic modulus of fiber

E_{mat} = Elastic modulus of matrix

Ɛ=Strain

$ε_{c1}$ = Strain at peak stress

$ε_{cm}$ = Maximum Concrete Strain

$ε_{fe}$ = Strain in the fiber

$Ɛ^{el}$=Elastic Strain

$ε_c^{in, h}$ =Inelastic compression strain

$ε_t^{cr, h}$ =Inelastic cracking strain

$Ɛ_{nom}$=Normalized Strain

$Ɛ^{pl}$=Plastic Strain

$Ɛ_0$=Maximum Strain

$ε_{S1}$ = Strain at bottom steel reinforcement

$ε_{S2}$ = Strain at top steel reinforcement

f= Stress

f_c= Cylindrical Compressive Strength

f_{cu}=Cubic Compressive Strength

f_{cm}= Mean Cylindrical Compressive Strength

f_{cr}/f_{ctm}= Mean tensile Strength

f_{ct}= Tensile Strength

f_{nom}=Normalized Stress

f_n=Reduced yield stress

f_o=Maximum Stress

f_y=Steel yield stress

f_u=Steel yield stress

G_i= Shear modulus of resin

G_c= Shear modulus of concrete

K= Beam Stiffness

K_c = Ratio of the second invariant on tensile meridian

l_b=Bond Length

M= Moment

M_{cr} = Cracking Moment

M_{RD} = Moment Capacity

m= Flow potential eccentricity

N_F=Normal Force

μ = Viscosity parameter

$ρ_s$ = Geometric Steel Ratio

σ= Axial Stress

$σ_{co}$ = Initial biaxial stress

$σ_{bo}$ = Initial uniaxial ratio

$\bar{σ}_c$= Effective uniaxial compression stress

$σ_f$ = Tensile strength of FRP

$σ_{fib}$ = Tensile strength of fiber

$σ_{mat}$ = Tensile strength of matrix

$\bar{σ}_t$= Effective uniaxial tensile stress

$τ_b$= Bond Shear Stress

$τ_{lim}$ = Longitudinal Shear Stress resistance

$τ_{max}$ = Maximum shear stress

ν= Poisson's Ratio

ψ = Dilation angle

Q_u= Ultimate Load

Q_{ser}=Serviceable Load

t_c= Concrete thickness

t_f= Fiber thickness

t_i= Resin thickness

Φ=Diameter

s_f=slip

T=longitudinal Shear Stress

T_{s1}= Tensile Force in bottom reinforcement

T_{s2}= Tensile Force in top reinforcement

V_{ED}= Shear Force

$V_{RD, cr}$= Cracking shear Force

V_{fib}= Volume fraction of fiber

V_{mat}= Volume fraction of matrix

W_c= Compression recovery factor

W_t= Tension recovery factor

Abstract

Carbon Fiber Reinforced Polymer (CFRP) has been proved to enhance the flexural strength of Reinforced Concrete (RC) beams and there is a wide range of application all over the world. As new strengthening technique Externally Bonded Reinforcement (EBR) FRP has developed and penetrated the market so quickly, however, its effectiveness on low strength concrete is questionable and there is also a minimum concrete compressive strength limit on some deign codes like ACI-2.R-08. The rationale behind this limit is not discussed in the code and measure that could be taken to improve FRP strengthening techniques at lower concrete grades is not yet known.

This research assesses different flexural strengthening techniques on medium and low concrete grades including the minimum limit recommended by ACI. A new CFRP anchorage technique is also proposed and its performance is compared with other prevailing application techniques. To do so, RC beams of medium and low concrete strength are casted in the laboratory and tested with a three point loading then the result is used to validate the concrete and steel material model on Abaqus non-linear finite element software. Other experimental results are also used to validate EBR CFRP and end wrapped CFRP strengthened beam models after different interaction models have been tried on the software.

With the best fitting models validated to represent CFRP strengthened beams, additional simulation works are done together with section analysis and other analytic manual calculations. With a one layer 1.4 mm thick SIKA Carbodur E-1014 CFRP Laminate, remarkable strength and stiffness increment is observed in all concrete grades and application techniques. However, beams with lower concrete compressive strength close to ACI limit are found prone to FRP end delamination at their ultimate capacity. More study was done on the delamination of these low strength beams and the new anchorage technique delayed the delamination of FRP and increased the ultimate load capacity. The other very important benefit gained from application of the new anchorage is that it dislocated the delamination initiation from the end of the FRP to the middle of the beam which is less brittle in nature compared to the one that initiates at the end of the FRP.

Chapter One
Introduction

1.1 General Introduction

Reinforced concrete (RC) structures are prone to significant strength and serviceability degradation. And it is because of the ever advancing strengthening and retrofitting techniques that RC still remained to be prominent construction material. One of the latest advancements in RC retrofitting is bonding of Fiber Reinforced Polymers (FRP) to the RC member. FRP composites consist of high number of small, continuous, directional non-metallic fibers with advanced characteristics embedded in a matrix of polymer resin.

The mechanical properties of composites are dependent on the fiber properties, matrix properties, fiber-matrix bond properties, and fiber amount and fiber orientation. The fibers, however, predominantly determine the stress bearing nature of the composite. The fibers also occupy the largest volume fraction up to 70%. A composite with all fibers in one direction is designated as unidirectional. If the fibers are woven, or oriented in many directions, the composite is bi- or multidirectional. Fibers can take the form of carbon, aramid, glass, basalt and other natural fibers. The former three, however, are the common types.

Carbon fibers have high strength, high stiffness and light-weight. They have a low thermal expansion but a high electrical conductivity. Generally, carbon fibers with a higher stiffness have lower tensile strength and vice versa.

Aramid fibers have high toughness and are not brittle in non-composite form as carbon and glass fiber. But they exhibit other weaknesses. The combination of their relatively high price, low compression and shear strength, difficulty in processing, low resistance against ultraviolet (UV) radiation and moisture has made the fibers less attractive for structural engineering.

Glass fibers are the least stiff and strong compared to aramid and carbon fibers, but they are the cheapest. Glass fibers are weak against highly acidic or alkaline environments and are also susceptible to creep.

The matrix material, or the resin, is the other constituent that holds the fibers together, fixes them in place, and provides the integrity of the composite material. One of the most important functions of the matrix is to transfer force between the fibers, but it also has to protect the fragile fibers against wear, impact and environmental degradation. If efficient resin is used it avoids the progressive failure of the fibers which limits the ultimate strength.

The most common adhesives are epoxies, polyester, phenolic and urethanes. Epoxies have qualities including high specific strength, good dimensional stability, high temperature resistance and good resistance to solvents and alkalis. Additionally, they exhibit a toughness that is superior to a lot of other civil engineering polymer.

One drawback is that they often have a limited resistance against acids. Most pre-cured Carbon Fiber Reinforcement Polymer (CFRP) composites are made with epoxy resins and they are also used extensively for dry sheets and fabrics acting as both adhesive and resin.

Polyester resins, compared to epoxies, are cheaper and easy to process and they are frequently used as resins for larger pultruded structural profiles. The mechanical properties though, are not as good as epoxies and the curing is highly exothermic and thus experience significant shrinkage.

Phenolic resins have advantageous properties with respect to fire. They have a high-resistance and emit a low amount of toxic fumes and smoke during fire However, they have a low toughness and are more hygroscopic than other resins, and therefore absorbed moisture will evaporate during fire resulting in severe damage to the bond. Polyurethane resins come in several different formulas and are generally a bit weaker than epoxies. On the other hand they have a high tolerance against chemicals and an adequate resistance against moisture; nevertheless they suffer from extensive curing shrinkage, creep and moisture movement.

Finally, in order to get a strong connection between the substrates, the adhesive has to get a good bond with the surface of each substrate. In the case where the substrate is a lot stronger than the adhesive it is important that the adhesive bond is not the weakest link and that the adhesive strength determines the strength of the bond. In order to get such a bond it is important that the application of the laminate is carried out in a proper way. This preparation is crucial for the final result of the strengthened beam. The surface of the strengthened member has to roughened up and the cleaned to get rid of all dust and dirt and then prepared with a primer to get a more suitable surface and filling cavities that would require large amounts of adhesive and would affect the behavior of the joint.

1.2 Historical Development of FRP's

1.2.1 Early Works

In the 1970's research and development of FRP reinforcement started in Europe, as well as in North-America and Japan. In Europe, FRP systems were developed as alternates to steel plate bonding. Bonding steel plates to the tension zones of concrete members with adhesive resins were shown to be viable techniques for increasing their flexural strengths. This technique has been used to strengthen many bridges and buildings around the world. Because steel plates can corrode, leading to a deterioration of the bond between the steel and concrete, and because they are difficult to install, requiring the use of heavy equipment, researchers have looked to FRP materials as an alternative to steel.

The use of FRPs in strengthening applications was suggested as a replacement for steel plates due to the rather significant shortcomings of steel plates such as durability, extra maintenance needed for the new steel plates including surface preparation, painting and regular inspections. The extra maintenance adds to the costs and complications of this traditional method. Additionally, there are several practical difficulties with the method due to the material properties of steel. The high density of steel makes it difficult to handle the plates on the installation site and usually heavy lifting machinery is needed for this purpose.

The plates are often cut in limited lengths, for transportation purposes, which necessitate splicing this in turn causes problems of joining the plates, which is mostly done by on-site welding, and creating poor fatigue details. These considerations are time-consuming and labor intensive. (Martin Fornander, 2013)

FRPs, however, have a high strength to weight ratio, a low maintenance cost, good fatigue properties, and a high resistance against corrosives such as alkalis, salts, and acids under a wide range of temperatures. In comparison to a steel strengthening system, an equivalent FRP system requires much fewer resources to install and being that it consists of a non-corrosive material. The non-corrosive characteristic of FRP is its most significant advantage.

Experimental work using FRP materials for retrofitting concrete structures was reported as early as 1978 in Germany (Wolf and Miessler, 1989). Research in Switzerland led to the first applications of externally bonded FRP systems to reinforced concrete bridges for flexural strengthening (Meier 1987; Rostasy 1987). FRP systems were first applied to reinforced concrete columns for providing additional confinement in Japan in the 1980s (Katsumata 1987).

Researchers in the United States have had a long and continuous interest in fiber-based reinforcement for concrete structures since the 1930s. Development and research into the use of these materials for retrofitting concrete structures, however, started in the 1980s through the initiatives of the National Science Foundation (NSF) and the Federal Highway Administration (FHWA). The research activities led to the construction of many field projects that encompassed a wide variety of environmental conditions.

Commercial applications of FRP materials especially (CFRP) began in the 1970s, initially being used in the field of sporting goods. In the 1980s, the FRP materials gradually started to be used in the field of transportation engineering. In the mid-1990s, because Japan's Kobe earthquake resulted in a great deal of civil transportation infrastructure disasters, FRP quickly developed into an important means for seismic reinforcement. Especially, the use of FRP as externally bonded reinforcement to retrofit existing structures has become commercially of considerable importance.

Among the different types of FRP's it was Glass Fiber Reinforcement Polymer (GFRP) that was used during the early days of FRP's. The initial developments took place in Germany where thick glass (GFRP) plates were used and in Switzerland where thin sheets of carbon (CFRP) were utilized (Meier 1987).

The development of codes and standards for externally bonded FRP systems is ongoing in Europe, Japan, Canada, and the United States. Within the last 10 years, the Japan Society of Civil Engineers (JSCE), the Japan Concrete Institute (JCI), and the Railway Technical Research Institute (RTRI) published several documents related to the use of FRP materials in concrete structures.

In Europe, Task Group 9.3 of the International Federation for Structural Concrete (FIB) published a bulletin on design guidelines for externally bonded FRP reinforcement for reinforced concrete structures (International Federation for Structural Concrete 2001).

ACI 440 (2002) has also prepared a design standard for FRP composites application, where it clearly states the different design standards to be used for redesigning structures for re-

strengthening reinforced concrete structures. Nanni (1993) also a leading researcher on Fiber reinforced plastics-studied the properties and Application of the system for concrete structures.
With all these advancements, delamination was a critical shortcoming always related to FRP's technology. In the last decade, the development of strong epoxy glue has led to a technique which has great potential in the tackling this drawback. Due to the diversity of input materials, epoxy resins have a very wide range of mechanical and physical properties, as well as processing conditions. As a result, they are the most versatile polymer binder for fiber composites, although more expensive than polyester and vinyl ester resins.

1.2.2 Recent Works (Retrieved from http://shodhganga.inflibnet.ac.in)

Some of the significant research works carried out on RC beams and columns for the past several decades using CFRP, GFRP, and Hybrid FRP are discussed below.

- Alessandra Aprile (2001), found that RCC beams strengthened by steel plates showed a ductile response, mainly due to yielding of the strengthening plate. The RCC beams strengthened by CFRP plates showed a brittle response, as the response was dominated by the elastic behavior of the plate.
- Francesco Bencardino (2002) conducted an experimental investigation of reinforced concrete beams strengthened in flexure and shear using externally epoxy bonded bidirectional carbon fiber fabric to overcome the bond slip and plate separation at the ends. In conclusion that the results reported herein show that CF fabrics can provide an effective and efficient alternative to laminates strengthening existing concrete structures.
- Maria Antonietta Aiello (2002) analyses to study the structural behavior of concrete beams reinforced with hybrid fiber reinforced polymer FRP-steel reinforcements. They observed from the experiment that the increase of stiffness is more evident for beams reinforced with FRP rebars placed near the outer surface of the tensile zone and steel rebars placed at the inner level of the tensile zone.
- Hedong Niu and Zhishen Wu (2006) analyzed the effect of interface bond properties on the performance of FRP-strengthened reinforced concrete (RC) beams in terms of concrete cracking, interface stress transfer, and failure mechanisms using nonlinear fracture mechanics based finite element analyses. They concluded that, low stiffness may be helpful to distribute more uniform stresses in both steel and FRP sheets, which may help to relieve local stress concentrations and reduce the likelihood of debonding in practice.
- Abdelhady Hosny (2006), made an elaborate study on the behavior of RC beams strengthened with hybrid fiber reinforced polymer (HFRP) laminates. They observed that use of CFRP and GFRP laminates for strengthening RC T-beam is an effective method to increase its ultimate load carrying capacity and using a combination of CFRP and GFRP laminates is an effective method to enhance the ductility of the strengthened beams.
- Muhammad and Shamim (2005) evaluated the effectiveness of glass Fiber reinforced polymer (GFRP) wraps in strengthening deficient and repairing damaged square concrete columns. Concluded square concrete columns externally retrofitted by GFRP wraps and tested under axial compression and cyclic loading, simulating seismic loads, showed pronounced un

retrofitted columns. Higher ductility and improved seismic performance can be achieved by retrofitting damaged square concrete columns with GFRP jackets.

- Nadeem (2010) presented the results of experimental study made on beams wrapped with CFRP and their test results clearly indicated that flexural strength can be substantially improved by externally bonding the CFRP sheets to the tension face of under-reinforced RC Beams. However, the percentage increase is dependent of steel reinforcement ratio. There is no universally accepted definition of structural ductility. In order to develop a rational and meaningful concept of ductility that may be applied to all structural materials, a reference base is required. The yield point of internal steel provides a very objective reference point to define ductility. However, it is the unique yield plateau of the stress-strain curve of steel which impart the structural member an ability to sustain load while undergoing large deformations. This is not that case when the reinforcing medium is fiber reinforced polymer (FRP), or a mixture of steel and FRP, as in the case of FRP sheet bonded RC beams, following expression was used to calculate the ductility index of control and CFRP strengthened beams:

$$\text{Ductility index} = \frac{Mid\ Span\ deflection\ at\ failure}{mid\ span\ deflection\ at\ tension\ steel\ yield}$$

- Yasmeen Taleb Obaidat presented the results of the experimental study conducted to investigate the behavior of structurally damaged full-scale reinforced concrete beams retrofitted with CFRP laminates in shear or in flexure. The main variables considered were the internal reinforcement ratio, position of retrofitting and the length of CFRP. The stiffness of the CFRP-retrofitted beams had increased compared to that of the control beams. Employing externally bonded CFRP plates resulted in an increase in maximum load. The increase in maximum load of the retrofitted specimens reached values of about 23% for retrofitting in shear and between 7% and 33% for retrofitting in flexure. More over retrofitting shifts the mode of failure to be brittle. The results showed that the main failure mode was plate debonding which reduced the efficiency of retrofitting.

- Jadhav and Shiyekar (2011) carried out experimental studies, to investigate the effect of length, width and number of layers of glass fiber reinforced polymer (GFRP) strips applied to the tension side of the RC Beam. The authors concluded that, the beam strengthened with different width and number of layers of glass fiber reinforced polymer (GFRP) strips exhibited relatively good ductile behavior. However it showed same load at yielding of steel. This was because the glass fiber reinforced polymer had higher initial stiffness. Hence, it contributed to strengthening more effectively. The load carrying of the strengthened beams increased by 7% to 35% when compared to the control beam.

- Ferrier (2011) examined the damage behavior of FRP-strengthened reinforced concrete (RC) Structures subjected to fatigue loading. Based on the research, two design force-strain relationships were proposed for hybrid carbon-glass FRP sheets, with and without consideration of hybrid effects. The specimen with two plies of the hybrid sheets (HF-2ply) had a hybrid FRP amount of approximately 75% of the maximum. The effective bond length of the tested hybrid FRP sheet was approximately 8 in. (200mm), and the bond shear stress capacity between the

hybrid FRP sheet and concrete was on the order of 3 MPa (430 psi), Comparable to that between the carbon FRP sheet and concrete.

- Antonio De Luca and Antonio Nanni (2011) analytically studied the single parameter methodology for the prediction of the stress-strain behavior of FRP confined RC square columns and concluded that, transverse/ diagonal dilation ratio -axial strain curves are influenced not only by the modulus of elasticity and the thickness of the jacket but also by the fiber type. However, it is believed that the validity of the theoretical framework is independent from the fiber type.

1.3 Statement of the Problem

One of the reasons that necessitate the retrofitting of existing structures is the revision of existing building codes. In Ethiopia, a code that has lasted for the last two decades is revised by a more conservative one. As a result, the new features of the recent code may regard some old buildings as unsafe. If this new features only belong to ultimate limit state, the already available simple external bonding of FRP to the RC substrate would retrofit the structure efficiently.

However, from effective depth calculation which allows the omission of deflection computation to limiting deflection values of different structural systems, vital changes are included on the serviceability limit state section of the new code. Serviceability retrofitting, especially deflection control is a difficult to attain by applying FRP because of the low stiffness of the material. And there is also another economic challenge related to sufficient amount of FRP application to address the serviceability requirement.

Given the high strength of FRP, relatively small cross-sectional areas are needed to reinforce concrete elements with respect to the ultimate limit state (strength considerations). On the other hand, to fulfill serviceability criteria, sufficient flexural stiffness should be available. Once cracked, the stiffness of reinforced concrete (RC) section significantly depends on the stiffness of the reinforcement. Due to small cross-sectional area needed for strength consideration and generally lower modulus of elasticity of most FRP's materials in comparison with steel, serviceability problems may arise when the design is based on the ultimate limit state only. This is also illustrated by the load deflection diagrams shown in Figure 1-1. (Stijn Matthys, 2000)

Designing a FRP RC member with similar strength as steel RC member (Curve 1 and 2), the obtained service load of the FRP cross-sectional area or by increasing the member depth (curve 3) is lower as a result of lower flexural stiffness. In this case, the ultimate load will generally be significantly higher. Hence, the high strength of the composite is not efficiently utilized.

In the flexural and shear retrofitting of RC beam and bridges the FRP are applied on the already deflected structures. Since there is no need for the use of formwork or up-lifting jacks; there is a chance for the deflected beams to remain deflected after the beam is retrofitted for flexure or shear. The repaired beam is experimentally and analytically proven to support immense amount of moment and shear afterwards but the deflection experienced in the process should be known ahead to be in accord with the serviceability limit states.

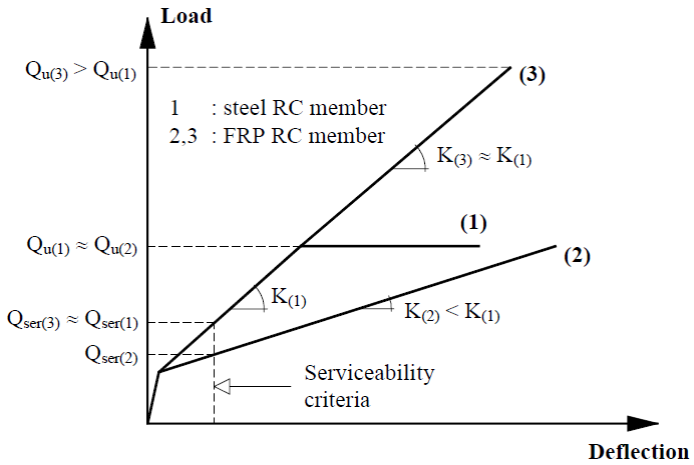

Figure 1-1: Steel Versus FRP reinforced concrete members (Stijn Matthys, 2000)

In fairly high grade concrete, experiments conducted to assess the flexural capacity increment attained by applying CFRP strengthening have proven that there is also important deflection decrement. However the construction trend in Ethiopia usually uses medium grade concrete around C-20/25 whose cylindrical compressive strength is close to the minimum strength recommended by ACI 440-08 for application of CFRP, i.e. 17 MPa. Hence without additional study and experimentation, medium grade concrete cannot be expected to yield similar improvement.

1.4 Aim and Scope of the Study

1.4.1 Research objective and aim of the thesis

This research aims at exploring the performance of CFRP strengthened and retrofitted C-20/25 concrete beams and asses application techniques which enhance the performance. The research focuses on flexure, specifically on load-deflection behavior of the RC beams. Different FRP application techniques will be evaluated to find out the most effective one with respect to the strength and stiffness of the beams.

The other objective of this research is to explore the rationale behind the minimum substrate compressive strength recommendation of ACI by taking a close look at the failure mode of CFRP strengthened concrete beams with the indicated compressive strength. If this research yields affirmative results, it dares a recommendation of CFRP bonding to RC beams for strengthening or retrofitting purpose in Ethiopia.

1.4.2 Scope of the Study

Experimental program will be conducted on RC beams with different application techniques side by side with a software simulation to be done on ABAQUS. Once the two results are found out to be in good agreement, the software simulation will be used to extend the study on various types of concrete strengths, steel ratio or application techniques. Analytic calculations will also be carried out to estimate the load carrying capacity and failure mode of both control and strengthened beams.

1.5 Layout of Chapters

The first chapter provides general ideas about the material Fiber Reinforcement Polymer (FRP) and its Externally Bonded Reinforcement (EBR) Techniques. Historical development and recent works are discussed as well. The background problem, objective of the thesis and methodology employed to proceed throughout the research work are also presented.

The second chapter brings detained information on different types of FRPs and constituent materials. Basic and Special techniques are presented. Among the different strengthening areas flexural strengthening is emphasized in the chapter.

The third chapter focuses on the experimental program carried out to cast the concrete beam specimens. Laboratory test results of constituent materials and the resulting concrete properties are presented. The tensile strength and other properties of reinforcement and the CFRP material are also presented. Finally the layout of the beam specimen, the loading setup and the reinforcement data are shown with the help of schematic diagrams.

The fourth chapter explains the initial validation process of the software Abaqus beginning from the discussion of different material models used to define the concrete material, reinforcement steel and the CFRP. Additional information is given on the final models used in the simulation work after carefully selecting the efficient ones. Two different models are tried for concrete-CFRP interface and then the one best fitting the experimental result is used for further simulation.

The fifth chapter discusses the conceptual design of a new end anchorage technique tried to better the load deflection of FRP EBR beams. The result with respect to the other application techniques is presented on load deflection diagrams. A study the rationale behind the minimum substrate compressive strength limit of ACI (ACI 2.R-08) is discussed in the chapter. Finally, the effect of concrete strength and end-anchorage on the ultimate load and stiffness increment is presented

The six chapter sums up the main findings obtained in the thesis and also provides additional information on further works and recommendation need to be noted. References and Annex are given at the end.

Chapter Two
Literature Review

2.1 Development of CFRP strengthened structures

This chapter briefly discusses the use of FRP to strengthen and retrofit RC structural members. The main focus will be on flexural beam strengthening and retrofitting works. Since almost 95% of all strengthening applications are carried out with CFRP due to its superior properties with regard to strength and stiffness, most of the discussion will be on CFRP.

Fiber reinforced plastic (FRP) reinforcement plays a very important role in the retrofitting and rehabilitation of reinforced concrete(RC) structural elements as an external reinforcements. Recent developments related to materials, methods and techniques for structural strengthening have been enormous. One of today's state of the art techniques is based on the use of fiber reinforced polymer (FRP) composites, which are currently viewed by structural engineers as "new" and highly promising materials in the construction industry. Moreover, recent developments have focused on the combination of continuous fiber based textiles with mortars (instead of resins, as in the case of FRP), leading to the development of the so-called textile reinforced mortars (TRM). Both FRP and TRM materials may be given the term "continuous fiber composites" or "advanced composites" or simply "composites". For comparison with steel, typical stress-strain diagrams for unidirectional composites under short-term monotonic loading are given in Figure 2-1.

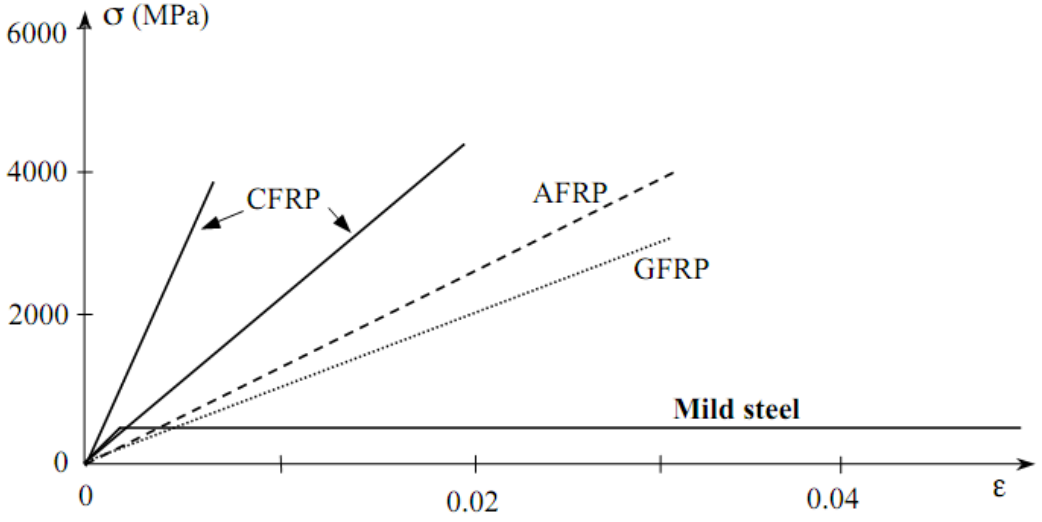

Figure 2-1: Uniaxial tension stress-strain diagrams for different unidirectional FRPs and steel. (Stijn Matthys, 2000)

CFRP = carbon FRP, AFRP = aramid FRP, GFRP = glass FRP

In the following sections the three main components, namely adhesives, matrices and fibers of a composite material strengthening system will be discussed briefly.

2.1.1 Properties of Structural Adhesives

Depending on the method of CFRP strengthening technique employed, different types of adhesives can be used. If manual lay-up is used, the adhesive is also the resin for the composite fibers, and if pre-formed FRP composites are used the composite has to be attached to the structural element using a separate adhesive.

The difference between the resins and the adhesives is that the adhesives need to be able to cure at in-situ, which often includes exposure to low temperature compared to the possibilities of higher controlled temperature while curing the resins in a factory. By means of an adhesive two materials can be connected to each other, so that full composite action can be developed. In the case of FRP Externally bonded Reinforcement (EBR), the adhesive is used to glue the FRP reinforcement onto the concrete surface and to provide a load path between these two materials.

The load transfer is normally achieved by stressing the adhesive in shear (stresses in the plane of the bond interface), although peel stresses (normal to the bonded surface) may occur as well. The choice of the adhesive depends on several factors, such as the type of substrates, the required performance, the environmental conditions and the possibilities with respect to application. Furthermore, the adhesive must be able to provide excellent bond over a long period of time, even when exposed to e.g. moisture and variable temperatures.

2.1.1.1 Adhesive requirements

To obtain a good performance of concrete structures strengthened with externally bonded FRP reinforcement, adhesives should meet certain requirements. Although detailed studies on the influence of material properties of adhesives on the performance of FRP EBR are rather limited, the following is generally required:

- Working characteristics with respect to mixing, application and curing should allow excellent joint quality, adequate adhesion to the concrete and the FRP (wetting ability), gap-filling properties, workability on overhead surfaces, etc. The adhesive should also be able to attach FRP without the need for temporary fixings.
- Bond quality and workability should not be unduly sensitive to limited variations in the quality of the prepared surfaces or the environmental conditions.
- With respect to durability, the adhesive should exhibit good moisture resistance, low creep, thermal stability and resistance to the alkaline nature of the concrete.
- The glass transition temperature of the adhesive should be significantly higher than the service temperature.
- The flexural modulus (E-modulus in bending) should fall within a specified range, generally taken as 2000 to 15000 N/mm^2. The lower limit relates to a restriction of creep,

the upper to minimize stress concentrations. Also, the fracture toughness of the adhesive should be sufficiently high.

- The minimum shear strength of the adhesive should be 12 N/mm^2 (at 20 °C).
- The permeability of the adhesive and its maximum moisture absorption should be limited. Generally, it is required that the equilibrium moisture content should not exceed 3 % by weight after immersion in distilled water at 20 °C.
- Depending on the use of the strengthened structure and the environmental conditions, specific aspects of influence on the adhesive may be of concern. The material properties of the adhesive should also be considered in relation to those of the concrete and the FRP.

2.1.1.2 Epoxy as structural adhesive

Epoxies offer high surface activity and good wetting properties for a variety of substrates, high cohesion (failure in the adhesive) and adhesion (failure in the bond interfaces) strength so that debonding is governed by the adherent strength, low shrinkage and low creep.

Given the numerous possibilities with respect to formulation, only epoxy adhesives should be used which are specifically produced for the construction industry. Generally, the formulations are complex as they are a blend of the epoxy resin, the hardener, fillers and additives. Fillers are used to reduce cost, assist gap-filling, reduce creep, etc. Diluents can be applied to reduce viscosity and may influence the pot life, flexibility and glass transition temperature. Flexibilisers can be used to improve impact resistance, peel strength and ductility, while toughеners improve fracture energy and fracture toughness.

Some typical values of the mechanical properties of epoxy adhesive, compared to those of concrete and steel, are given in Table 2-1. For properly formulated epoxy adhesives, generally no primer on the FRP or the concrete surface is required (for steel plate bonding a primer is normally applied on the steel).

Property		Epoxy adhesive	Concrete	Steel
Compressive Strength	[N/mm^2]	55-100	25-150	200-2000
Tensile Strength	[N/mm^2]	9-20	1-6	200-2000
Modulus of Elasticity	[N/mm^2]	500-20000	20000-50000	≈ 200000
Coefficient of thermal Expansion	[10^{-6}/°C]	25-30	8-12	≈ 10
Density	[Kg/m^3]	1450-1550	≈ 2400	≈ 7800
Poisson ratio		≈ 0.30	0.15-0.2	0.30

Table 2-1: Typical properties of epoxy adhesive compared to concrete and steel

2.1.2 Polymer matrices

The polymer matrix of a FRP material consists of a resin binder (polymer binder) and normally some fillers and additives. Primarily the matrix has to bind the fibers together, provide lateral support to the fibers, protect the fibers from their surroundings, offer a load transfer medium and may beneficially influence some FRP material properties. In addition, the matrix selection is also important with respect to composite process ability and cost.

The polymer matrix of a FRP material consists of a resin binder (polymer binder) and normally some fillers and additives. Primarily the matrix has to bind the fibers together, provide lateral support to the fibers, protect the fibers from their surroundings, offer a load transfer medium and may beneficially influence some FRP material properties. In addition, the matrix selection is also important with respect to composite processability and cost.

For structural fire composites, among which FRP reinforcement for concrete, unsaturated polyester, vinyl ester and epoxy are often used as polymer binder. From these resins, polyesters are most general purpose and frequently applied, given the good processability, fairly good properties and low cost. Vinyl esters process essentially like polyesters, but provide improved mechanical and chemical performance. Epoxy resins are more expensive than polyesters and vinyl esters, but are largely used in high-performance composites as they generally have the best mechanical properties, good adhesion properties and excellent resistance to chemicals and solvents. Some typical properties of these polymers are given in table 2-2.

	Epoxy	polyester	Phenolic	Polyurethane
Modulus of Elasticity (GPa)	2.6-3.8	3.1-4.6	3.0-4.0	0.5
Tensile Strength (MPa)	60-85	50-75	60-80	15-25
Strain to failure (%)	1.5-8.0	1.0-2.5	1.0-1.8	10
Poisson's ratio	0.3-0.4	0.35-0,38	NA	0.4
Density (Kg/m^3)	1110-1200	1110-1250	1000-1250	1150-1200
Coefficient of thermal expansion ($10^{-6}/^oC$)	30-70	30-70	80	40

Table 2-2: Typical properties of resins *(Martin Fornander)*

2.1.2.1 Epoxy Resins

Epoxy resins are made of low-molecular weight organic liquid resins containing epoxide groups (rings of two carbon and one oxygen atom). Epoxies have qualities including high specific strength, good dimensional stability, high temperature resistance and good resistance to solvents and alkalis.

Additionally, they exhibit a toughness that is superior to a lot of other civil engineering polymers. Epoxies have good adhesion to most materials and exhibit a low shrinkage, usually 2-3%, during polymerization. One drawback is that they often have a limited resistance against acids. Most pre-cured CFRP composites are made with epoxy resins and they are also used extensively for dry sheets and fabrics acting as both adhesive and resin.

2.1.3 Fibers Used in FRP's

There are three different types of fibers commonly used in civil engineering; carbon, aramid and glass fibers. The main fibers used in structural engineering are carbon and glass fibers and for strengthening purposes almost 95% are carbon fibers (*H. Nordin, 2005*). For strengthening of structures in bending using prestressed FRPs, carbon fibers are used for their suitable properties such as high strength and stiffness. Typical properties for the different fibers are presented in Table 2-3.

Material	Tensile Strength (MPa)	Modulus of Elasticity (GPa)	Density (Kg/m^3)	Modulus of elasticity to density ratio(Mm^2/s^2)
Carbon	2200-5600	240-830	1800-2200	130-380
Aramid	2400-3600	130-160	1400-1500	90-110
Glass	3400-4800	70-90	2200-2500	31-33
Steel	280-1900	190-210	7900	24-27

Table 2-3: Typical properties for the different fibers

2.1.3.1 Carbon Fibers

Carbon fibers have high strength; high stiffness and they are light-weight. They have a low thermal expansion but a high electrical conductivity. There are different types of carbon fibers which are categorized depending on the manufacturing process:

- High-strength (HS),
- High-modulus (HM),
- Ultra-high-modulus (UHM).

Generally, carbon fibers with a higher stiffness have lower tensile strength and vice versa. UHM carbon fibers are very brittle and therefore CFRP composites require special care when handled. Carbon fibers are the stiffest and strongest reinforcing fibers for polymer composites. They are very resistant against creep and fatigue and have a very good chemical, UV light and moisture resistance. Hence, carbon fibers are very durable and have excellent mechanical properties. As the fibers are electrically conducting, they can give galvanic corrosion in contact with metals. The wetting of the fibers by resins is not easy, so that surface treatments are normally needed. In this respect, carbon fibers are often provided with an epoxy size treatment which protects the fibers against abrasion (improved handling) and offers an epoxy matrix compatible interface. (Stijn Matthys, 2000)

2.1.3.2 Glass fibers

Glass fibers are made of silicon oxide with the addition of small amounts of other oxides and are formed by extruding molten glass and fiber stretching. As glass fibers are very surface active and hydrophilic, individual fibers are generally coated by a sizing agent immediately after fiber forming. The sizing also acts to minimize abrasion damage and to aid coupling with polymer matrices.

Glass fibers are also characterized by high tensile strength, good electrical resistivity, good thermal resistance and low price glass fibers are known to degrade in the presence of water, acid and alkaline solutions. Also, they exhibit a considerable creep or stress rupture behavior, meaning that the tensile strength gradually decreases under constant stress.

Given the low durability of glass fibers, it is important to select a suitable and protective matrix. The use of AR-glass fibers with higher chemical resistance is of interest as well. (Stijn Matthys, 2000)

2.1.3.3 Aramid fibers

In the 1980s the first prestressing tendons were manufactured with aramid fibers, usually presented under their commercial names; Kevlar and Tarpon. Today very few manufacturers produce them. Aramid fibers have high toughness and are not brittle in non-composite form as carbon and glass fiber, but they exhibit other weaknesses. The combination of their relatively high price, low compression and shear strength, difficulty in processing, low resistance against ultraviolet (UV) radiation and moisture has made the fibers less attractive for structural engineering. [Martin Fornander, 2013]

With respect to durability, aramid fibers generally exhibit a low or moderate resistance against acids, a moderate resistance against alkalis and a poor resistance against ultraviolet radiation. Due to the interaction of water with the polymer structure, they are sensitive to moisture as well. Because of these aspects, the fibers should be embedded in a matrix which is carefully chosen to provide additional protection. To improve the bond between fibers and matrix, surface treatments may be used. (Stijn Matthys, 2000)

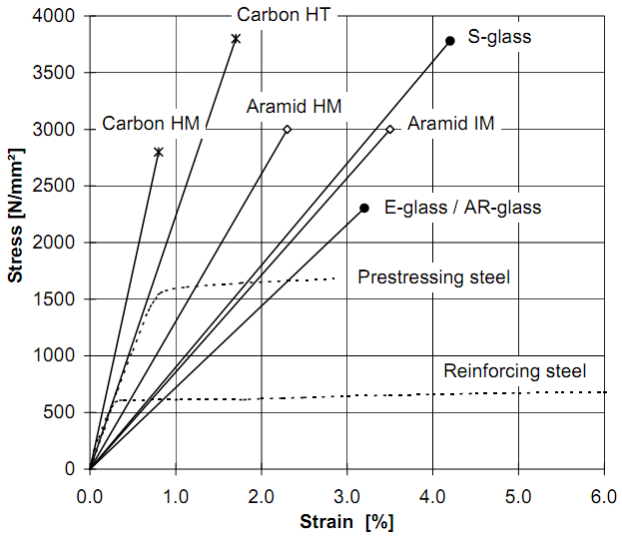

Figure 2-2: Tensile stress-strain behavior of reinforcing fibers (Stijn Matthys, 2000)

2.2 Techniques for FRP strengthening

2.2.1 Basic techniques

The basic FRP strengthening technique, which is most widely applied, involves the manual application of either wet lay-up (so-called hand lay-up) or prefabricated systems by means of cold cured adhesive bonding. Common in this technique is that the external reinforcement is bonded onto the concrete surface with the fibers as parallel as practically possible to the direction of principal tensile stresses. Typical applications of the hand lay-up and prefabricated systems are illustrated in Figure 2-3.

(a) *(b)*

Figure 2-3: Basic FRP EBR Application Technique (FIB 14)

(a) Hand lay-up of CFRP sheets or fabrics. (b) Application of prefabricated strips.

2.2.2 Special techniques

Besides the basic technique, several special techniques have been developed. Without aiming to provide a complete overview of these special techniques, a number of them are briefly explained in the following sections.

2.2.2.1 Automated wrapping

The FRP strengthening technique through automated winding of tow or tape was first developed in Japan in the early 90s and a little later in the USA. The technique, shown in figure 2-4, involves continuous winding of wet fibers under a slight angle around columns or other structures (e.g. chimneys, as has been done in Japan) by means of a robot. Key advantage of the technique, apart from good quality control, is the rapid installation.

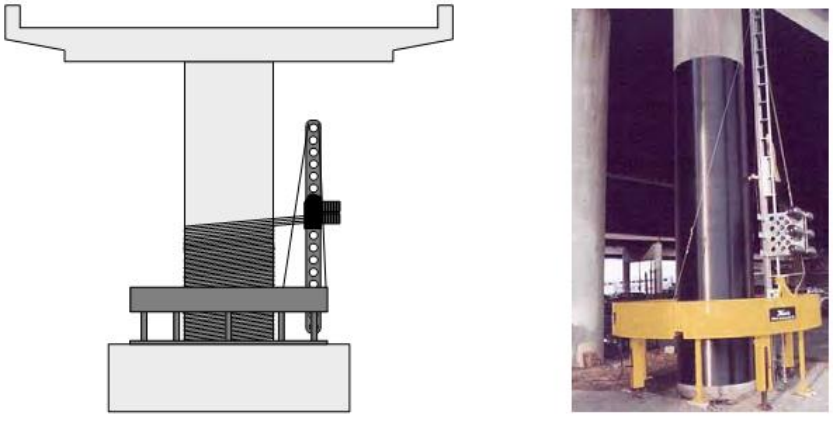

(a) (b)

Figure 2-4: Automated RC column wrapping. (a) Schematic. (b) Photograph of robot-wrapper.

2.2.2.2 Prestressed FRP

In some cases it may be advantageous to bond the external FRP reinforcement onto the concrete surface in a prestressed state. Both laboratory and analytical research (e.g. Triantafillou 1992, Deuring 1993) shows that prestressing represents a significant contribution to the advancement of the FRP strengthening technique, and methods have been developed to prestress the FRP composites under real life conditions.

Prestressing the strips prior to bonding has the following advantages:

- provides stiffer behavior as at early stages most of the concrete is in compression and therefore contributing to the moment of resistance.
- crack formation in the shear span is delayed and the cracks when they appear are more finely distributed and narrower (crack widths are also a matter of bond properties).
- closes cracks in structures with pre-existing cracks.
- improves serviceability and durability due to reduced cracking.
- improves the shear resistance of member as the whole concrete section will resist the shear, provided that the concrete remains uncracked.
- the same strengthening is achieved with smaller areas of stressed strips compared with unstressed strips.
- with adequate anchorage, prestressing may increase the ultimate moment of resistance by avoiding failure modes associated with peeling-off at cracks and the ends of the strips.
- the neutral axis remains at a lower level in the prestressed case than in the unstressed one, resulting in greater structural efficiency.
- prestressing significantly increases the applied load at which the internal steel begins to yield compared to a non-stressed member.

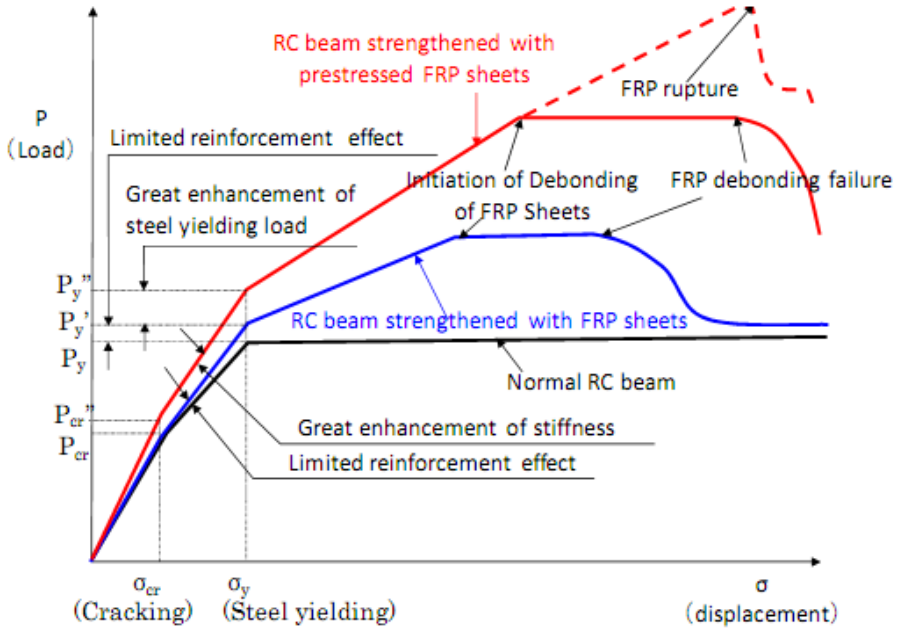

Figure 2-3: Load Deflection curves of FRP strengthened RC beams

When the prestressing force is too high, failure of the beam due to release of the prestressing force will occur at the two ends, due to the development of high shear stresses in the concrete just above the FRP. Hence the design and construction of the end zones requires special attention. Tests and analysis have shown that if no special anchorages are provided at the ends, FRP strips shear-off (from the ends) with prestress levels in the order of only 5-6% of their tensile strength (for CFRP).

The concept for applying a prestressed FRP strip is shown schematically in figure 2-6.

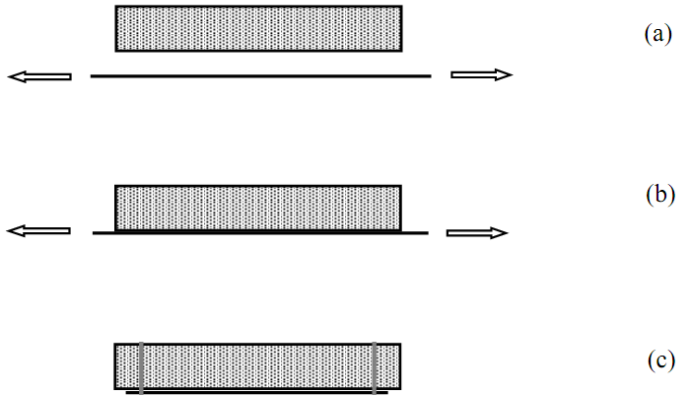

Figure 2-4.: Strengthening with prestressed FRP strips
(a) Prestressing; (b) bonding; (c) end anchorage and FRP release

Prestressing of column jackets (active confinement) can be achieved by pretensioning the fiber bundles during winding or with unstressed jackets by making use of, e.g., expansive mortar or injection of mortar or epoxy under pressure.

2.2.2.3 Near Surface Mounted (NSM) Reinforcement or FRP inside slits

By reason of the problems in the bondage between concrete surfaces and superficially fastened CFRP lamellae a new method of application was developed in the late nineties, the so-called "slotted-in CFRP lamellae" method (figure 2-6). By use of that, carbon fiber lamellae can be fixed in slots vertically in to the surface of the concrete element and thus to essentially improve the ductile behavior and eliminate the danger of a brittle failure, in contrast to the superficially fastened lamellae. For this purpose, slots are incised normal to the concrete element, to a depth smaller than the concrete cover.

Since the concrete cover has often a small and varying value, for the implementation of this method it is of utter importance to know the values and therefore the exact measurements should be included already in the design stage. In order to avoid damaging the stirrups or the lateral reinforcement by incising the slots, the available concrete cover should be of at least 25 mm. In case of bi-axial layers of reinforcement the application is hard to be realized.

Depending on the geometry of the lamellae (thickness up to 2 mm), these slots are usually 15 to 30 mm deep and up to 3 mm wide. After careful cleaning of the slots, the CFRP lamellae are finally fixed inside by use of epoxy resin.

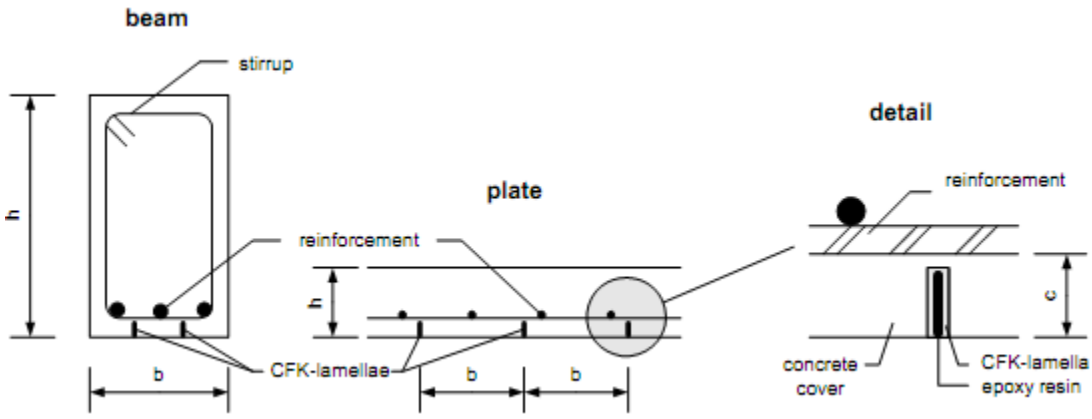

Figure 2-5: Strengthening with slotted-in lamellae (FIB 14)

This method in comparison to the superficially fastened CFRP lamellae features the following advantages: [Blaschko A, 2001]

- Better behavior of the bondage between lamellae and concrete surface, so more efficient usage of the lamellae and selection of smaller lamellae cross sections
- Unevenness of the concrete surfaces can be easily adapted to, by a proper slot depth
- Incising of the slots is often less expensive than evening and roughening of the concrete surfaces in case of superficially fastened lamellae
- Slotted-in lamellae are protected from mechanical damage, while they exhibit a more favorable performance in case of fire

Ideal fields of application of slotted-in lamellae are:

- Increase of resistance in negative moments (joint moments)
- Slots in compression members (increase of tension components of moments)

At this point, it should also be mentioned that CFRP lamellae as strengthening components can be applied not only in concrete structures but also in wood and especially in steel and composite constructions.

2.2.3 Other techniques

There are some more special techniques used for particular cases and resemble the basic technique in many ways. Some examples of these techniques are:

- The use of heating devices, which allow fast curing of the bond interface and wet lay-up FRP types. The technique makes use of heating blankets, electrical heaters or infrared (IR) heaters. In the case of CFRP the heat may even be generated by an electric current, as CFRP is

electrically conducting (and yet resistant against an electric current). By applying heat to the FRP EBR the curing time may be considerably reduced, a higher glass transition temperature is obtained and the application is possible in cold regions or during cold seasons.

- The use of Fusion-bonded pin-loaded straps. The strap comprises a number of non-laminated layers formed from a single, continuous, thin tape, which consists of fibers in a thermoplastic matrix. The outside, final layer of the tape is fixed to the previous layer by a fusion bonding process. Such a system enables the individual layers to move relative to each other, thus reducing the unwanted secondary bending stresses. Careful control of the initial tensioning process allows inter-laminar shear stress concentrations to be reduced, so that a uniform strain distribution in all layers is achieved.
- Prefab type of composite material systems are mostly applied in the form of straight strips. However, these prefab systems can also be produced in other forms, depending on the foreseen application. By shaping them, prefab systems can be employed in applications where normally the more flexible wet lay-up systems are used. For shear strengthening of beams, pre-manufactured angles can be used.
- The other application technique is textile-reinforced mortar (TRM) jacketing. e FRP strengthening technique suffers from some problems associated with the epoxy resins, including the problematic behavior at high temperatures and the relatively high cost. One possible solution to alleviate these problems would be the mere replacement of resins with inorganic binders. However, as a consequence of the granularity of the mortar, penetration and impregnation of conventional fiber sheets is very difficult to achieve; also, mortars cannot wet individual fibers, unlike resins. Bond conditions in cementitious composites could be improved and fiber-matrix interactions could be made tighter when continuous fiber sheets are replaced by textiles.

These materials comprise fabric meshes made of long woven, knitted or even unwoven fiber roving in at least two (typically orthogonal) directions (Figure 2-7).

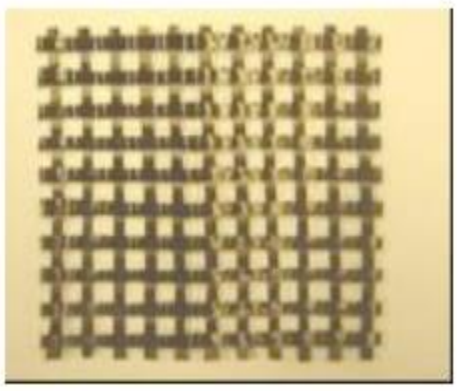

(a)

(b)

(c)

Figure 2-6: Different types of fiber orientations of FRP's

(a) Bidirectional carbon fiber and (b) multidirectional glass fiber textiles (c) Textile-reinforced mortar (TRM) jacketing.

2.3 Flexural Strengthening by EBR FRP

Reinforced concrete elements, such as beams and slabs, may be strengthened in flexure through the application of composites to their tension zones, with the direction of fibers parallel to that of high tensile stresses. The concept is illustrated in figure 2-8, which also shows a practical application.

Figure 2-7: *Flexural strengthening* of RC *beam with CFRP strips (FIB 14)*

The analysis for the limit states for such elements may follow well-established procedures for reinforced concrete structures, provided that: (a) the contribution of external reinforcement is taken into account properly; and (b) special consideration is given to the issue of bond between the concrete and the external reinforcement, through the use of an appropriate bond model. Central to the analysis of these elements is the identification of all the possible failure modes. These failure modes may be divided into two types:

(a) those where full composite action of concrete and external reinforcement is maintained until the concrete reaches crushing in compression or the composite material fails in tension (such failure modes may also be characterized as "classical"). Schematic illustration of these failure types is given below in figure 2-9:

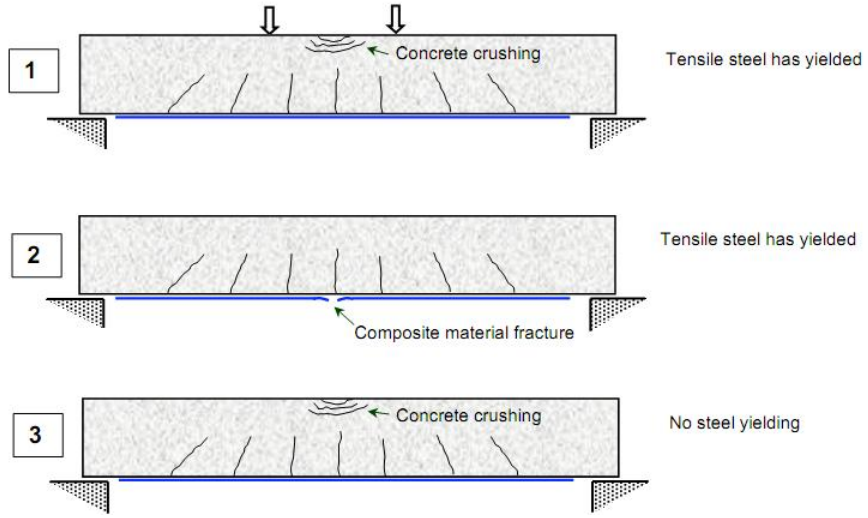

Figure 2-8: Full composite action failure types (FIB 14)

(b) those where composite action is lost prior to type (a) failure, due to debonding of the composite material. Most failures observed in tests of RC flexural members with EBR are caused by peeling off of the EBR element. As discussed above, the weakest point in the bond between the EBR and the concrete is in the concrete layer near the surface. Depending on the starting point of the debonding process, the following failure modes can be identified.

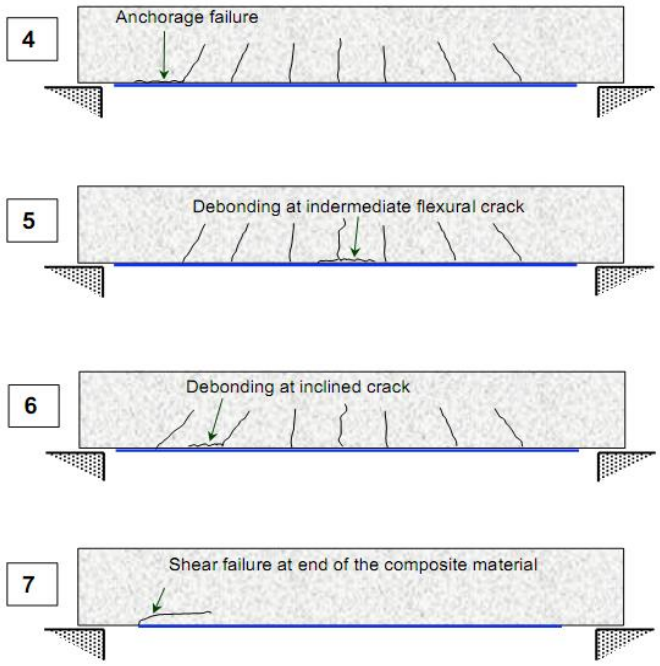

Figure 2-9: Loss of composite action (4-6) and end-shear (7) failure modes associated with flexural strengthening.(Fib 14)

Debonding of the external reinforcement is dealt with through the use of a proper bond model, which allows the calculation of the maximum force carried by the composite material based on force – bond length relations.

2.3.1 Bond behavior

The behavior of the bond between externally bonded FRP and concrete can be analyzed in bond tests, such as the one illustrated in a simplified form in Figure 2-11.

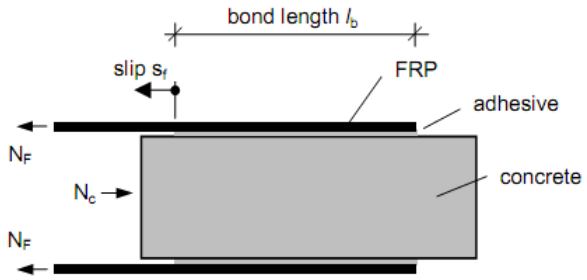

Figure 2-10: Simplified bond test (FIB 14)

The behavior of the bond between concrete and reinforcement can be characterized by the shear-slip relation. This relates the shear stress which is locally transferred between concrete and reinforcement to the displacement, that is the slip, between the two materials.

Shear-slip relations for different types of reinforcement are shown in Figure 2-12. The bond of EBR is very stiff compared to the bond of embedded deformed steel bars, but the total load capacity of the bond is much lower (the area under the curves in Figure 2-12 indicates the energy, which can be borne in the reinforcement by bond). The difference in bond characteristics influences the division of the tensile force into the embedded and the externally bonded FRP reinforcement. For design purposes, the shear-slip behavior may be simplified and modeled according to various degrees of complexity.

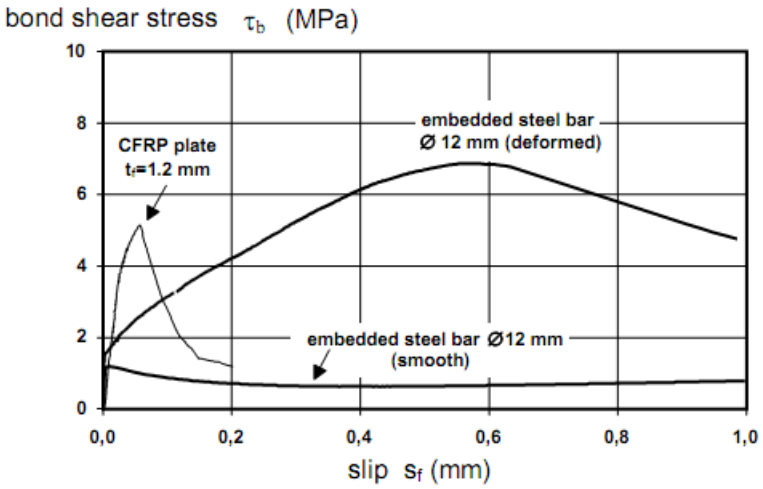

Figure 2-11: Shear stress - slip relations for different types of reinforcement (FIB 14)

Chapter Three
Experimental Design

3.1 Material Properties

3.1.1 Concrete

3.1.1.1 Cement: Pozzolana Portland cement(PPC) that meets the requirement of Ethiopian national standard EN1177-1:2005 with a specific gravity of 3.15 gm/cc is used.

3.1.1.2 Fine and Coarse aggregates: In order to investigate their properties for the required application, different tests were carried out which includes:

- silt content
- sieve analysis
- specific gravity and absorption capacity
- moisture content
- unit weight

Sieve Analysis and fineness modulus for sand

Locally available sand was purchased and the sieve analysis was done on a quartered 500 gm sand sample according to ASTM recommendation.

Sieve Size (mm)	Cumulative Coarser (%)	Percentage Passing (%)	% Pass According to ASTM
9.5	0.000	100.000	100
4.75	4.082	95.918	95-100
2.36	16.327	83.673	80-100
1.18	38.776	61.224	50-85
0.6	71.429	28.571	25-60
0.3	92.857	7.143	10-30
0.15	96.939	3.061	2-10
pan	100.000	0.000	
The fineness modulus is 3.204			

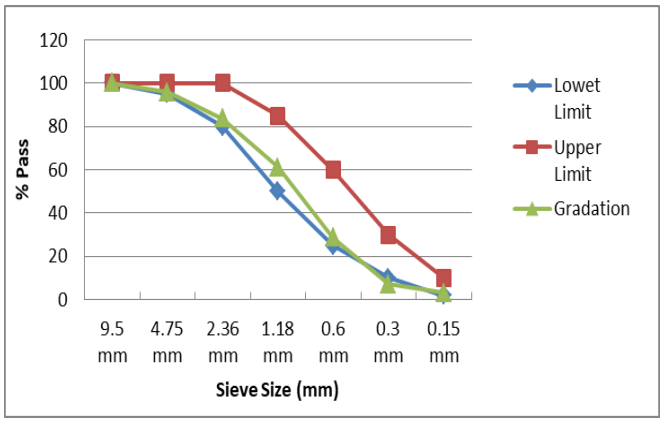

Table 3-1: Sieve analysis and gradation for sand

The coarse aggregate used for the experiment had a gap graded gradation and it was blended with finer, 01 aggregates, to yield the following result. The nominal aggregate size is set as 19.5 mm which is recommended to beam by ACI.

Tests on silt content, specific gravity, Unit weight and moisture content were made according to AAiT laboratory manual, ASTM C138, C127, C128 and C70 respectively. Test results are summarized in the table below.

Sieve Size (mm)	Cumulative Coarser (%)	Cumulative Passing (%)	% Pass According to ASTM
37.5 mm	0.000	100.000	100
25.5 mm	0.000	100.000	100
19.5 mm	1.158	98.842	95-100
12.5 mm	39.575	60.425	
9.5 mm	73.842	26.158	25-55
4.75 mm	95.849	4.151	0-10
FM=	2.104		

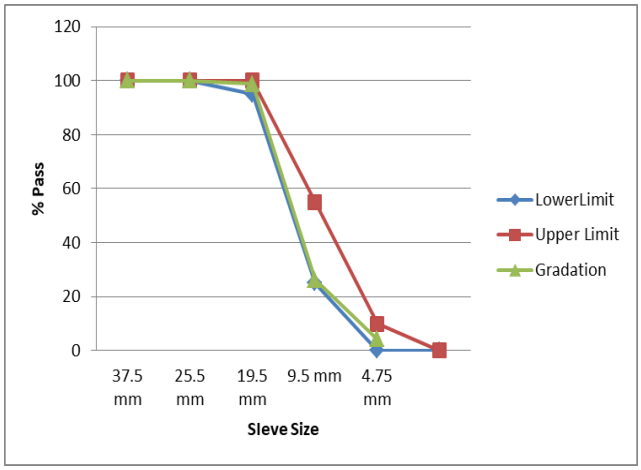

Table 3-2: Sieve analysis of and gradation for coarse aggregates

No	Test Description		Sand	Coarse Aggregate
1	Silt Content		3.14%	-
2	Absorption Capacity		3.76%	-
3	Specific gravity	Bulk	1.722	2.488
		Bulk(SSD)	1.93	2.605
4	fineness modulus		3.204	2.104
5	Unit Weight		1243.23 kg/m^3	1450.94 kg/m^3
6	Moisture Content		9.89%	0.61%

Table 3-3: Summarized results of aggregate tests

With the materials listed above and based on the recommendation of ACI 211. 4R-08, the following mix ratios based on weights are prepared with three different water to cement ratios.

Mix Design-1

W/C= 0.4
Slump= 62 mm
Water= 132 kg/m^3 Sand=688 kg/m^3
Coarse aggregate=1104 kg/m^3
Cement=336 kg/m^3 =>1:2.05:3.28 (Cement: Sand: Coarse Aggregate)

Mix Design-2

W/C= 0.43
Slump= 66 mm
Water= 145 kg/m^3

Sand=688 kg/m^3
Coarse aggregate=1104 kg/m^3
Cement=336 kg/m^3 =>1:2.05:3.28 (Cement: Sand: Coarse Aggregate)

Mix Design-3

W/C= 0.47
Slump= 77 mm
Water= 160 kg/m^3
Sand=688 kg/m^3
Coarse aggregate=1104 kg/m^3
Cement=336 kg/m^3 =>1:2.05:3.28 (Cement: Sand: Coarse Aggregate)

3.1.1.3 Test Specimen and Mean Compressive strength

Twelve beams with the same cross section and length are casted for this study. The beams are grouped in to three based on their concrete compressive strength and for each group a control RC beam is set. Beams within 3 MPa range of the control beam's cylindrical compressive strength are compared with that control beam. All of the beams are reinforced with two 8mm diameter top bars and two 10mm diameter bottom bars with 17 web reinforcement 8mm diameter bars aligned at 100 mm spacing.

Strengthened beams are bonded with CFRP at the soffit. The end-U wrap anchored beams additionally have a 100 mm wide wrap of same CFRP sheet throughout the side face of the beam near the support as indicated in figure 3-3. The same SIKA product Carbodur E1014 CFRP sheet is used for all strengthening with 1 layer. The detailed schematic diagram is given in figure 3-3.

Spec.	Type Of strengthening	Age at Test (Days)	f_{cu} (N/mm^2)	ρ_s (%)
BC1	Unstrengthened	34	33.52	0.7
BF1	EBR Strengthened		29.73	
BF2.	EBR Strengthened		33.52	
BC2	Unstrengthened		27.14	
BF3	EBR Strengthened		27.14	
BF4	EBR Stren.+End Slit Anchor		27.14	
BC3	Unstrengthened		21.49	
BF5	EBR Strengthened		21.49	
BF6	EBR Stren +End wrap Anchor		21.49	
BF7	Strengthened		23.05	
BF8.	EBR Stren. + End wrap Anchor		23.05	
BF9.	EBR Stren. +End Slit Anchor		23.05	

Table 3-4: Test beams detailed section and loading

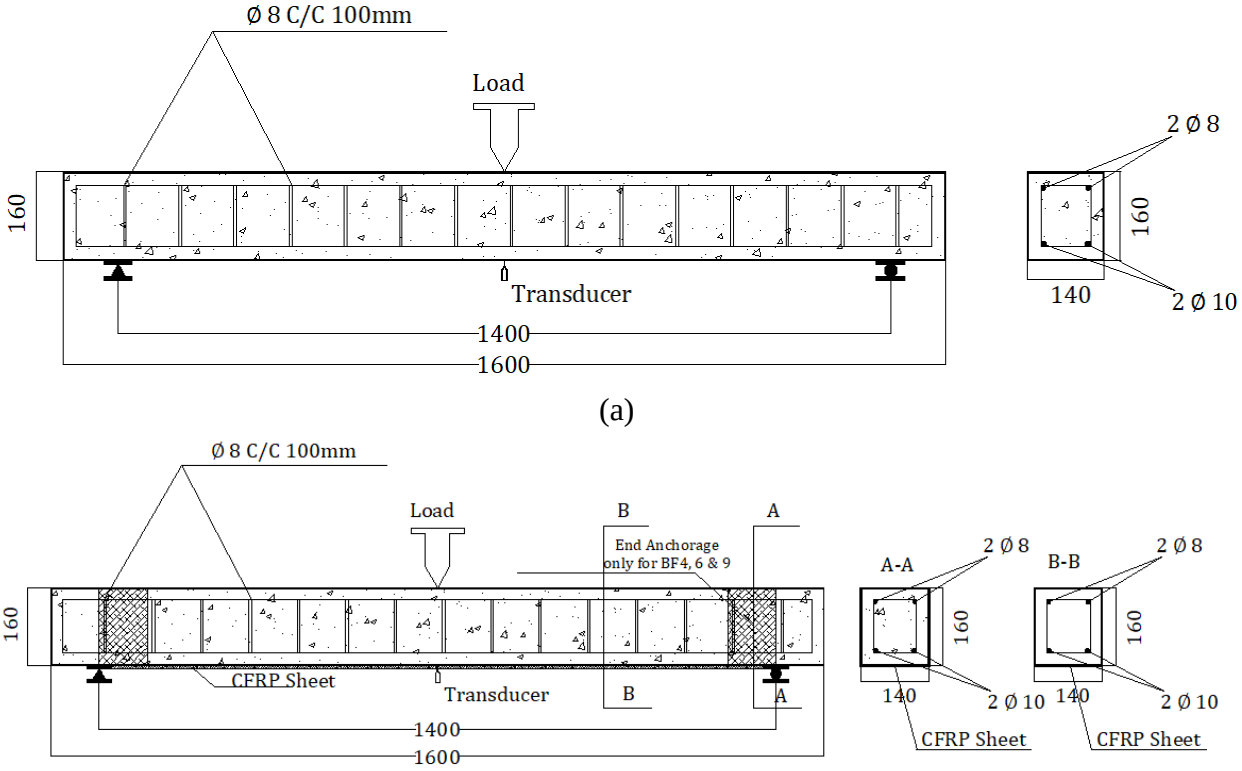

Figure 3-1: Schematic diagram of control and strengthened beams
(a) Control beams BC1, BC2 and BC3 (b) Strengthened beams

End slit anchored beam have the same arrangement with end wrap anchored beam with the CFRP sheet inserted in the beam slit created near the support at the soffit part of the beam. More information about this type of anchorage is provided in chapter five.

3.1.2 Reinforcement steel and CFRP

The properties of the reinforcement steel are obtained from a tensile strength test in the laboratory and that of the Carbodur E-1014 CFRP sheet are found from the manufacturer website.

Type	Dimension (mm)	Yield Strength (N/mm^2)	Tensile Strength (N/mm^2)	Ultimate Strain (%)	E-modulus (N/mm^2)
Rebar S500	Φ 10	545.37	632.38	24	200000
Rebar S400	Φ 8	445.63	592.85	30	200000
Carbodur E-1014	100×1.4(1)	-	2200	1.22	180000

(1) Global Dimension

Table 3-5: Properties of Reinforcement steel and Carbodur E1014

3.2 Specimen Preparation and Test Procedure

The beams were cured for 15 days after casting and left thereafter in an open door area to be replenished by the rain which was falling continuously during the time. No formwork of the beam was removed before 7 days of the test except the side formworks which were removed 24 hours after casting. The beams were tested by one point loading as shown in figure 3-3 the deflection was measured at mid span by electronic potentiometer displacement transducer. The load was also applied at mid span by hydraulic jack of 300 KN capacity. And the results are recorded by a data logger connected to a load cell and the transducer.

Figure 3-2: Beam loading set-up

Figure 3-3: Data Logger

Chapter Four
Initial validation Model

4.1 Validation of the Control (RC) Beam

4.1.1 Material Definitions

Material definition is the first task of every simulation work. It significantly affects the accuracy of the final result. The material library in Abaqus allows most engineering materials to be modeled, including metals, plastics, rubbers, foams, composites, granular soils, rocks, and plain and reinforced concrete. But when none of the existing material models included in the ABAQUS material library accurately represents the behavior of the material to be modeled, the user can also write an algorithm that defines the material constitutive equations and feed the software through UMAT or VUMAT subroutine of the software.

4.1.1.1. Concrete

Concrete by itself is a composite material. It is made of cement, mortar, and aggregates. The thermo-chemical interaction between these constituents results in a unique building material. One of the most important characteristics of concrete is low tensile strength, which results in tensile cracking at a very low stress compared with compressive stresses. The tensile cracking reduces the stiffness of the concrete component.

Several issues in the current practice of constitutive modeling of concrete material need to be addressed. First, concrete is a non-homogeneous and anisotropic material, the mechanical behavior of which is nonlinear (Kupfer, 1969). Its compressive strength increases as it is loaded in a biaxial compressive state, but decreases as the tensile stress is increased under biaxial compression–tension. Moreover, the ductility of concrete under biaxial stresses is also dependent on the stress state.

Concrete exhibits a large number of micro-cracks, especially at the interface between coarser aggregates and mortar, even before the application of any external loads. The presence of these micro-cracks has a great effect on the mechanical behavior of concrete, since their propagation (concrete damage) during loading contributes to the nonlinear behavior at low stress levels and causes volume expansion near failure. Many of these micro-cracks are initially caused by segregation, shrinkage or thermal expansion of the mortar. Some micro-cracks may develop during loading because of the difference in stiffness between aggregates and mortar. Since the aggregate mortar interface has a significantly lower tensile strength than the mortar; it constitutes the weakest link in the composite system. This is the primary reason for the low tensile strength of concrete.

Before yielding has occurred concrete elasticity is defined simply isotropic. The isotropic elasticity defines the slope of the stress/strain curve in both tension and compression until the plastic limit is reached. Other general parameters of concrete used in this model include poison's

ratio and density. The density of normal weight concrete is approximately 2400 kg/m^3 While the corresponding poison's ratio of concrete is 0.2 (MacGregor and White, 2009).

Case specific modulus of elasticity of concrete is read from the new Ethiopian building code (EBCS EN 1992-1-1:2013) table 3.1. The table recommends using the following empirical formula to relate the mean cylindrical compressive strength (f_{cm}) of concrete with the secant elastic modulus (E_{cm}).

$$E_{cm} = 22[\frac{f_{cm}}{10}]^{0.3}, \text{ } f_{cm} \text{ in MPa.} \qquad (4.1)$$

The failure behavior of concrete is governed by complex degradation processes starting within the aggregate-matrix interface. These processes are shown in figure 4-1. The aggregate-matrix interface contains micro-cracks that exist even before any load is applied to concrete (Figure 4-1.a). The formation of these micro-cracks is primarily due to stress and strain concentrations resulting from the incompatibility of the elastic moduli of the aggregate and cement paste components. Strain concentrations at the aggregate-mortar interface may also occur as a result of volume changes in the concrete due to shrinkage and/or thermal effects resulting from the difference in thermal coefficients of various constituents.

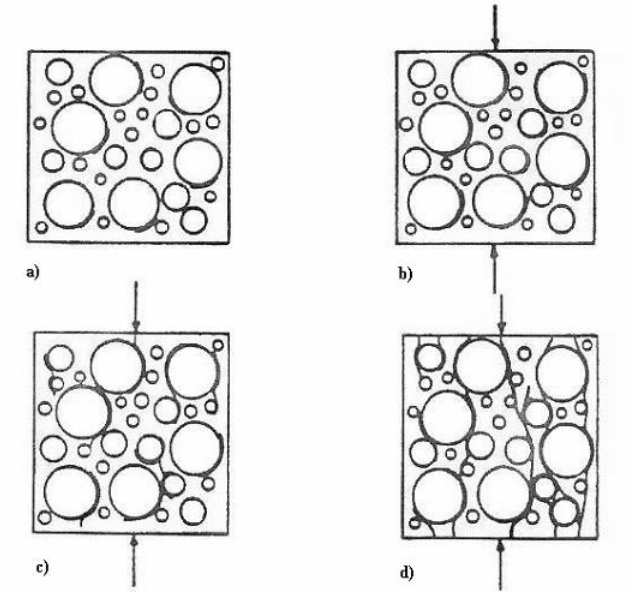

Figure 4-1: Aggregate-matrix interface: a) prior to loading, b) 65% of ultimate load, c) 85% of ultimate load, d) failure load (ZIad Taqqiedin, 2008)

It is observed that under different magnitudes of the applied load, the concrete behavior can be summarized in four stages shown in Figure 4-2. The first stage is observed during 30-60% of the ultimate strength (shown as 45% in Figure 4-2).

In this initial stage, one can observe the highest tensile strain concentration at particular points where new micro-cracks are initiated as shown in Figure 4-1.b. At this load state, localized

cracks are initiated, but they do not propagate (stationary cracks). Hence, the stress-strain behavior is linearly elastic. Therefore, $0.3f_c$ is usually proposed as the limit of elasticity. Beyond this limit, the stress-strain curve begins to deviate from a straight line. Stresses up to 70-90% of the ultimate strength (shown as 85% in Figure 4-1.c) characterize the second stage.

In this stage, as the applied load is progressively increased, the crack system multiplies and propagates as shown in Figure 4-1.c. The increase of the internal damage in concrete, revealed by deviation from the linear elastic behavior, reduces the material stiffness and causes irrecoverable deformation in unloading. Although the relief of strain concentration continues during this stage, void formation causes the rate of increase of the tensile strain in the direction normal to that of branching to increase with respect to the rate of increase of the strain in the direction of branching (Kotsovos and Newman, 1977). The start of such deformation behavior is called "onset of stable fracture propagation" (OSFP). In this load stage, the mortar cracks tend to bridge the aggregate-matrix bond cracks.

A third stage shown in Figure 4-2 extends up to the ultimate strength. Interface micro-cracks are linked to each other by mortar cracks as shown in Figure 4-1.c, and void formation (dilation) begins to have its effect on deformation at this stage. The start of this stage is called "onset of unstable fracture propagation" (OUFP). This level is easily defined since it coincides with the level at which the overall volume of the material becomes a minimum. In this stage, the progressive failure of concrete is primarily caused by cracks through the mortar. These cracks merge with bond cracks at the surface of nearby aggregates and form crack zones of internal damage. Following that, a smoothly varying deformation pattern may change and further deformation may be localized.

A fourth stage defines the region beyond the ultimate strength. In this region, the energy released by the propagation of a crack is greater than the energy needed for propagation. Therefore, the cracks become unstable and self-propagating until complete disruption and failure occurs. In this stage, the major cracks form parallel to the direction of the applied load, causing failure of the concrete. The volume of voids increases dramatically causing a rapid dilation of the overall volume of concrete as shown in Figure 4-1.d.

All the above mentioned stages are for the uniaxial compression case. Stages I, (II and III), and IV could be categorized into the linear elastic, inelastic, and the localized stages respectively. Understanding these stages is crucial for the development of any concrete model.

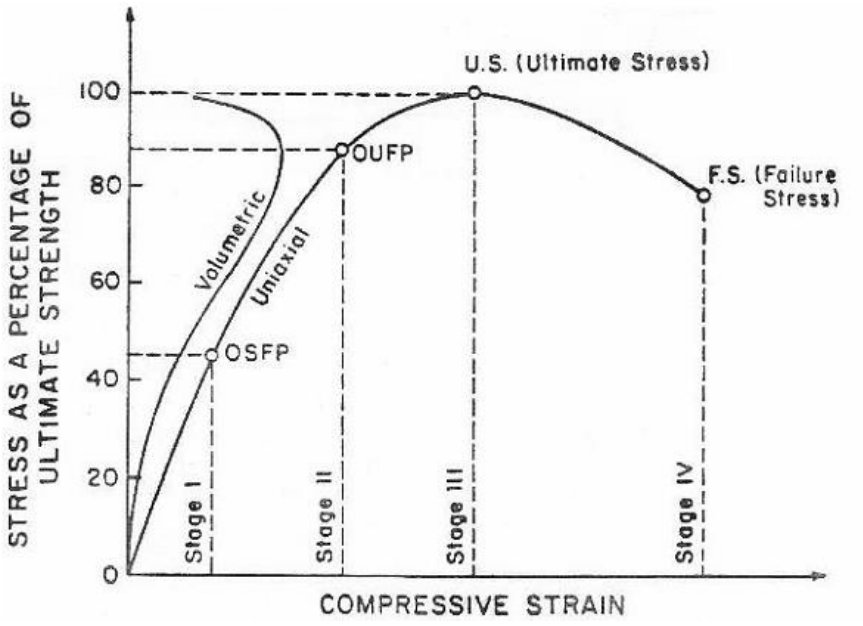

Figure 4-2: Uniaxial compression stress-strain relation of concrete (ZIad Taqquidin, 2008)

Figure 4-3 shows a typical uniaxial tension stress-elongation curve. In general the limit of elasticity is observed to be about 60-80% of the ultimate tensile strength. Above this level, the aggregate-matrix interface micro-cracks start to grow. As the uniaxial tension state of stress tends to arrest the cracks much less frequently than the compressive stage of stress, one can expect the interval of stable crack propagation to be quite short, and the unstable crack propagation to occur much earlier. That is why the deformation behavior of concrete in tension is quite brittle in nature. In addition, the aggregate-matrix interface has a significantly lower tensile strength than the matrix, which is the primary reason for the low tensile strength of concrete.

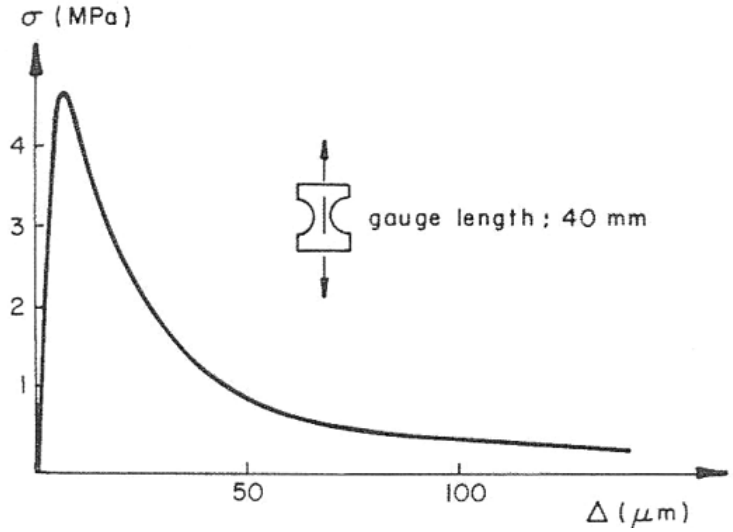

Figure 4-3: Uniaxial tensile stress-strain curve (ZIad Taqquidin, 2008)

Cracking models define concrete property after yielding. This finite element model (FEM) will focus on the cracking behavior of concrete. Current methods of finite element modeling for reinforced concrete are separated in to two general categories. The first category of concrete modeling uses a lumped parameter model which smears cracking over an effective mesh area, also known as smeared cracking model. The second category modeling takes in to account the time dependent damage of the concrete and is also known as the concrete damage plasticity model. These models will be discussed further in this section. (Joshua S. Tyau, 2009)
These general cracking models have been generally calibrated typically using loading cases, such as beam load test and column load tests typically modeled with 2-dimensional elements.

4.1.1.1.1 Smeared cracking Model (Simulia, 2009)

The concrete smeared cracking model efficiently reduces stiffness properties of the concrete over an area that has exceeded tensile yield stress. This smeared model does not track individual cracks but distributes the effect of these cracks. Constitutive calculations are performed independently at each integration point of the finite element model. The presence of cracks enters into these calculations by the way in which the cracks affect the stress and material stiffness associated with the integration point.
This model is most efficiently used for use with concrete shell elements where reinforcement is typically defined in layers. The smeared cracking model does not take in to account compression damage, but ultimate compression yields stress may be specified in the elastic properties. The smeared cracking model is not used for this model.

4.1.1.1.2 Concrete Damage Plasticity (Simulia, 2009)

The term damage mechanics has been conventionally used to refer to models that are characterized by a loss of stiffness or a reduction of the secant constitutive modulus. Plasticity by itself fails to address the softening behavior of concrete under tension and compression caused by damage propagation due to micro-cracking in the material. On the other hand, damage mechanics is concerned with the description of this progressive weakening of solids due to the development of micro-cracks and micro-voids. Damage theory in concrete materials can therefore represent the post-peak region.
Concrete damage can be characterized as a reduction in the material stiffness. Stiffness reduction in tensile loading is less than that under compressive loading and therefore, more damage occurs in tension than in compression. Thus, the characterization of material damage in tension and in compression should be considered when modeling the response of plain concrete, justifying the use of multiple damage variables.
In a simple plasticity model after yielding has occurred, if force is removed, the residual plastic strain is found by a rebound function of the modulus of elasticity. Damage parameters of the CDP model modify this rebound function to include damage effects as shown in figure 4-3. The CDP model also accounts for cyclic loading effects where a recovery factor can be specified to account for the amount of total inverse loading strength available after damage has occurred.

The effects of these damage parameters change the inherent constitutive equations that are used to define the material properties each of individual element. As these constitutive equations change, the element affected will in essence behave as a different material from concrete element that has not yielded.

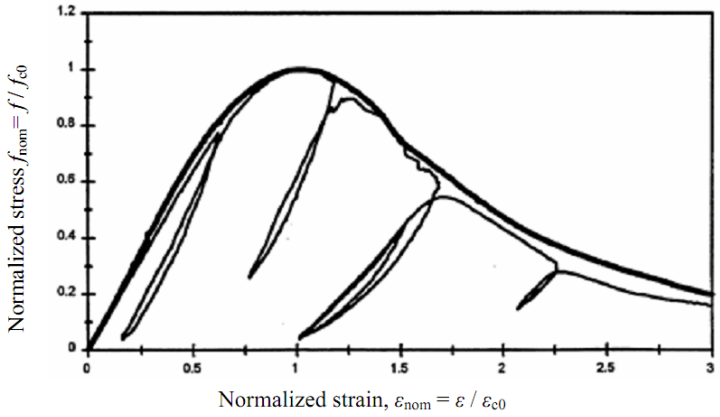

(a)

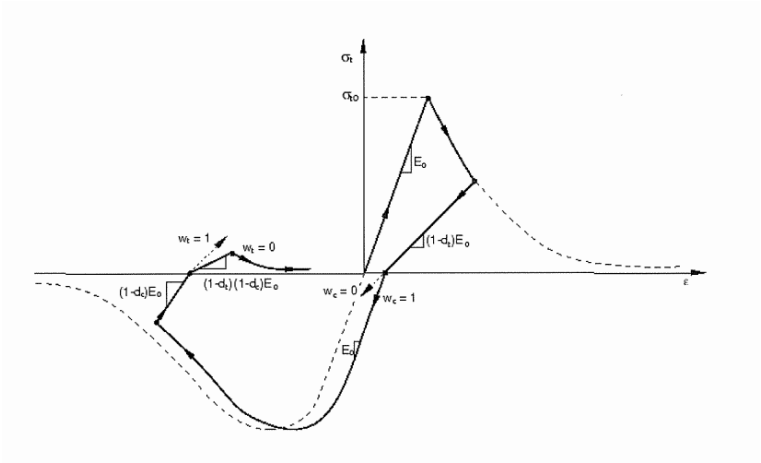

(b)

Figure 4-4: Concrete Response to different loading scheme (a): Concrete response to monotonic and cyclic compression load (data from Bahn and Hsu, 1998) (b): Concrete damage plasticity damage parameters (ZIad Taqquidin, 2008)

The variables in figure 4-3.a are defined as follow:

- E_o= Concrete Modulus of Elasticity
- d_c= Compression damage parameter
- d_t= Tension damage parameter
    - Damage parameters must range between 0<d<1 to avoid instability from rebound slopes
- W_c= Compression recovery factor
- W_t= Tension recovery factor, ε= Strain, σ= Stress

Typical values for compression recovery range from 0.85-0.99 while for tension typical values range from 0.01-0.1. These typical values show that the compression cycle following tension

cycle will retain a significant fraction of total compressive strength. This can be physically observed as cracks in the concrete close retaining compressive resistance. In contrast, a tension cycle following an extreme compression cycle where high compression damage has occurred would retain only a small portion of the ultimate tensile strength.

Constitutive Equations for CDP (Milad Hafezolghorani and Farzad Hejaz, 2007)

The isotropic damaged elasticity and the isotropic tensile and compressive plasticity were used in the concrete damaged plasticity model to study the behavior of concrete in a non-elastic manner. The total strain tensor ε was comprised of the elastic part ε_{el} and the plastic part ε_{pl}.

1) $\varepsilon = \varepsilon^{el} + \varepsilon^{pl}$ *(4.2)*

2) $\sigma = D^{el} : (\varepsilon - \varepsilon^{pl})$ *(4.3)*

3) $\bar{\sigma} = D_o^{el} : (\varepsilon - \varepsilon^{pl})$ *(4.4)*

4) $D^{el} = (1-d)\, D_o^{el}$ *(4.5)*

The nominal stress with the degraded elastic tensor from (4) could be rewritten as follows:

5) $\sigma = (1-d)\, D_o^{el} : (\varepsilon - \varepsilon^{pl})$ *(4.6)*

The damage plasticity constitutive model was based on the following stress–strain relationship:

6) $\sigma = (1-d).\bar{\sigma} \rightarrow \sigma = (1-d_t)\bar{\sigma}_t + (1-d_c)\bar{\sigma}_c$ *(4.7)*

, where d_t and d_c were two scalar damage variables, ranging from 0 (undamaged) to 1 (fully damaged). The damage model used for concrete was based on plasticity and considered the failure process of tensile cracking and compressive crushing. Isotropic hardening variables were expressed by inelastic compression strain $\varepsilon_c^{in,\ h}$ and cracking strain $\varepsilon_t^{ck,\ h}$, which include the plastic hardening strain $\varepsilon^{pl,h}$ plus the residual strain due to damages.

7) $\varepsilon^{pl,h} = \begin{bmatrix} \mathcal{E}_t^{pl,h} \\ \mathcal{E}_c^{pl,h} \end{bmatrix}$; $\dot{\varepsilon}^{pl} = h(\varepsilon^{pl,h}, \bar{\sigma}).\ \dot{\varepsilon}^{pl}$,

$\dot{\varepsilon} = \dot{\varepsilon}^{el} + \dot{\varepsilon}^{pl}$ *(4.8)*

Hardening variables were used to control the development of the yield or failure of the surface. These variables were connected to the processes of tension and compression loading. The behavior of the concrete was explained by the assumption that concrete damage plasticity utilized the yield function, $f(\varepsilon^{pl,h}, \bar{\sigma})$, which represented the yield surface in effective stress space to determine the states of damage or failure.

Figure 4-4 indicated that the uniaxial compressive and tensile response of concrete was assumed to be influenced by damaged plasticity, and this assumption formed the basis of the model. The uniaxial compressive and tensile responses of concrete with respect to the concrete damage plasticity model subjected to compression and tension load were given by:

9) $\sigma_t = (1-d_t)\, E_o\, (\varepsilon_t - \mathcal{E}_t^{pl,h})$ *(4.9)*

10) $\sigma_c = (1-d_c)\, E_o\, (\varepsilon_c - \mathcal{E}_c^{pl,h})$ *(4.10)*

Given the nominal uniaxial stress, the effective uniaxial stress $\bar{\sigma}_t$ and $\bar{\sigma}_c$ were derived as follows;

11) $\bar{\sigma}_t = \frac{\sigma_t}{1-d_t} = E_o\,(\varepsilon_t - \varepsilon_t^{pl,h})$ *(4.11)*

12) $\bar{\sigma}_c = \frac{\sigma_c}{1-d_c} = E_o\,(\varepsilon_c - \varepsilon_c^{pl,h})$ *(4.12)*

, where compressive strain ε_c equaled $\varepsilon_c^{pl,h} + \varepsilon_c^{el}$ and tensile strain ε_t equaled $\varepsilon_t^{pl,h} + \varepsilon_t^{el}$

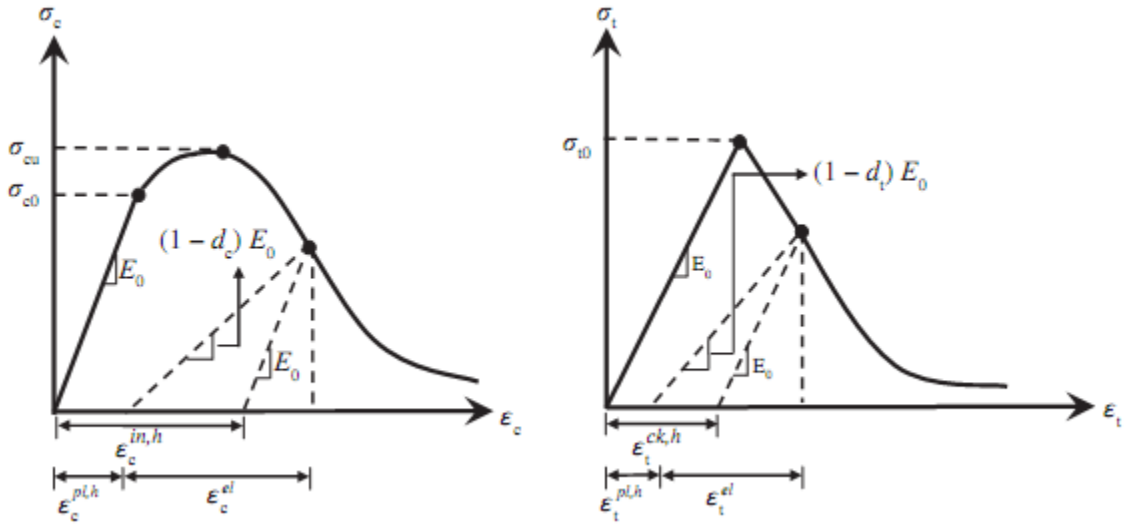

(a) (b)

Figure 4-5: Response of concrete to a uniaxial loading condition: (a) Compression, (b) Tension

Simplified Damage Plasticity Model for Concrete

Generally, uniaxial compressive behavior could be characterized by either experimental tests or existing constitutive models such as the one proposed on EBCS EN 1992-1-1:2013 which is employed as follow:

$$\frac{\sigma_c}{f_{cm}} = \frac{k\eta - \eta^2}{1 + (k-2)\eta} \qquad (4.13)$$

Where, $\eta = \varepsilon_c/\varepsilon_{c1}$, ε_{c1} is the strain at peak stress. It is taken as 0.002 for the curve fitting.

$K = 1.05\,E_{cm} \times |\varepsilon_{c1}| / f_{cm}$, where E_{cm} and f_{cm} are the secant elastic modulus and the mean compressive strength of the concrete respectively. Equation (4-13) assumed a nonlinear behavior for concrete from the beginning to the end. However, defining the behavior of concrete up to 40% of its strength in the elastic phase was important in determining the effective elastic modulus. In other words, the constitutive model came into effect when the compressive strength was 60% of the concrete compressive strength. The softening phase, the post peak region, continued until 10 % of the unconfined cylinder compressive strength was reached.

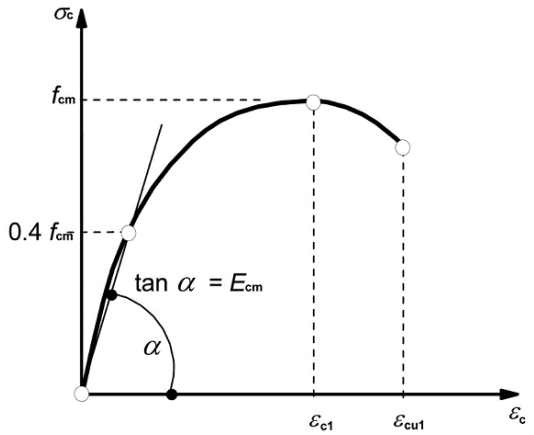

Figure 4-6: Schematic representative of the stress-strain relation of concrete

According to Figures 4-5.a and b, inelastic hardening strain in compression $\varepsilon_c^{in,h}$, was derived as follows:

$$\varepsilon_c^{in,h} = \varepsilon_c - \frac{\sigma_c}{E_o} \qquad (4.14)$$

Compression damage (dc) was based on inelastic hardening strain in compression $\varepsilon_c^{in,h}$ that controlled the unloading curve slope. Given that dc increased with respect to an increase in $\varepsilon_c^{in,h}$, it could be expressed as follows:

$$d_c = 1 - \frac{\sigma_c}{f_{cm}} \qquad (4.15)$$

The tangent of the curve decreased with respect to the initial tangent (modulus of elasticity, E_0) due to the damage when plastic strains increased in brittle materials (such as concrete and concrete-like material) as shown in figure 4-5.a. The damage parameter (d_c) was 0 at the maximum compressive stress, and thereafter, it began to decrease and continued decreasing until 0.9 was reached with respect to 10% remaining strength in large strains.

In addition to these basic parameters that identify stress/strain relationships, parameters based up on the micro structure of concrete must also be identified. For the purpose of this finite element model, these parameters include dilation angle ψ, flow potential eccentricity m, initial biaxial/uniaxial ratio σ_{co}/σ_{bo}, the ratio of the second invariant on tensile meridian K_c, and viscosity parameter μ. The dilation angle was equal to volume strain over shear strain. The dilation angle for concrete was usually 20 to 40, which affected material ductility.

Consequently, the dilation angle had considerable effects on the entire model. An increase in the dilation angle increased the system flexibility. From a practical viewpoint, the internal dilation angle depended on certain parameters, including plastic strain and confined pressure. An increase in plastic strain and confined pressure decreased the internal dilation angle. The material has a constant dilation angle for a large range of pressure stresses used for the confinement of the material.

The default flow potential eccentricity was ε = 0.1, and by raising the value of, the curvature of the flow potential increased. If the default flow of potential eccentricity had a value much lower

than the default value, there could be convergence problems when the confining pressure is not high. The ratio of initial equi-biaxial compressive yield stress to initial uniaxial compressive yield stress was given by f_{bo}/f_{co}, and its default value was 1.16 (Simulia, 2009). The Abaqus software used a null default viscosity parameter so that the visco-plastic regularization did not occur.

These parameters are related to yield surface of individual finite concrete elements. As previously mentioned, concrete has different yield stresses in compression and tension; in essence a yield surface attempts to envelope these stresses in order to create an interaction relationship. As simple concrete yield surface in plane stress is shown in the figure 4-7.

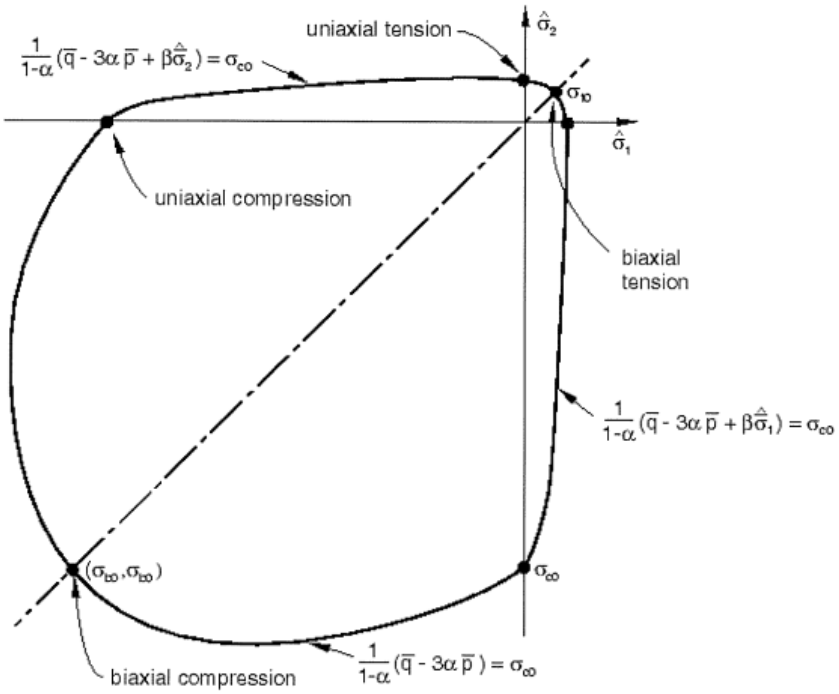

Figure 4-7: Concrete yield surface in plane stress

The CDP and Plasticity parameters for one of the concrete strengths found in the expermentation are given in the table below. These parameters for the rest of concrete grades are presented in Appendix A.

Material parameter	f_{cu}= 33.54 Mpa	Plasticity Parameter	
		Dilation angle	31
		Eccentricity	0.1
Concrete Elasticity		f_{b0}/f_{co}	1.16
E (GPa)	29.571	K	0.666
N (Poisson Ratio)	0.2	Viscosity	0
Concrete Compressive Behavior		Concrete Compressive Damage	

Stress (MPa)	Inelastic Strain	Damage Parameter (d_c)	Inelastic Strain
10.72	0	0.00	0
19.23	0.000141975	0.00	0.000141975
24.29	0.000407606	0.00	0.000407606
26.56	0.00077382	0.00	0.00077382
26.52	0.001222947	0.00	0.001222947
24.55	0.001741229	0.08	0.001741229
20.97	0.00231779	0.21	0.00231779
16.00	0.002943923	0.40	0.002943923
9.85	0.003612572	0.63	0.003612572
2.68	0.00431796	0.90	0.00431796

Table 4-1: Material properties for concrete with CDP model

Uniaxial Tensile Behavior

In concrete damage plasticity models, the plastic hardening strain in tension $\varepsilon_t^{pl,h}$ was derived (see figure 4-5.b) as follows;

$$\sigma_t = (1-d_t)\, E_o\, (\varepsilon_t - \varepsilon_t^{pl,h}) \qquad (4.16)$$

$$\varepsilon_t^{cr,h} = \varepsilon_t - \frac{\sigma_t}{E_o} \qquad (4.17)$$

$$\varepsilon_t^{pl,h} = \varepsilon_t - \frac{\sigma_t}{E_o}\left(\frac{1}{1-d_t}\right) \qquad (4.18)$$

$$\varepsilon_t^{pl,h} = \varepsilon_t^{cr,h} - \frac{d_t}{1-d_t}\left(\frac{\sigma_t}{E_o}\right) \qquad (4.19)$$

Although concrete had many constitutive models in the tension phase, there is no significant difference in the result due to the brittle behavior of concrete. Engineers seldom define the tension behavior of concrete in numerical modeling. This is mainly because the interaction between reinforcement and concrete is simplified and because certain changes in the stress strain relation of concrete in the tension phase must be made to consider bar slips in concrete.

The tensile strength of concrete is directly read from ES-EN-1992, table 3.1. In this paper, 1% of the tensile strength was considered during the analysis regardless of the realistic condition to prevent numerical instability. In contrast, correspondence strain value, where stress is 1% of the ultimate tensile strength, was taken as 10 times the percentage of the strain, in which stress was equal to ultimate tensile strength. The tension CDP parameter for the concrete illustrated in the table 4-1 is presented in the following table 4-2.

Concrete tensile behavior		Concrete tension damage	
Yield Stress (MPa)	Cracking Strain	Damage parameter (d_t)	Cracking Strain
2.6	0	0	0
0.026	0.00087924	.99	0.00087924

Table 4-2- Simplified Tension CDP Parameters of concrete

According to the aforementioned damage plasticity formulation derived in this section, five different concrete grades are defined and the results are presented in Appendix A. The general framework of the damage plasticity formulation was clearly stated and could be extended to other concrete grades.

4.1.1.2. Steel Reinforcement

Reinforcement comes in different types and shapes. Those most commonly used are the deformed circular cross-sectional bars. The spiral deformation pattern on the bars strengthens the mechanical bond between the bars and concrete. The properties of reinforcing steel, unlike concrete, are generally not dependent on environmental conditions or time. Thus, the specification of a single stress-strain relation is sufficient to define the material properties needed in the analysis of RC structures.

Typical stress-strain curves for reinforcing steel bars used in concrete construction are obtained from coupon tests of bars loaded monotonically in tension. For all practical purposes steel exhibits the same stress-strain curve in compression as in tension. The steel stress-strain relation exhibits an initial linear elastic portion, a yield plateau, a strain hardening range in which stress again increases with strain and, finally, a range in which the stress drops off until fracture occurs. The extent of the yield plateau is a function of the tensile strength of steel.

Two different idealizations, shown in figure 4-8.a, are commonly used depending on the desired level of accuracy (ASCE 1982). The first idealization neglects the strength increase due to strain hardening and the reinforcing steel is modeled as a linear elastic, perfectly plastic material, as shown in figure 4-8.a. This assumption underlies the design equations of the ACI code. If the strain at the onset of strain hardening is much larger than the yield strain, this approximation yields very satisfactory results. This is the case for low-carbon steels with low yield strength.

If the steel hardens soon after the onset of yielding, this approximation underestimates the steel stress at high strains. In several instances it is necessary to evaluate the steel stress at strains higher than yield to more accurately assess the strength of member's at large deformations.

Therefore, the stress-strain idealization will take the form of the second type as shown in figure 4-8.b. The parameters of these models are the stress and strain at the onset of yielding, the strain at the onset of strain hardening and the stress and strain at ultimate stress.

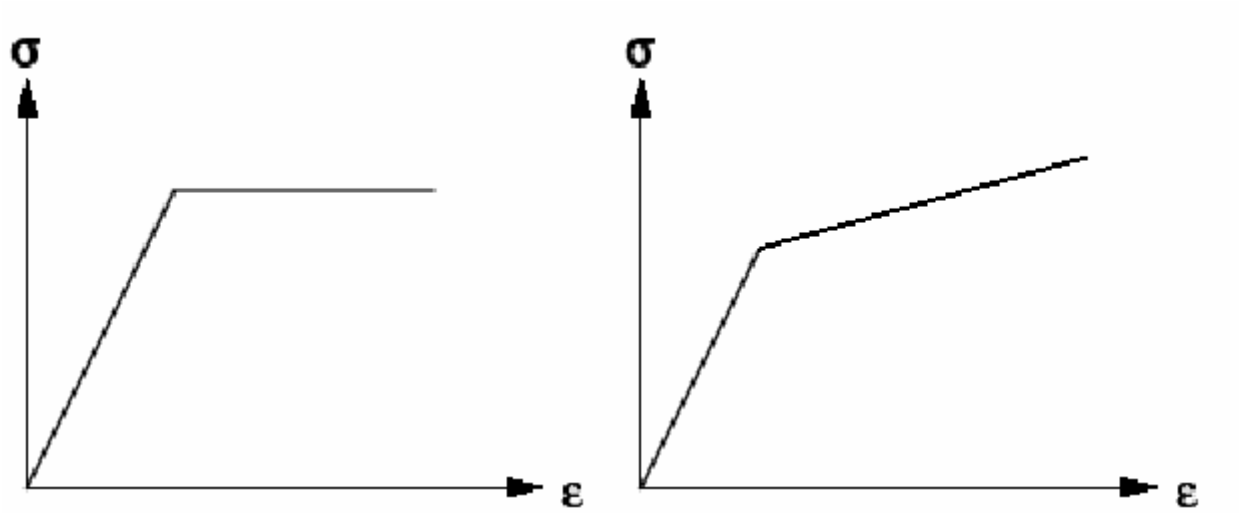

(a) (b)

Figure 4-8: Idealizations of the steel stress-strain curves.

4.1.2 Interaction at Steel – Concrete Interface

Utilization of RC as a structural material is derived from the combination of concrete and reinforcing steel into structural elements. Concrete is strong and relatively durable in compression while reinforcing steel is strong and ductile in tension and in compression.

Maintaining this composite action requires transfer of load between concrete and steel. This load transfer is referred to as bond and is idealized as a continuous stress field that develops in the vicinity of the steel-concrete interface. For RC structures subjected to moderate loading, the bond stress capacity of the system exceeds the demand allowing steel and the surrounding concrete to behave as a unit (full bond). However, further application of external loads results in an increase in the stresses in the interface between concrete and steel. It also results in localized bond demand that exceeds the bond capacity, resulting in the deterioration of that capacity, a localized damage that gradually spreads to the surrounding material, and a significant movement between the reinforcing steel and the surrounding concrete. Therefore, the properties of the interface between concrete and steel is very important in the analysis of RC structures. (Ziad N. Taqieddin, 2008)

Reduction of yielding stress

Reinforcing steel is usually modeled as a linear elastic, linear strain hardening material with a yield stress f_y. However, when reinforcing bars are surrounded by concrete, the average behavior of the stress–strain relation is quite different, as shown in figure 4-9. The most strikingly different feature is the lowering of the yield stress below f_y. Yielding of an RC member occurs when the steel stress at a cracked section reaches the yield strength of the bare bar. However, the average steel stress at a cracked element still maintains an elastic stress that is less than the yield strength, because the concrete matrix located between cracks is still partially capable of resisting tensile forces, owing to the bond between the concrete and the reinforcement. Determination of

element stiffness on the basis of the yielding of steel at a cracked section where a local stress concentration appears in the steel may result in overestimation of the structural response at the post-yielding range.

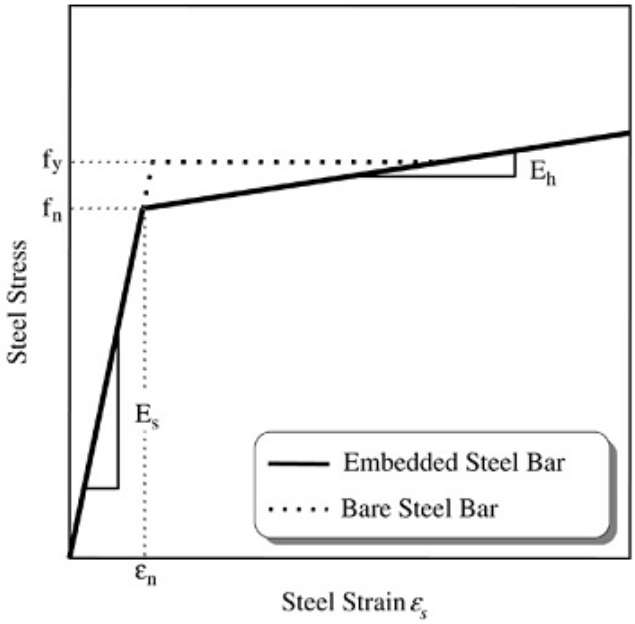

Figure 4-9: Stress–strain relation of steel (Belarbi and Hsu)

Considering these factors, the following linear average stress–strain relation, which was introduced by Belarbi and Hsu from experimental data, is used in this paper to revise the monotonic envelope curve of steel.

$$\sigma_s = E_s.\varepsilon_{s,}\varepsilon_s \le \varepsilon_n \qquad (4.20)$$

$$\sigma_s = f_n + (0.02 + 0.25\beta)E_s(\varepsilon_s - \varepsilon_n), \varepsilon_s \ge \varepsilon_n \qquad (4.21)$$

, where σ_s and ε_s represent the average strain and stress, respectively, and f_y and ε_y are the yield stress and the corresponding yield strain of a bare steel bar, respectively. As shown in Eq. (4.17) the average stress σ_s is a linear function of the parameter β,

$B = \frac{(f_{cr} / f_y)^{1.5}}{\rho}$, where f_{cr} is the tensile strength of the concrete, f_y is the tensile strength of the concrete and ρ is the percentage of the steel ratio and must be greater than 0.5%

$$\varepsilon_n = \varepsilon_y(0.93 - 2B) \qquad (4.22)$$

$$f_n = E.\varepsilon_n \qquad (4.23)$$

In this study the reinforcing steel is modeled as a linear elastic, linear strain hardening material with reduced steel yield stress f_n, as proposed by Belarbi and Hsu. The steel yield stress

reduction is applied only for the bottom reinforcement steel in the tension zone. The accuracy of the steel stress strain model is further evaluated by a beam flexure capacity manual calculation using both reduced and the original yield stress values conducted on the control beams. All control beams have the same cross section and reinforcement provision as shown in the figure 3-3(a), except for the concrete strength as shown in the table 4-3.

Beams	Concrete Compressive strength (f_{cm}), MPa	Mean Concrete tensile strength (f_{ctm}), MPa	Original Yield Stress, MPa		Reduced Yield Stress according to Belarbi and Hsu, MPa
			Phi 8	Phi 10	Phi 10
BC1	26.816	2.15	445.63	545.37	468.231
BC2	21.712	1.7	445.63	545.37	491.1337
BC3	17.192	1.5	445.63	545.37	500.4176

Table 4-3: Control beam specimen concrete strength and reinforcement data

The loading setup was similar to all of the three control beams as shown on figure 3-3(b). The summary of the failure load results of the experiment and manual failure load calculation method by using both reduced and original steel yield stress is presented below in table 4.4. Section analysis of the beams to find failure loads and neutral axis depth is presented in Annex B.

Beams	Failure Load Experiment Result	Failure Load Manual calculation Result, Original steel yield stress		Failure Load Manual calculation Result, Reduced steel yield stress	
	Load, KN	Load, KN	% difference	Load, KN	% difference
BC1	30.01	27.38	-8.76	24.23	-19.26
BC2	29.89	26.37	-11.78	24.19	-19.07
BC3	23.26	25.37	9.07	23.59	1.42

Table 4-4: Failure load result comparison

In the table, the original yield stress resulted better approximation compared to the reduced yield stress for two of the beams. But the reduced yield stress almost perfectly estimated the failure load of the third beam. To clearly decide which value better estimates the experimental result neutral axis depth comparison is made in the table 4-5 below.

Beams	Failure Load Experiment Result	Manual calculation Result, Original steel yield stress		Manual calculation Result, Reduced steel yield stress	
	N.A Depth, mm	N.A Depth, mm	Difference, %	N.A Depth, mm	Difference, %
BC1	27	31.89	18.11	29.8	10.37
BC2	30	35.79	19.30	33.94	13.13
BC3	35	40.71	16.31	38.33	9.51

Table 4-5: The comparison of neutral axis depth calculations

$$\% \text{ difference} = \frac{(Manual\ Calculation\ Result - Expeimetal\ result)}{Expeimetal\ result} \times 100\ \%$$

In table 4-4, the original yield stress gives closer lower bound ultimate failure load values than the reduced yield stress for two of the beam with in a vicinity of 10%, while calculation using the reduced yield stress doubled the error to around 20%. However in one of the beams the reduced yield stress calculation almost perfectly estimated the failure load with a percentage difference of 1.42 % whereas the calculation based on the original yield stress resulted an upper bound value with an error seven times bigger. On the other hand, in the neutral axis depth comparison, shown in table 4-5, closer values are found in the case of reduced yield stress calculation in all of the beams. And all the results are upper bound values with a value greater than the experimental result.

In this simulation work the reduced steel yield stresses proposed by Belarbi and Hsu are used because of the following reasons:

- The tension stiffening effect which is the rationale behind the yield stress reduction is not taken in to account by the CDP model used for the simulation
- A perfect bond between the steel reinforcement and the concrete is modeled in the simulation work which is not the case in reality. Therefore the reduced yield stresses are used to take in to account the capacity reduction caused by bond slip and other related effects

The manual calculation with the reduced yield stress resulted closer results than the one with original for all the neutral axis depth comparisons and a very accurate result for one of the ultimate failure load comparisons.

4.1.3 Simulation Results and Comparisons

According the aforementioned material definitions and interaction properties, the initial RC beam validation simulation model is made for all the three control beams and the result is presented as follow in comparison to the experimental results (see figure 4-11).

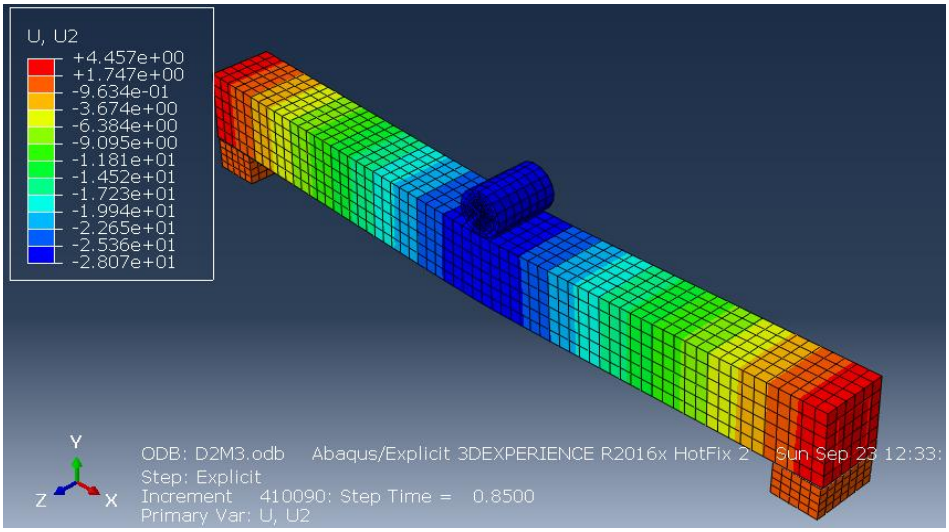

Figure 4-10: Control beam Abaqus model

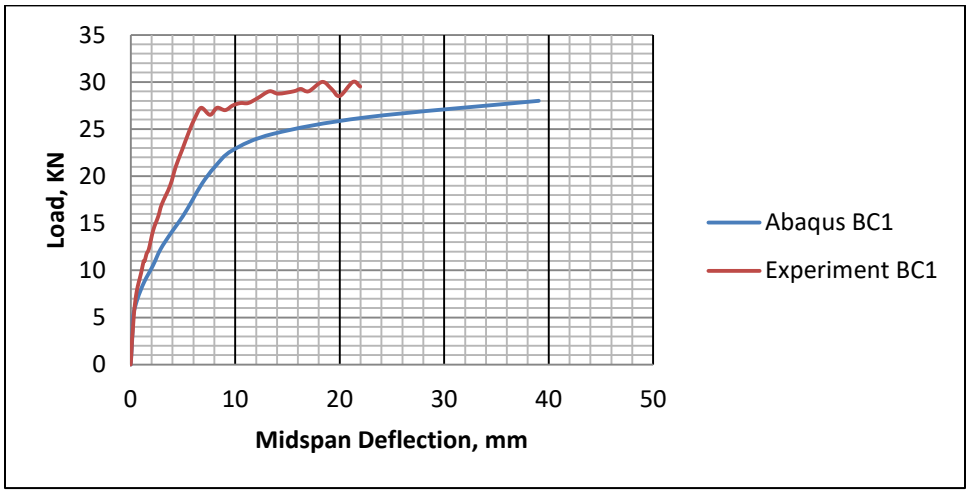

(a)

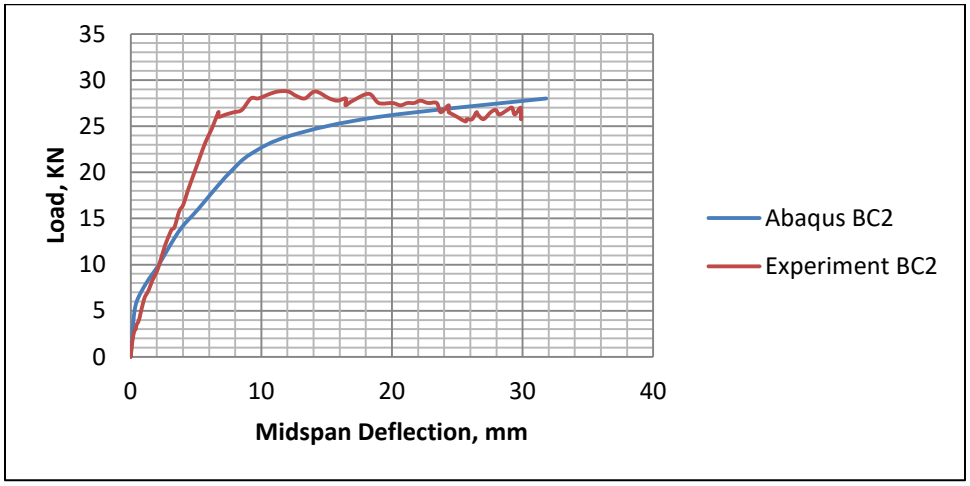

(b)

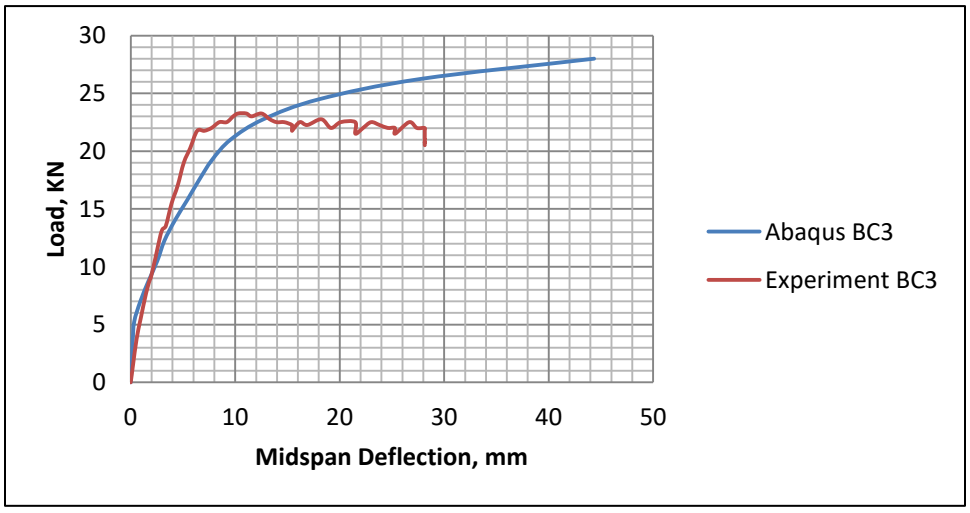

(c)

Figure 4-11: Load deflection diagram (a) BC1 (b) BC2 (c) BC3

As shown on figure 4-11, the simulation model can be taken to represent the experimental results with in an acceptable margin of error. The following section will discuss the validation work for CFRP strengthened beams.

4.2 Validation of the EBR CFRP Strengthened Beam

4.2.1 Material Property

4.2.1.1 Concrete

For this validation work, beams casted by Yasmeen T. Obaidate in Lund University are used. The beams had a rectangular cross-section of 150 mm width and 300 mm height, and were 1960 mm long. The mean compressive strength was determined in compressive tests 28 days after casting of three 300 mm by 150 mm diameter cylinders. The average concrete compressive strength was 29 MPa. The CDP parameters of the concrete are defined on Abaqus as shown in table 4-6 below.

Material parameter	f_{cu}= 33.54 Mpa	Plasticity Parameter	
		Dilation angle	31
		Eccentricity	0.1
Concrete Elasticity		f_{b0}/f_{co}	1.16
E (GPa)	29.571	K	0.666
ν (Poisson Ratio)	0.2	Viscosity	0
Concrete Compressive Behavior		Concrete Compressive Damage	
Stress (MPa)	Inelastic Strain	Damage Parameter (d_c)	Inelastic Strain
11.60	0	0.00	0
20.48	0.000133498	0.00	0.000133498
25.99	0.000384916	0.00	0.000384916
28.62	0.000736336	0.00	0.000736336
28.80	0.001173292	0.00	0.001173292
26.86	0.001683982	0.06	0.001683982
23.09	0.00225868	0.19	0.00225868
17.72	0.002889297	0.38	0.002889297
10.93	0.003569053	0.62	0.003569053
2.90	0.004292221	0.90	0.004292221
Concrete tensile behavior		Concrete tension damage	
Yield Stress (MPa)	Cracking Strain	Damage parameter (d_t)	Cracking Strain
2.3	0	0	0
0.023	0.000759601	0.99	0.000759601

Table 4-6: CDP and Plasticity parameters of the concrete

4.2.1.2 Reinforcement Steel

The reinforcement steel is modeled as an elastic linear plastic hardening material. The steel yield stress of the bottom reinforcements (Φ12) are reduced according to the recommendation of Belarbi and Hsu to account for the tension stiffening effect. Details of the material properties for the reinforcing steel are given in table 4-7.

Nominal Diameter (mm)	Elastic Modulus (GPa)	Yield Stress (MPa)	Reduced Yield Stress (MPa)	Ultimate Stress (MPa)	Ultimate Strain
8	209	490	-	600	0.15
10	211	520	-	741	0.151
12	207	495	397.97	760	0.167

Table 4-7: Mechanical properties of steel bars.

The beams were designed to have insufficient flexural strength to obtain a pure flexural failure. They had tension reinforcement (2Φ12mm), compression reinforcement (2Φ10) and the steel bars were tied together with 8 mm stirrups c/c 100 mm along the beam. In all the beams, the clear concrete cover to the main flexural reinforcement was set to 25 mm. This cover was expected to avoid splitting bond failure. Geometry and reinforcement are shown in figure 4-12.

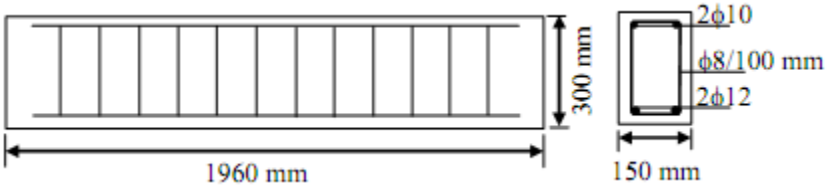

Figure 4-12: Geometry and reinforcement of EBR FRP beam validation

The beams were tested in four point bending. The span between the supports was 1560 mm and the load was applied at points dividing the length into three equal parts as shown in figure 4-13.

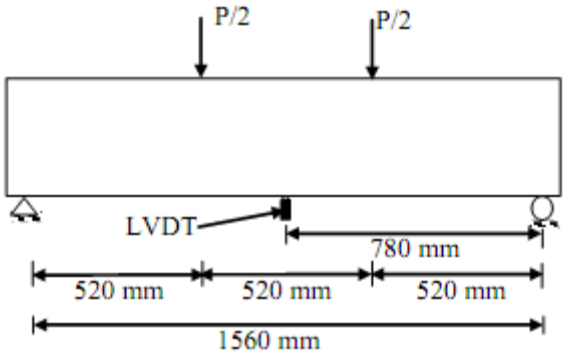

Figure 4-13: Supports, loading and position of Linear Variable differential Transducer (LVDT)

4.2.1.3 CFRP

As a first characterization, the type and the dimensions of a FRP EBR system are of interest to know. This data deals with fiber type, adhesive type, system type (prefab or wet lay-up), fiber orientation(s), width, length and nominal thickness. The definition of the nominal thickness may be as follows.

For prefab FRP types, which are produced with small tolerances on the dimensions, the nominal thickness is generally taken as the global thickness. Alternatively, referring to the fibers as principle stress bearing component, the equivalent dry fiber thickness can be used. This nominal thickness is obtained as the ratio of the fiber mass per area (kilogram of fibers per unit area) and the fiber density. In the case of wet lay-up FRP types, the final thickness after in-situ impregnation may vary considerably and is difficult to determine. Therefore, generally reference is made to the equivalent dry-fiber thickness, which is related to the fiber orientation.

As demonstrated in figure 4-14(a), the FRP properties differ significantly from the properties of the fibers. Hence, using the equivalent dry fiber thickness to characterize composite properties is rather confusing. Moreover, for fiber composites, this definition of the nominal thickness results in unrealistically high values of the modulus of elasticity and the tensile strength, as reference is made to a nominal thickness which is considerably lower than the actual thickness of the cured FRP. For this study the global thickness of the CFRP sheet from the manufacturer is used.

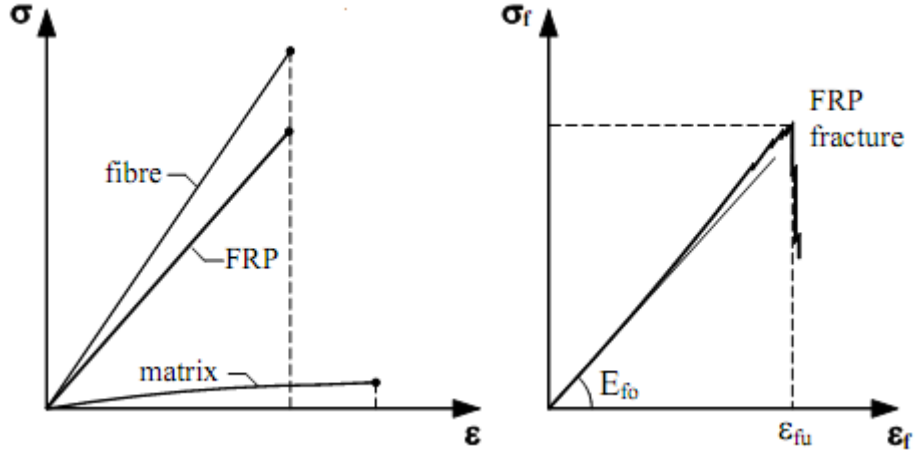

(a) (b)

Figure 4-14: Tensile stress-strain behavior, (a) rule of mixture, (b) actual

In structural engineering, normally the materials dealt with are basically isotropic. This is no longer the case for FRP materials, which are orthotropic due to the mostly unidirectional orientation of the continuous fibers. When the fibers are made available in multiple directions, the FRP can be assumed as quasi-isotropic. Because of the anisotropy, the various possibilities with respect to constituent materials and the influence of the production process, material properties of FRP EBR systems depend on a lot of factors.

Therefore, material properties are preferably determined on the final products (the FRP reinforcement and the adhesive) by standard testing.

Tensile strength and stress-strain behavior

FRP elements primarily act as tensile reinforcement, so that the tensile stress-strain behavior is of basic interest for design. Given the mechanical characteristics and volume fractions of the constituent materials, it is possible to estimate the basic properties of unidirectional FRP elements based on the rule of mixture simplification. The FRP tensile stress (based on the global thickness) is given as:

$$\sigma_f = \sigma_{fib} V_{fib} + \sigma_{mat} V mat \qquad (4.24)$$

$$= \sigma_{fib} V_{fib} + \sigma_{mat}(1-V_{fib}) \qquad (4.25)$$

Where σ_f = tensile strength of the FRP,

σ_{fib} = tensile strength of the fiber, V_{fib}= Volume fraction of the fiber

σ_{mat} = tensile strength of the matrix, V_{mat}= Volume fraction of the matrix

Similarly, the modulus of elasticity and Poisson ratio are obtained as:

$$E_f = E_{fib} V_{fib} + E_{mat}(1-V_{fib}) \qquad (4.26)$$

$$\nu_f = \nu_{fib} V_{fib} + \nu_{mat}(1-V_{fib}) \qquad (4.27)$$

As the fibers are the main tensile stress bearing element and as the fiber volume fraction is relatively high, the axial response of the FRP in tension is basically a reflection of that of the fibers. Compared to the fibers, the axial strength and modulus of elasticity of the FRP are lower. Other properties of FRP's include;

- Typically, the density of FRP reinforcement equals 1400 to 2200 kg/m^3. Compared to steel; FRP is about 4 times lighter.
- The coefficient of thermal expansion (CTE) of steel and concrete are about the same and equal roughly 12×10^{-6}/°C. As a result, thermal stresses at the bond interface of the steel reinforcement and the concrete are generally not significant.
- In general, the shear strength of the FRP (as well as the adhesive) is superior to that of the concrete. For wet lay-up FRP types with a large number of layers, the inter-laminar shear strength may be critical. Although primarily subjected to axial tension, the application of FRP EBR requires transfer of the tensile force to the concrete, resulting in multi-axial stresses (especially in the anchorage zones). Due to this load transfer, mainly shear stresses are generated, which act on the interior of the FRP as well as on the bond interface.

The CFRP bonded to the RC beams is supplied by FOSROC. The laminate had a thickness of 1.2 mm, a width of 50 mm and the elastic modulus 165 GPa. The mean ultimate stress of the three

specimens was 2640 MPa, with the strain corresponding to the failure load being 0.0154. This test also showed that the behavior of the CFRP is linear elastic up to failure.

In order to simulate damage, the beams were preloaded before retrofitting. The preloading was done with the same setup as described in figure 4-13. First the beams were loaded until cracks appeared; the load was 95 KN for beams. The beams were then removed from the test machine and turned over to retrofit them with CFRP. The soffit of the beam was retrofitted with CFRP laminates 50 mm wide and of three different lengths, 1560 mm (series RF1), 1040 mm (series RF2) and 520 mm (series RF3) as shown in figure 4-15.

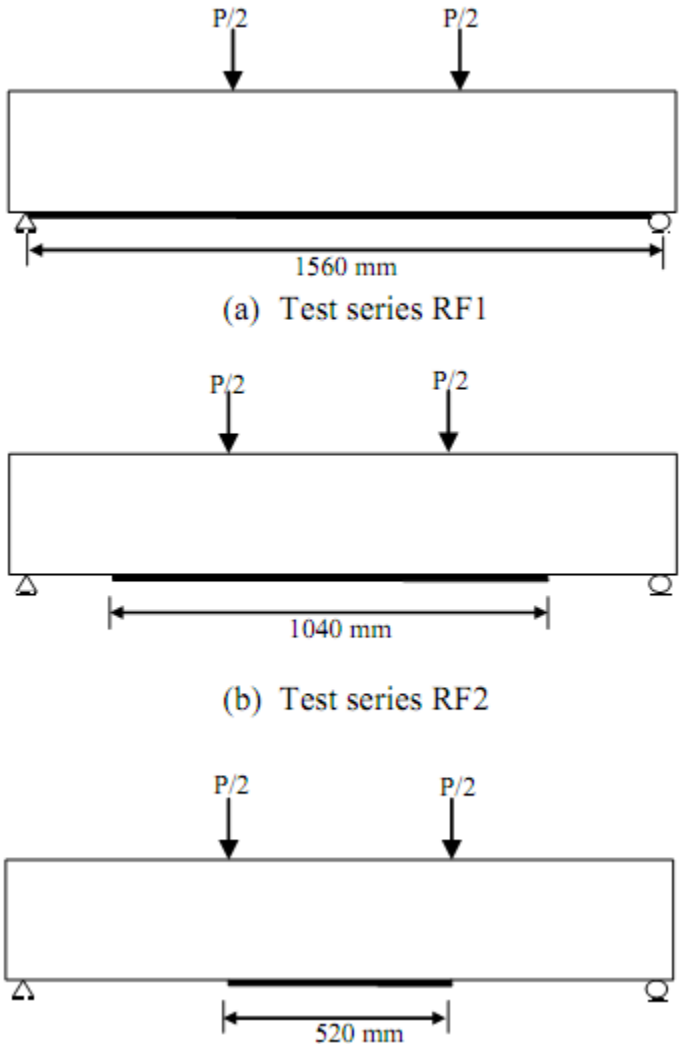

Figure 4-15: Lengths of CFRP laminate in test series RF1, RF2 and RF3.

4.2.1.4 Adhesive

Structural adhesives can be formulated for a wide range of properties. Due to the complex nature of these formulations, estimation of the mechanical properties is difficult and hence requires material testing. With this respect, in various normative references are provided. In principle, the adhesive provides a shear load path between the concrete and the FRP. As a result, the shear and adhesion strength of the adhesive are of mayor concern. For structural adhesives it is generally required to have shear strength of at least 12 N/mm^2 and adhesion strength in terms of pull-off tensile strength of at least 15 N/mm^2. In the case of a FRP/concrete joint, the latter condition means that adhesion is stronger than the concrete tensile strength. For cold cured epoxy adhesives, often used for structural bonding, the shear strength equals 15 to 35 N/mm^2. The flexural modulus of epoxy adhesives should be within the 2000 to 15000 N/mm^2 range. (Stijn Metthys, 2000) The shear modulus of epoxy varies from 0.5 GPa to 0.9 GPa.

The material used in the experiment and this validation model for the bonding of CFRP plates to the concrete is an epoxy adhesive with compressive strength equal to 40 MPa and it was applied with a total thickness equal to 1 mm.

4.2.2 CFRP Laminate-RC Beam Bond Behavior

Two different models were used to represent the interface between concrete and CFRP. In the first model the interface was modeled as a perfect bond while in the second it was modeled using a cohesive zone model. Figure 4-15 shows a graphic interpretation of a simple bilinear traction separation law written in terms of the effective traction τ and effective opening displacement δ. The interface is modeled as a rich zone of small thickness and the initial stiffness K_o is defined as equation (4.20).

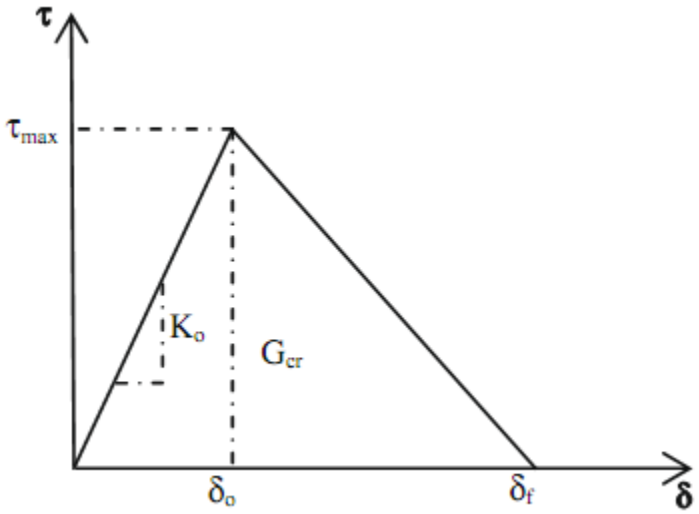

Figure 4-16: Bilinear traction–separation constitutive law.

$$K_o = \frac{1}{\frac{t_i}{G_i} + \frac{t_c}{G_c}} \qquad (4.28)$$

, where t_i is the resin thickness, t_c is the concrete thickness, and G_i and G_c are the shear modulus of resin and concrete respectively. The values used for this study were t_i =1 mm (Adhesive thickness), t_c =25 mm(Concrete cover) , G_i=0.7 GPa, and G_c = 11.65 GPa.

The shear modulus of the epoxy resin is not given therefore; average shear modulus of the epoxy resins is taken in the simulation. Since the range of the shear modulus of epoxy resins is narrow the assumed value will not be expected to cause significant error. The shear modulus of the concrete is calculated indirectly by using a relationship between elastic modulus (E), shear modulus (G) and poisons ratio (ν) of isotropic materials.

$$G = \frac{E}{2(1+\nu)} \qquad (4.29)$$

The defined bond slip is derived from the well-kNown Coulomb's frictional model for surfaces sliding along their contact surface. The basic concept of the Coulomb friction model is to relate the maximum allowable frictional (shear) stress across an interface to the contact pressure between the contacting bodies. In the basic form of the Coulomb friction model, two contacting surfaces can carry shear stresses up to a certain magnitude across their interface before they start sliding relative to one another; this state is kNown as sticking. The Coulomb friction model defines this critical shear stress ,(τ_{max}), at which sliding of the surfaces starts as a fraction of the contact pressure, p, between the surfaces (τ_{max}=μP). The stick/slip calculations determine when a point transitions from sticking to slipping or from slipping to sticking. The fraction, μ, is kNown as the coefficient of friction. (Simulia 2009)

Equation (4.26) provides an upper limit for the maximum shear stress, τ_{max}, giving τ_{max} = 4.3 MPa in this case:

$$\tau_{max} = 1.5\beta_w f_{cr} \qquad (4.30)$$

$$\text{where; } \beta_w = \sqrt{\left(2.25 - \frac{b_f}{b_c}\right) \Big/ \left(1.25 + \frac{b_f}{b_c}\right)} \qquad (4.31)$$

and b_f is CFRP plate width, b_c is concrete width and f_{cr} is concrete tensile strength.

4.2.3 Result and Comparison

A total of six Abaqus models (one perfect bonding and one cohesive model for each of the three CFRP strengthened beams) and three experimental results are compared. In the experiment, all beams experienced a brittle failure mechanism, however in this case sudden debonding of the CFRP plate from the concrete occurred without concrete splitting. This failure was due to high shear stress occurring at the ends of the CFRP. The properties of the adhesive are probably important in relation to the debonding failure. A lower stiffness and higher fracture energy will probably weaken the tendency of debonding. For RF2 and RF3, debonding occurred earlier than for RF1.

The main reason leading to this is that RF2 and RF3 do not have a full anchorage length outside the maximum moment region, hence higher shear stress concentration will occur compared to for the longest CFRP. Experimental results and Abaqus simulation result are presented in the following figures;

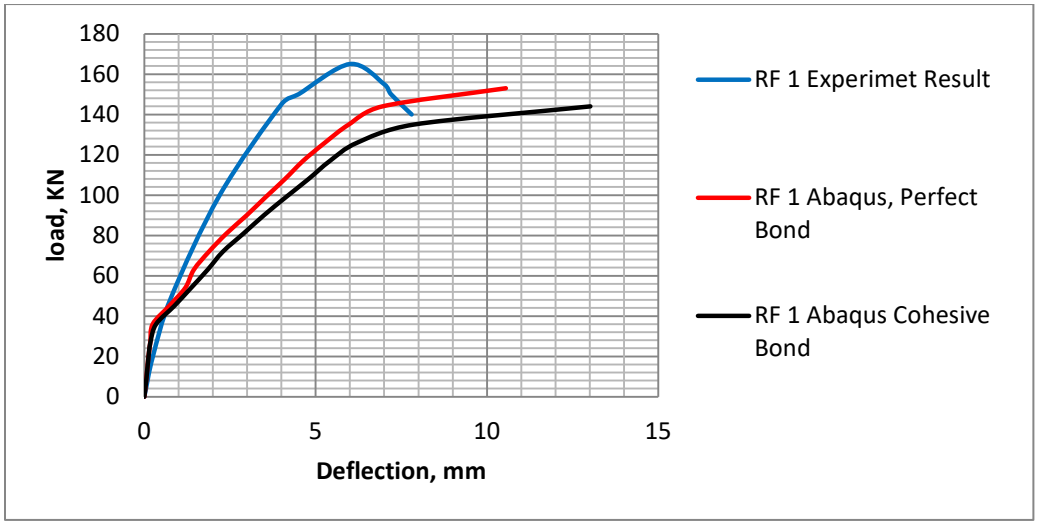

(a)

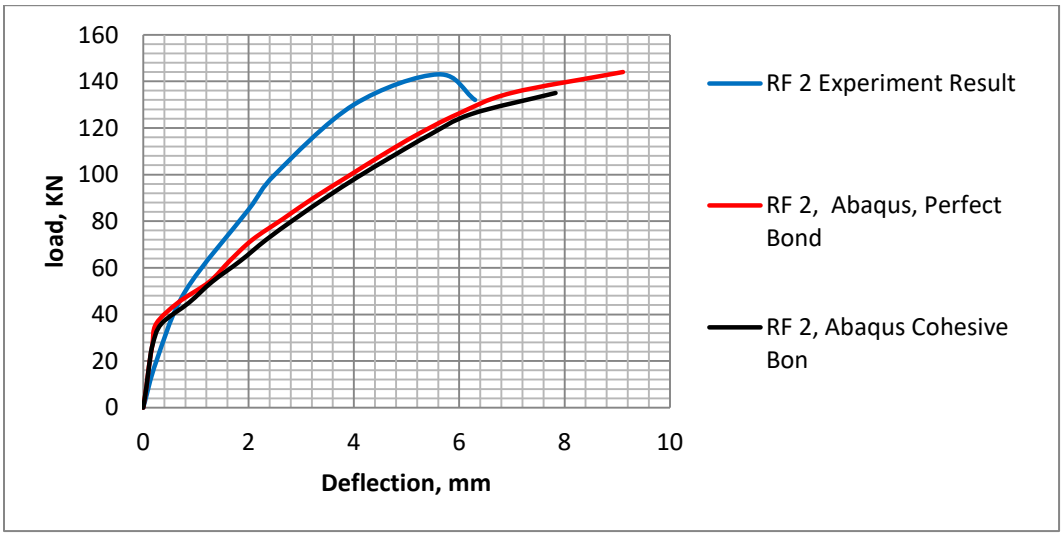

(b)

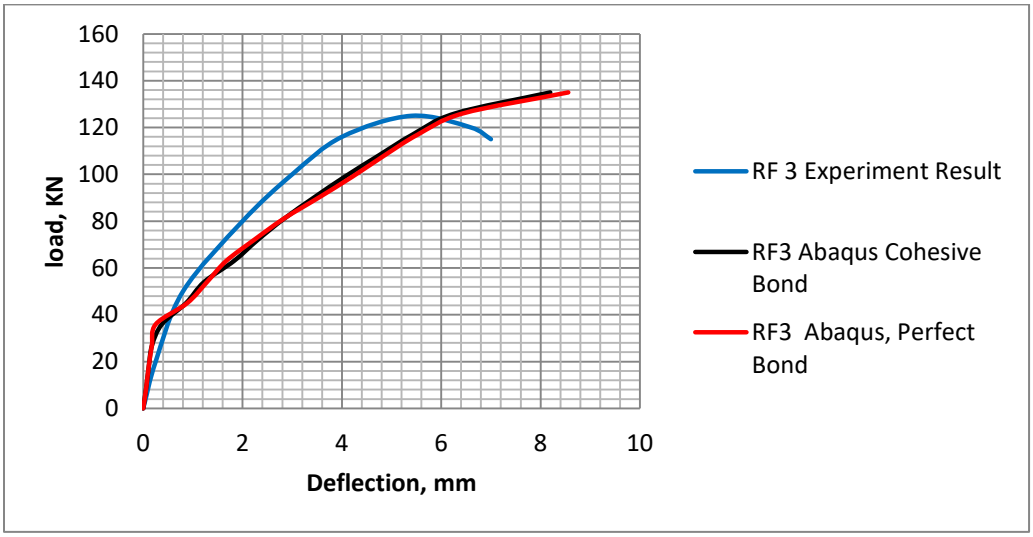

(c)

Figure 4-17: Abaqus simulation and experiment result comparison (a) RF1 (b) RF2 (C) RF3

As shown on the figure it is perfect bond that simulated the experimental result more accurately. As long as the debonding is not initiated in the adhesive, which is not the case for structural epoxies, perfect bond can be used to simulate the interface between CFRP and the concrete beam substrate.

In all the three cases, lower bound Abaqus simulation results were found which assured that in other simulation works where experimental result could not be found, the simulation will not be over estimating the moment capacity of the CFRP strengthened beam. On the other hand, a trial and error ultimate strength calculation method recommended on ACI-440.2R-08 section 10.2 over estimated the section capacity around 237.89 kN.m. Since the calculation is based on section analysis, same ultimate load estimation is made for all the three beams which results 43.31 %, 67.53 % and 88.87 % over estimation error for the case of RF1, RF2 and RF 3 respectively. The calculation of the ultimate load estimation according to ACI is presented in Annex C.

4.3 Validation of End Wrap Anchored CFRP Strengthened Beam

In another work done to see the efficiency of Abaqus model in representing CFRP end wrapped beams, a single beam experimented by Stijn Matthys in a PhD dissertation work in Ghent university is used. The beam has a width of 200 mm, a total depth of 450 mm, a span of 3.8 m and a total length of 4 m. A clean cover of 25 mm is provided to a steel reinforcement of, $\varrho(A_s/bd)$=0.96% and additional one layer of Carbodur S1012 CFRP laminate with 100 mm width and 1.2 mm thickness, and extra 330 mm wide end anchorage with Replark MRK-M2-20 is attached to the beam. The extra anchorage is provided for the beam was obtained by a means of U shaped wrapping around the soffit and the side faces of the beam. The dimension of the beam and the test set up are shown in figure 4-18.

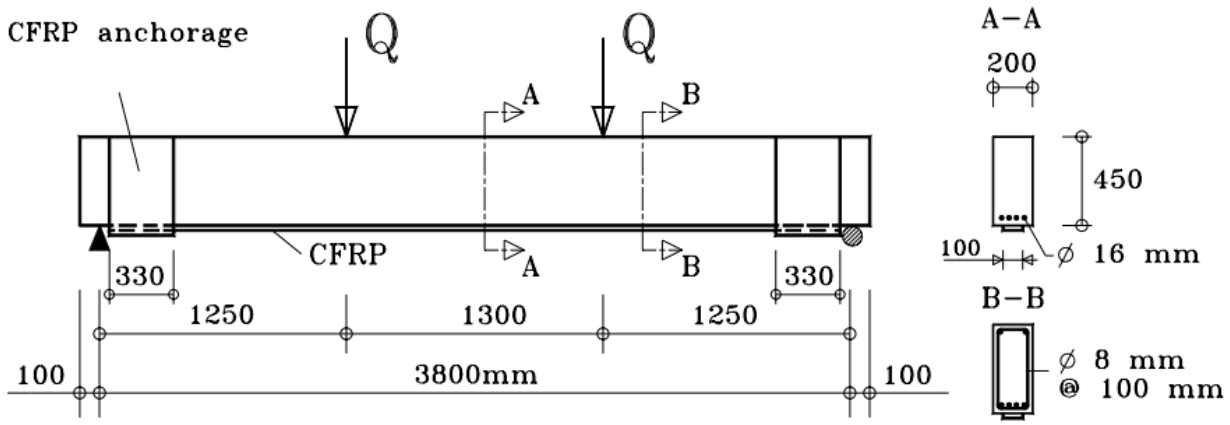

Figure 4-18: Test set-up and specimen dimension of End anchored validation beam

The mean compressive cylindrical strength f_{cm} at the 28th day was 32.8 MPa. For the internal reinforcement deformed steel bars with a minimum guaranteed characteristic yield strength of 500 MPa is used. Mechanical properties of reinforcement materials used in the research are presented in table 4-8.

Type	Dimensions, mm	Yield Strength, MPa	Tensile Strength, MPa	Ultimate Strain, (%)	E-modulus, MPa
Rebar S500	Φ 16	590	690	12.4	200000
Carbodur S1012	100 x 1.2 (1)	-	3200	1.85	159000(3)
Replark MRK-M2	100 x 0.11(2)	-	3500	1.25	233000(3)

(1) Global thickness, (2) Equivalent dry-fiber thickness, (3) Tangent modulus at the origin

Table 4-8: Mean properties reinforcement materials

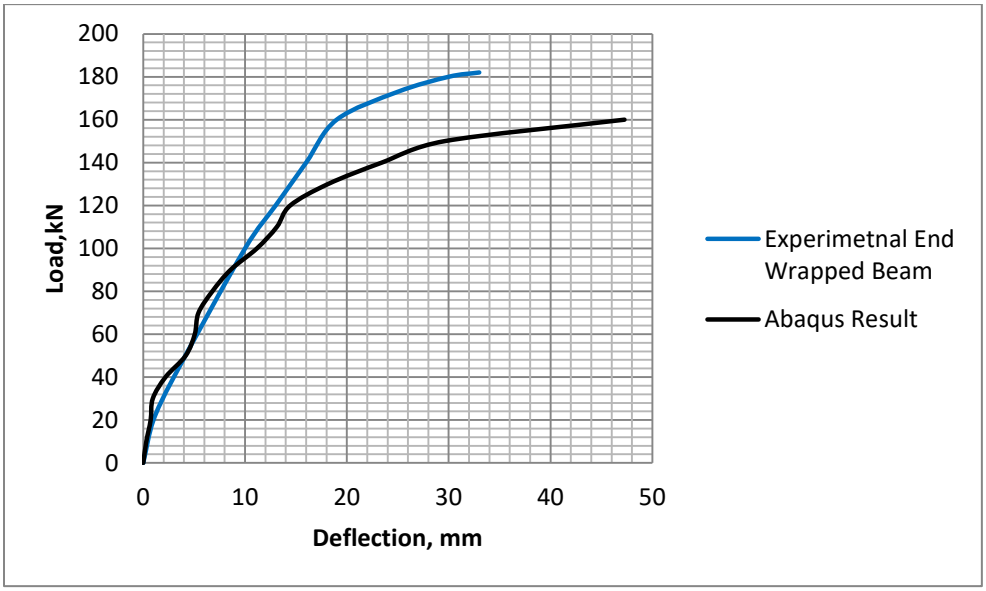

Figure 4-18: Abaqus simulation and experiment result comparison for End anchored beam

No new material or interface model was tried in this simulation work. CDP model for the concrete, elastic linearly hardening model for the steel with yield strength reduction

recommended by Belarbi and Hsu, elastic model for both CFRP laminates and perfect bond is used to simulate CFRP concrete interactions in all cases.

The simulation result remained to yield a lower bound result assuring once again the simulation works to be done will not be exaggerating the real behavior of CFRP end anchored beams.

Chapter Five
Conceptual Design and Modeling of the End Slit Anchored Beam

5.1 Conceptual Design

Research works on end anchored EBR CFRP beam have reported that it has improved the ultimate load, stiffness and ductility of a beam compared to the Externally Bonded Reinforcement (EBR) CFRP beam with no end anchors. For example Al-Amery investigated the combined shear-flexural strengthening of RC beams. It was found that a significant improvement in the beam strength up to 95% is gained due to the use of CFRP strips to anchor the CFRP sheets. It was found that the dominant mode of failure observed in the beams with strips was a ductile flexural failure with excessive yielding of internal steel prior to the rupture of CFRP sheets and crushing of the concrete.

The other important FRP application technique that current research works have proved to be beneficiary over other customary EBR application techniques is Near Surface Mounted (NSM) EBR. It first developed with the aim of protecting the CFRP material from environmental and chemical damages. However it has additional advantages of improving the bond between the CFRP and the surrounding concrete to give a higher flexural capacity and assure the FRP sheets attain higher ultimate strain. NSM basically consists of the following steps;

a) Cutting grooves of specified dimensions at designed
b) Cleaning the grooves to ensure proper bonding between the epoxy adhesive and concrete.
c) Placing the epoxy paste into the grooves to fill 2/3 of the groove depth.
d) Inserting the strengthening materials (rods or strips) in the groove
e) Placing additional epoxy paste to ensure that the grooves are completely filled and then leveling the surface by removing excessive adhesive and
f) Curing

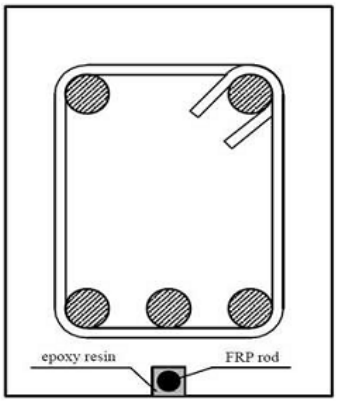

Figure 5-1: Application of FRP rod in NSM method

Therefore, it is evident that this application technique demands additional effort than the usual EBR techniques. Especially cutting of thin grooves in the concrete beam is costly and time consuming. Moreover, unlike the CFRP rod, it could be inconvenient with laminates since the laminates cannot easily be rolled and inserted to the groove.

With the aim of tackling the aforementioned challenge and at the same time benefitting from the advantages of end-anchorage, the idea of end slit anchors is proposed. This new technique avoids cutting of grooves throughout the length of the beam and limits the slits to the area near the end of the beams. Therefore the cutting process will not be costly as in the case of NSM EBR. If the concrete beam is intended for strengthening from the beginning slit creating plastic or other material with the dimension of the slit could be used as a mold fixed with the soffit formwork to remove it later when the concrete hardens and create the slit. Figure 5-dd demonstrates the slit creating material fixed to the formwork during the experimental work.

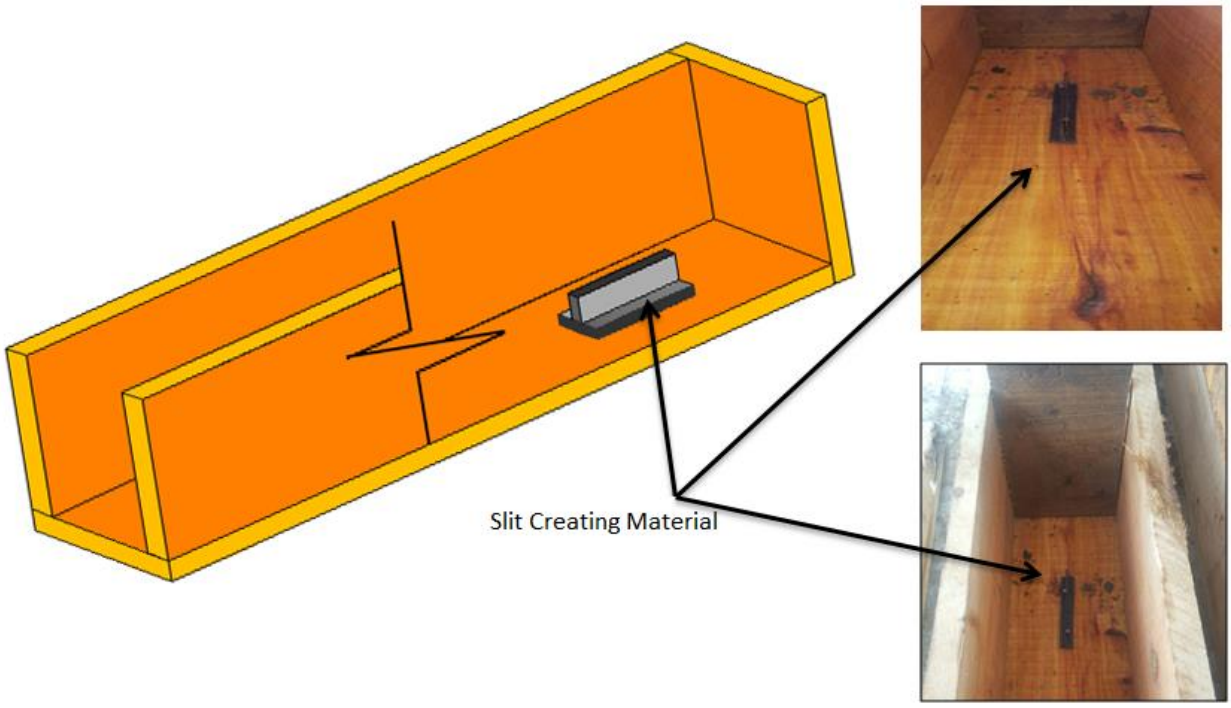

Figure 5-2: Slit creating material

The CFRP material will be bonded to the concrete beam as usual between the end slits and as it reached the slits the CFRP laminate will be inserted and bonded with epoxy into the slits giving it anchorage effect. Additionally if there is an end wrap anchorage that covers the side faces and the soffit of the beam, it could also be inserted and bonded to the slit together with the longitudinal laminate giving it more fixity. The CFRP laminate could also be externally covered by mortar case as in the case of Textile Reinforced mortar (TRM) if environmental and chemical attacks are likely to occur.

5.2 Modeling of End-Anchored CFRP Strengthened Beam

In this section the simulation result of the nine CFRP strengthened beams, (BF1, BF2 BF3 BF4 BF5 BF6 BF7 BF8 and BF9), casted in the laboratory are presented in the already validated models using Abaqus finite element software. The experimental results of these beams are not presented in this paper.

The next phase of this study will discuss the results of the experiment in depth. Effect of concrete strength on delamination and flexural capacity and end-anchorage effect on the load deflection of the beams is discussed in this chapter based on the simulation result.

5.2.1 Material Property and Beam Layout

The CFRP application techniques vary from simple EBR with no anchors to EBR with U-wrap and End-Slit anchor. The specimen types and loading set up of the beams can be seen on table 3-4 and figure 3-3. For the modeling work, the RC part is modeled by a CDP model as discussed earlier in chapter four, and the steel reinforcement bar is modeled as discrete wire element embedded in the concrete beam. The stress-strain diagram of the steel is defined as an elastic linear strain hardening model with a yield stress reduction recommended by Belarbi and Hsu. The CFRP laminate, Sika Carbodur E1014 supplied by SIKA is assumed with Sikadur 30 in the modeling.

Mechanical Properties	Curing time	Curing Temperature	
		15^0c	35^0c
Compressive Strength (Mpa)	1 day	55	90
	3 days	70	90
	7days	75	90
Tensile Strength (Mpa)	1 day	20	26
	3 days	23	27
	7days	26	29
Shear Strength (Mpa)	1 day	4	17
	3 days	15	18
	7days	16	18
Tensile Adhesion Strength @23°c, (Mpa)	7 days	Concrete Substrate	> 4
	7 days	Steel Substrate	> 21
Compressive Elastic Modulus @ 23^0c (MPa)			9600
Tensile Elastic Modulus @ 23^0c (MPa)			11,200
Shrinkage (%)			0.04
Coefficient of Thermal Expansion			$2.5x10^{-5}$ / °C

(a)

Material Property		Mean	Characteristic
Tensile Strength (MPa)		2200	2000
Modulus of Elasticity (GPa)		180	170
Elongation at Break (%)		1.22	1.18
Density (g/cm3)		1.55	
Section Property	**Width, mm**	**Thickness, mm**	**Cross-section Area, mm^2**
Dimensions, mm/mm^2	100	1.4	14
Fiber Volume Content (%)	> 70		

(b)

Table 5-1: Material property (a) Sikadur-30 (b) Sika Carbodur E1014

5.2.2 Modeling Results

In a simulation result presented below the load deflection diagram of all beams and the failure load estimation for the beams according to ultimate failure load estimation of ACI trial and error calculation is shown. Additionally, for unanchored CFRP Strengthened beams of each group, a rough load deflection analytic estimation according to EC-2 is done assuming the CFRP as bottom reinforcement and the result is presented in figure 5-3. In the first group there are two unanchored beams and the analytic calculation represents BF 2 beam. The load-deflection curve obtained is modified to attain the plateau at the failure load estimated by ACI calculation. The procedure followed for the analytic calculation is presented in Annex-D.

Control beam BC1 serves as control for BF1 and BF2 and these beams are labeled as group 1. BC 2 serves as control for group 2, BF3 and BF4 beams, whereas BC 3 serves as a control for group 3, BF5, BF6. BF7, BF8 and BF9 beams. Some results like BF 1 and BF 2 have similar behavior because of the closeness in compressive strength. BF 7 is also omitted because it has exactly the same curve with BF 5. The enhancement attained by end anchorage can also be studied on the same figure in comparison with the others.

As shown on figure 5-3 (a) in the first group (BC1, BF1 and BF 2) a flexural load increment of 73.33 % is attained compared with the experimental result. There is also significant stiffness increment both around service loads and ultimate load. Deflection at yield point of the strengthened beams and the control beam is similar.

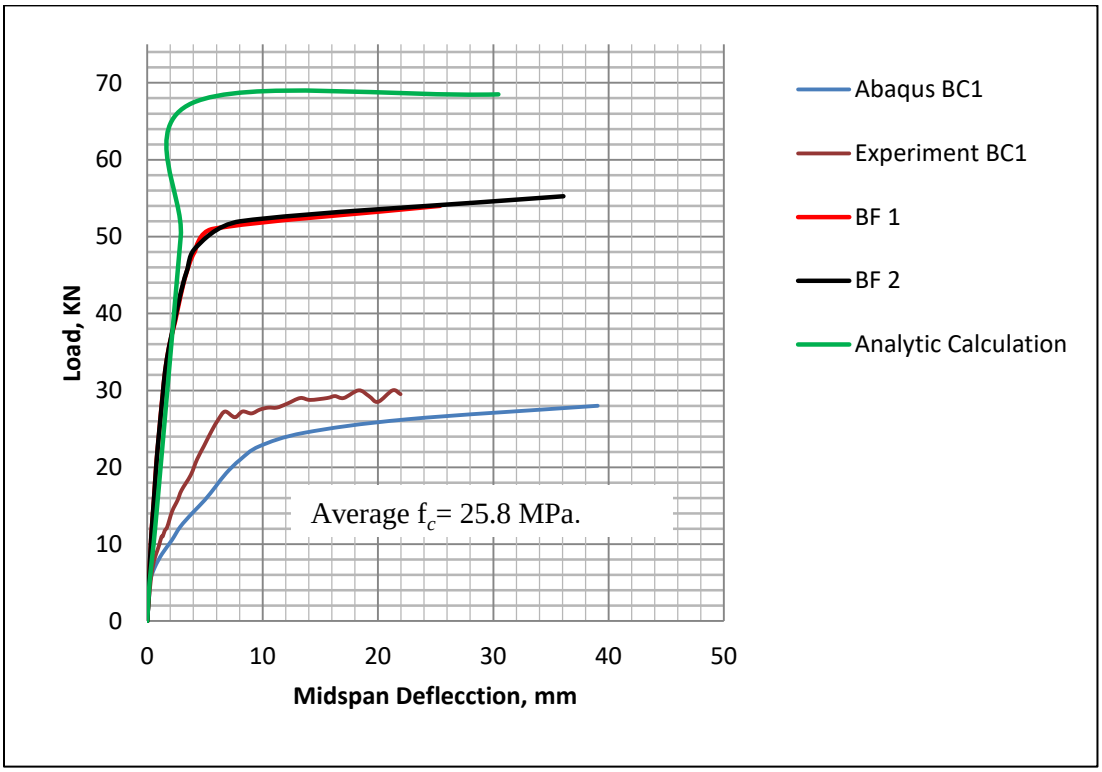
Load, KN
Midspan Deflecction, mm
Average f_c= 25.8 MPa.
Abaqus BC1
Experiment BC1
BF 1
BF 2
Analytic Calculation

(a)

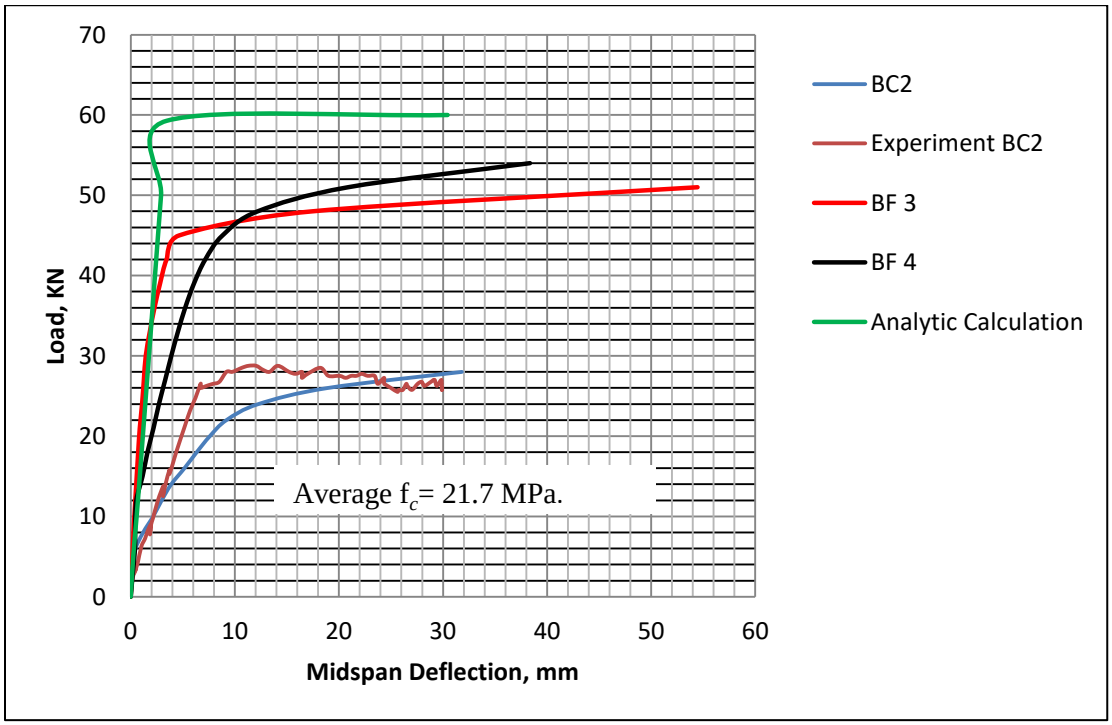
Load, KN
Midspan Deflection, mm
Average f_c= 21.7 MPa.
BC2
Experiment BC2
BF 3
BF 4
Analytic Calculation

(b)

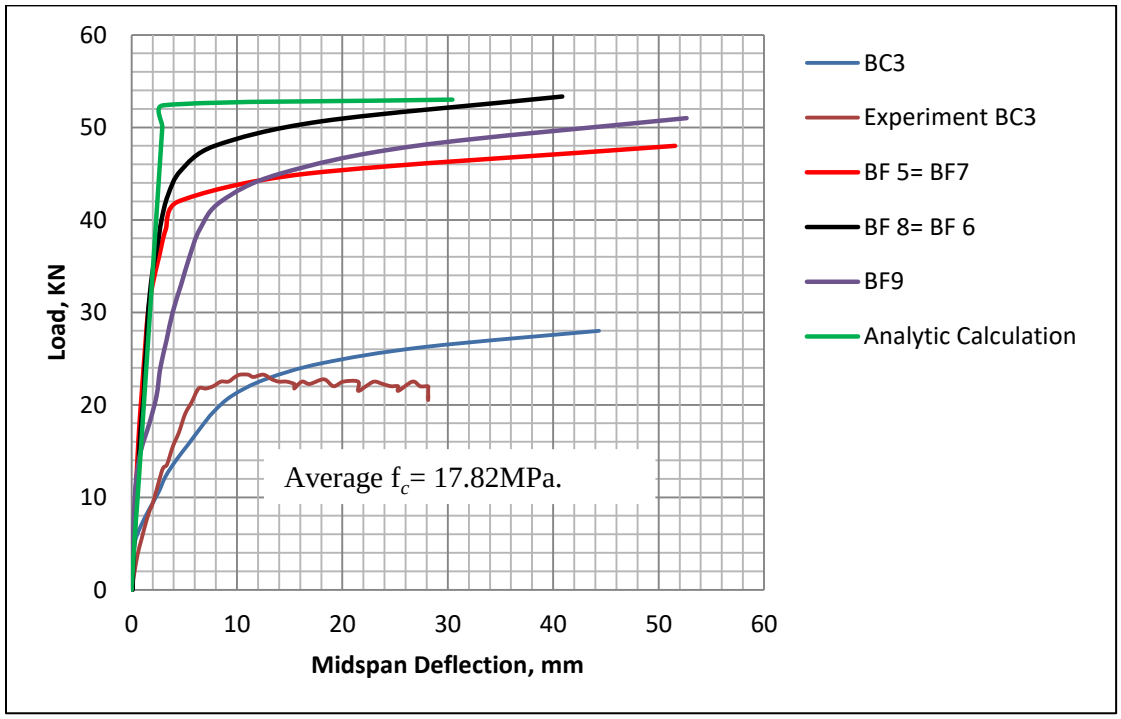

(c)

Figure 5-3: Load deflection diagram for strengthened beams (a) group 1 (b) group 2 (c) group 3

With regard to stiffness, the load in the control beam had to be raised by 120%, 104% and 130 % to bring the beam to maximum serviceable deflection of 5.6 mm according to EBCS-EN 1992 in the first, second and third group respectively. Generally, there is no extra stiffness increment attained by end anchorages. In the second group the failure load increment lower to 59.94 %, as the compressive strength of the concrete lowers from an average value of 25.8 MPa for the first group to 21.7 MPa in the second group. Finally, the third group came with an ultimate load increment of 85.95 % defying ACI minimum concrete substrate limit. The following section discusses more about the contradiction.

5.3 Effect of Concrete Strength on Delamination and Flexural Capacity

A direct relationship between concrete strength and flexural strength increment attained by the CFRP was observed in the first two groups. The flexural strength increment reduced as the concrete grade of the beams lower. But sudden increment was observed in the case of the third group with the lowest concrete strength. Since perfect bond is assumed in the modeling the interface model functions regardless of delamination issue. Therefore to study this phenomena, BF 5 beam, which has a concrete strength (f_c=17.19 MPa) close to ACI minimum concrete substrate strength limit (17 MPa), is modeled on SIKA Carbodur design software. Material strength is increased by the safety factor (1.5 for concrete and 1.15 for steel) and the load is decreased by the load safety factor (1.35, for permanent load) used by the software to remove the

effect of safety factors and to bring the load to ultimate failure level. The tables illustrate the state of different delamination failure modes at moment the first and the second group beams, table 5.2 a and b, fail by full composite action of concrete crashing after the steel has yielded and; the third group, by concrete crashing before the steel yielded. Additionally reduced steel yield strengths are used in the design for consistency with the simulation work.

The software shows BF5 beam can resist a concentrated midpoint load of 40.5 KN. The software compares the capacity of the beam against the three different types of delamination and the yield strain of the FRP against the strain in it. In a row added to compare the capacity versus the load or stress in the section, Group three beams, BF 5 specifically, see figure 5-2(c), show the lowest ratio in longitudinal shear near ends of FRP and anchorage failure. Especially anchorage delamination is on the verge of occurrence. The following tables are extracted from the report prepared by the software.

Failure Type	Comparison	Results	Capacity/ Load(Stress)
Shear Crack induced FRP Separation	$V_{ED} \leq V_{RD,\ Crack}$	20.49 kN ≤ 72.11 kN	3.52
Strain in the FRP	$\varepsilon_{mt} \leq \varepsilon_{fd}$	0.00215 ≤ 0.00899	4.18
Longitudinal shear near ends of FRP	$T \leq \tau_{lim,c}$	0.75 MPa ≤ 1.28 MPa	1.71
Anchorage	$T_d \leq T_k$	31.83 kN ≤ 37.82 kN	1.19

(a)

Failure Type	Comparison	Results	Capacity/ Load(Stress)
Shear Crack induced FRP Separation	$V_{ED} \leq V_{RD,\ Crack}$	20.99 kN ≤ 71.29 kN	3.40
Strain in the FRP	$\varepsilon_{mt} \leq \varepsilon_{fd}$	0.00222 ≤ 0.00899	4.05
Longitudinal shear near ends of FRP	$T \leq \tau_{lim,c}$	0.80 MPa ≤ 1.14 MPa	1.43
Anchorage	$T_d \leq T_k$	33.24 kN ≤ 35.68 kN	1.07

(b)

Failure Type	Comparison	Results	Capacity/ Load(Stress)
Shear Crack induced FRP Separation	$V_{ED} \leq V_{RD,\ Crack}$	20.25 kN ≤ 70.25 kN	3.47
Strain in the FRP	$\varepsilon_{mt} \leq \varepsilon_{fd}$	0.00210 ≤ 0.00899	4.28
Longitudinal shear near ends of FRP	$T \leq \tau_{lim,c}$	0.77 MPa ≤ 0.97 MPa	1.26
Anchorage	$T_d \leq T_k$	32.10 kN ≤ 32.95 kN	1.03

(c)

Table 5-2: FRP Separation failure and anchorage,
(a) group one beam BF2, (b) group two beam BF3, (c) group three beam BF5

The other beams have a higher ratio with this regard at their failure point. Beams in group two can be designed to resist a load up to 41.98 KN and at that point the FRP separation failure scenario is presented in table 5-2 (b). Group one beams, on the other hand, can be designed to resist a load up to 40.97 kN and at that point are less likely to be delaminated from the CFRP laminate according to the higher ratio indicated in table 5-2 (a).

Therefore the result shows that the minimum substrate compressive strength is set not because no flexural strength increment is attained at that concrete strength rather, the beams is prone to anchorage failure and longitudinal shear debonding near FRP end. These are brittle failures that could cause sudden stress transfer from the FRP to the steel reinforcement and cause catastrophic damage or collapse of the structure ultimately.

FIB Bulletin 14, under section 4.6.5 states that verification of bond interface cracking that are usually initiates at FRP ends is not necessary if extra anchorage is provided. Despite the fact that, cohesive bond model have underestimated the ultimate load capacity and the stiffness of FRP strengthened beams in the validation work, for the sake of assessing delamination mitigation by the use of end anchorages, BF5 beam with two different end anchorage types is modeled using cohesive CFRP-RC beam interaction model discussed earlier in section 4.2.2. The following topic discusses the modeling result.

5.4 Effect of End Anchorage on Load-Deflection Behavior

In a simulation work done to check if end wrap anchorage will mitigate the delamination of BF 5 beam, the end anchor altered the location delamination initiated from the end of the FRP as in the case of the unanchored beam, to the middle of the beam. But the load at which the delamination occurred and the ultimate load are almost the same for both cases. The simulation used cohesive model for both cases.

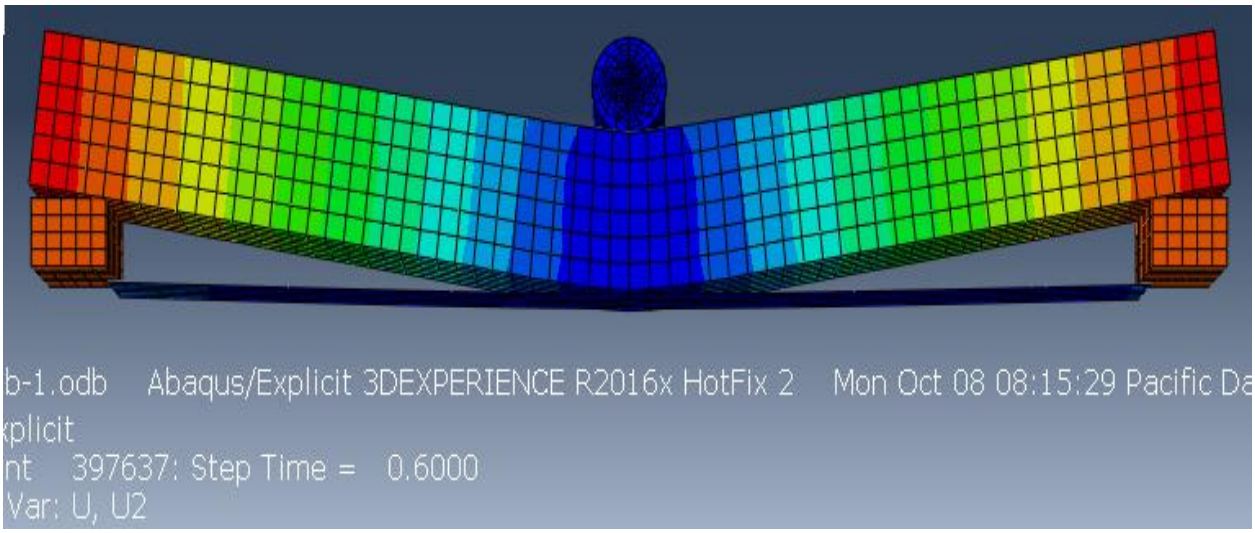

Figure 5-4: Delamination of CFRP sheet of unanchored BF 5 beam

The new proposed end slit anchorage, however, resulted a very good result in terms of both ultimate load increment and stiffness enhancement. As shown on figure 5-6, it has a 21.7 % increment at load corresponding to 10 mm relative to both EBR and end wrap anchored BF 5 beams. At maximum serviceable deflection the load increment is as high as 33.33 %. The other benefit of the end slit anchorage technique is the fact that delamination initiated lately at the middle of the beam, it can, therefore, be recommended to enhance the load-deflection behavior of low concrete grade CFRP strengthened beams both for ultimate load and stiffness enhancement.

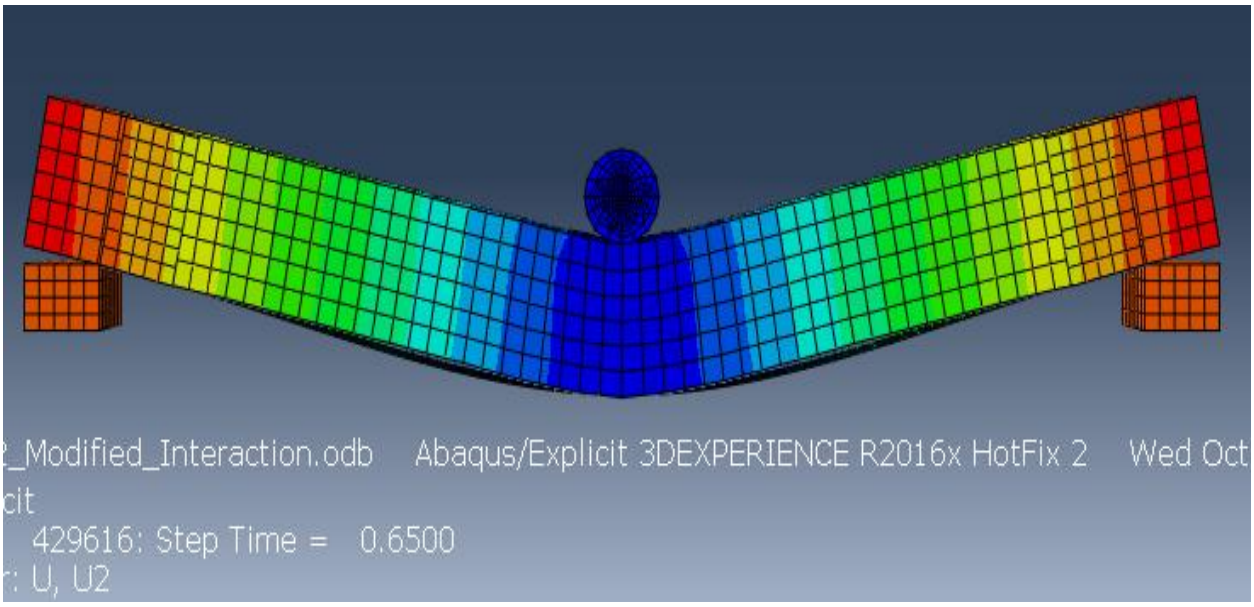

Figure 5-5: Delamination of the End wrap anchored BF 5 beam

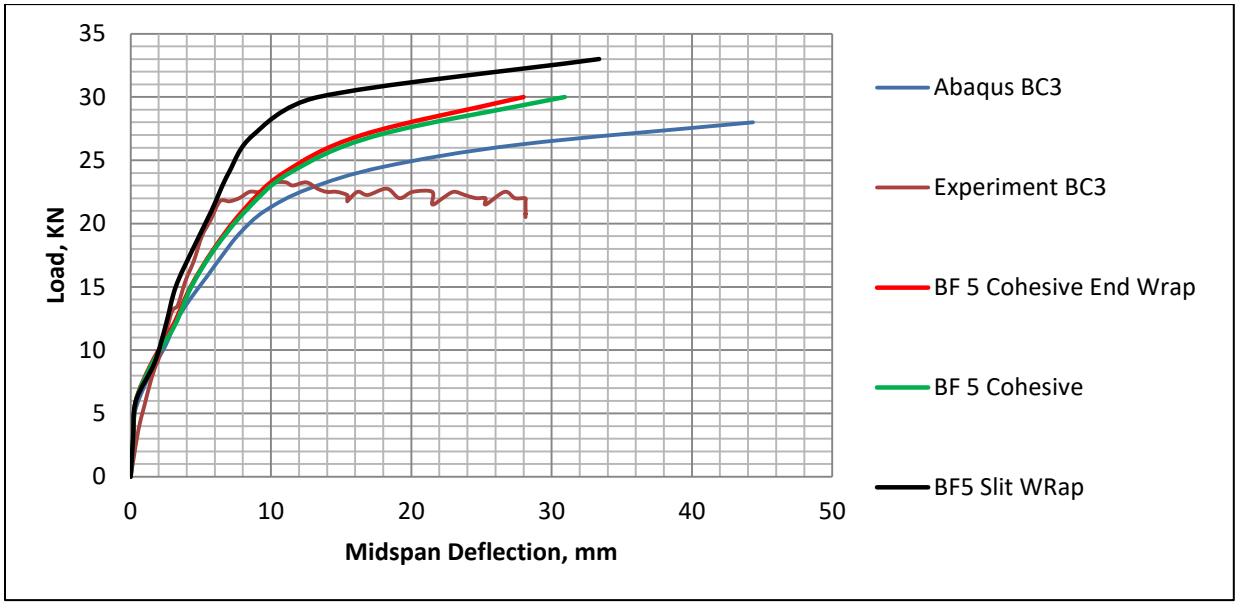

Figure 5-6: Load deflection diagram of BF 5 and End anchored beams

Chapter Six
Conclusion and Recommendation

6.1 Conclusion

This research aimed at flexural strengthening of medium and low grade concrete. To do so, different EBR CFRP application techniques have been modeled on Abaqus non-linear finite element software and the simulation work is compared with experimental results. Different material and interface interaction models have been used and their result is verified with manual calculation and experimental results to find the best fitting model. Concrete damage plasticity model for concrete and elastic linear strain hardening model of reinforcement steel material models are found to effectively represent the experimental results. In the steel material model, the yield strength is reduced by the factor recommended by Belarbi and Hsu (1994) to account for tension stiffening.

Two phases of software validation works are carried out in this thesis. In the first phase three RC control beams casted in the experimental program, tested with a three point loading with the load and deflection both applied and recorded at the center of the beams, are used to validate the RC beam model. In addition to the control beams nine strengthened beams are casted in the laboratory with different anchorage techniques. All beams had the same cross-section and steel reinforcement provision. They are grouped in to three based on concrete compressive strength, and for each group one control beam serves as a reference.

The second validation work focused on CFRP strengthened RC beams. All material models validated in the first phase are used with additional two perfect and cohesive CFRP RC beam interface interaction models available for choice to represent the true nature. CFRP EBR beams with different laminate length casted and experimented by Talieb Y. Obadiat in Lund University are used to find out the more effective one. Provided that strong epoxy, stronger than concrete in shear strength and able to avoid adhesion failure, is used, perfect bond bettered than cohesive bond model in all cases.

The validation works have proved, therefore, that Abaqus can represent experimental results very well. Then the strengthened beams were modeled and analyzed to raise the failure load and the stiffness of the control beam with a factor of 60-85 % and 105-130% respectively. The stiffness increment calculation is made based on control and CFRP EBR beam load comparison corresponding to the maximum serviceable deflection according to EBCS-EN-1992. The end wrap further raised the ultimate load by up to 13 % but it generally didn't have significant effect on stiffness.

A new anchorage technique is also proposed in this thesis as a combination of end anchorage and near surface mounted (NSM) applications. The new anchorage technique is called end slit anchorage and it is discussed to ease the difficulty, inconvenience and also minimize the costly groove cutting process of NSM application technique. In the modeling work the new end slit anchorage technique showed a failure load increment of up to 6.25% compared to the usual EBR CFRP application.

A special focus was made on ACI minimum compressive strength limit, i.e 17 MPa, of concrete substrate to be strengthened by FRP. Failure type and ultimate load resisted by a beam with the cylindrical compressive strength of 17.12 MPa is studied in comparison to a control RC beam with the same compressive strength. The result showed that the EBR CFRP beam shows

immense load increment but delamination is more likely and sudden to happen at that concrete strength which causes brittle failures. Therefore it will be wise to note ACI recommendation for a safe design of EBR FRP systems. To study the effect of end wrap anchor on the delamination of this beam, cohesive interaction model is used because it takes the interface interaction property as a function of the strength of concrete. The end wrap anchor altered the location delamination initiated but it had insignificant effect on the load deflection of the CFRP EBR beam.

Finally, an end slip wrap anchorage proposed in this paper as a new application technique is used to mitigate the delamination and it resulted a very good result with ultimate load increment up to 25% and significant deflection decrement both at serviceable and ultimate load. The other important benefit gained was delayed delamination that initiated at the middle of the beam.

6.2 Recommendation

In this thesis, the performance of flexural strengthening CFRP application techniques is discusses for C-20/25 concrete RC beams. The research basically combined experimental and software simulation results for the study. The following recommendations are forwarded at the completion of this research work.

- The new end slit anchorage technique should be tried with different slit lengths to prepare a guideline which recommends optimal slit length for the load increment needed.
- The concrete CFRP interface should be further studied to capture both delamination and load-deflection behavior of CFRP strengthened beams
- The new end slit anchorage should be experimentally tried in the laboratory to see other parameters the software simulation failed to capture
- Ductility enhancement is not covered in this research work. Therefore experimental or software simulation should be carried out to study the effect of end slit anchorage on ductility of the beam with a modeling that best captures the post-peak behavior of RC beams and unloads when the beams fail,
- Experimental Investigation should also be carried out with different epoxy strengths to point out the limit at which delamination of CFRP cause no improvement on the load deflection behavior of RC beams

Apart from this research work, failure criteria and design procedures on both ACI and FIB are limited to few EBR FRP application techniques therefore more focus should be given to researches in this area and bring the experience and design methods of practitioners like SIKA to the same table to include special application techniques in the design.

References

1. Abaqus/CAE Users Guide, Dassault Systems (DS) Simulia Abaqus 2016
2. ACI 211. 4R-08,Guide for selecting proportions for high strength concrete using Portland Cement and other cementitious materials, 2008
3. ACI 318-08, Building Code Requirements for Structural Concrete and Commentary, American Concrete Institute, 2008
4. ACI 440.2 R-08, Guide for the Design and Construction of Externally Bonded FRP Systems for Strengthening Concrete Structures, American Concrete Institute, July 2008
5. Belarbi A, Hsu TTC, "Constitutive laws of concrete in tension and reinforcing bars stiffened by concrete", ACI Structural Journal 1994; 91(4): 465–74.
6. Beza Fekadu and her colleagues, "Seismic Retrofitting Of Reinforced Concrete Beams Using Fiber Reinforced Polymer Sheets", BSc. Thesis, Addis Ababa Institute of Technology(AAiT), 2015
7. Blaschko A., "The bearing behavior of concrete structural compounds with slotted-in CFRP lamellae, German", Dissertation, TU Munich, June 2001
8. EBCS EN 1992-1-1:2013, Ethiopian Building Code Standard, Design of Concrete Structure, 2013
9. EN 1992, Eurocode 2: Design of concrete structures: General rules and rules for buildings, November 2002
10. FIB, Bulletin 14, Task Group 9.3, "Design and use of externally bonded fiber reinforced polymer reinforcement (FRP EBR) for reinforced concrete structures', July 2001
11. Joshua S. Tyau, "Finit Element Modeling of Reinforced Concrete Using 3-dimensional solid elements with discrete rebar", MSc. Thesis, Brigham Young University, 2009
12. H. B. Kupfer, H. D. Hilsdorf and H. Rusch, "Behavior of Concrete under Biaxial Stresses," ACI Journal, 1969
13. H. Nordin, "Strengthening structures with externally prestressed tendons strengthening structures with Literature review," 2005.
14. Hyo Gyoung Kwak, Jin Kook Kim, "Implementation of bond-slip effect in analyses of RC frames under cyclic loads using layered section method", Elsevier, Korea Advanced Institute of Science and Technology, Republic of Korea, April 2006
15. James MacGregor and James White, Reinforced Concrete Mechanics and design, fifth edition, 2009
16. Kotsovos M.D. and Newman J.B, "Behavior of Concrete under multiaxial stress", ACI Journal, 1977
17. Luke, P. S., Leeming, M. B. and Skwarski, A. J. (1998), ROBUST results for carbon fibre. Concrete Engineering International, 2(2), 19-21
18. Martin Fornander, Patrik Nihlmark, "A New Method for using Prestressed Fibre-Reinforced Polymer Laminates for Strengthening and Repair of Structural Members", MSc. Thesis, Chalmers University of Technology, Goteborg, Sweden 2013

19. Meier, U. (1987), Bridge repair with high performance composite materials. Material & Technik, 4, 125-128 (in German).
20. Milad Hafezolghorani, PhD Candidate; Farzad Hejaz, Journal, Structural Engineering International, University of Putra Malaysia, Selangor, Malaysia, February 2017
21. Nanni, A., 1995, "Concrete Repair with Externally Bonded FRP Reinforcement," Concrete International, V. 17, No. 6, June, pp. 22-26
22. Stijn Matthys, "Structural Behavior and Design of Concrete Members Strengthened with Externally bonded FRP reinforcement", PhD Dissertation, Ghent University, 1999,
23. Thomas T. C. Hsu and Y. L. Mo, Unified Theory of Concrete Structures, First Edition, University of Houston, USA, 2010
24. Triantafillou T. C., Deskovic N. and Deuring, M. (1992), "Strengthening of concrete structures with prestressed fiber reinforced plastic sheets". ACI Structural Journal, 89(3), 235-244.
25. Yasmeen Taleb Obaidat, "Structural Retrofitting of Reinforced Concrete Beams Using CFRP", Division of Structural Mechanics, LTH, Lund University, Lund, Sweden, 2010
26. Ziad N. Taqieddin, "Elasto-plastic and damage modeling of reinforced", Doctoral Dissertations, Louisiana State University and Agricultural and Mechanical College, ztaqie1@lsu.edu, 2008

Annex A

Concrete Damage Plasticity (CDP) Parameters

Plasticity and simplified Concrete Damage Plasticity parameters for all the five concrete strengths used in the simulation work are presented below.

1. f_{cu}=33.52 MPa, f_{cm}=26.90 MPa Concrete strength of BC1 and BF2

Material parameter	f_{cu}= 33.54 Mpa	Plasticity Parameter	
		Dilation angle	31
		Eccentricity	0.1
Concrete Elasticity		f_{b0}/f_{co}	1.16
E (Gpa)	29.571	K	0.666
ν (Poisson Ratio)	0.2	Viscosity	0
Concrete Compressive Behavior		Concrete Compressive Damage	
Stress (MPa)	Inelastic Strain	Damage Parameter (d_c)	Inelastic Strain
11.6	0	0	0
20.48	0.000133498	0	0.000133498
25.99	0.000384916	0	0.000384916
28.62	0.000736336	0	0.000736336
28.8	0.001173292	0	0.001173292
26.86	0.001683982	0.06	0.001683982
23.09	0.00225868	0.19	0.00225868
17.72	0.002889297	0.38	0.002889297
10.93	0.003569053	0.62	0.003569053
2.9	0.004292221	0.9	0.004292221
Concrete tensile behavior		Concrete tension damage	
Yield Stress (MPa)	Cracking Strain	Damage parameter (d_t)	Cracking Strain
2.3	0	0	0
0.023	0.000759601	0.99	0.000759601

2. f_{cu}=29.73 MPa, f_{cm}=23.784 MPa, Concrete strength of BF1

Material parameter	f_{cu}= 29.73 Mpa	Plasticity Parameter	
		Dilation angle	31
		Eccentricity	0.1
Concrete Elasticity		f_{b0}/f_{co}	1.16
E (Gpa)	28.53	K	0.666
ν (Poisson Ratio)	0.2	Viscosity	0
Concrete Compressive Behavior		Concrete Compressive Damage	
Stress (MPa)	Inelastic Strain	Damage Parameter (d_c)	Inelastic Strain
9.51	0.0000000	0.000	0.0000000
17.46	0.0001552	0.000	0.0001552
21.90	0.0004422	0.000	0.0004422
23.68	0.0008296	0.000	0.0008296
23.37	0.0012954	0.013	0.0012954
21.41	0.0018234	0.096	0.0018234
18.12	0.0024016	0.235	0.0024016
13.73	0.0030210	0.420	0.0030210
8.44	0.0036746	0.644	0.0036746
2.38	0.0043568	0.900	0.0043568
Concrete tensile behavior		Concrete tension damage	
Yield Stress (MPa)	Cracking Strain	Damage parameter (d_t)	Cracking Strain
2.15	0	0	0
0.0215	0.000574788	0.99	0.000574788

3. f_{cu}=27.14 MPa, f_{cm}=21.71 MPa, Concrete strength of BC 2, BF 3 and BF 4

Material parameter	f_{cu}= 27.14 Mpa	Plasticity Parameter	
		Dilation angle	31
		Eccentricity	0.1
Concrete Elasticity		f_{b0}/f_{co}	1.16
E (Gpa)	27.76	K	0.666
ν (Poisson Ratio)	0.2	Viscosity	0
Concrete Compressive Behavior		Concrete Compressive Damage	
Stress (MPa)	Inelastic Strain	Damage Parameter (d_c)	Inelastic Strain
8.69	0.0000000	0.000	0.0000000
16.22	0.0001655	0.000	0.0001655
20.22	0.0004687	0.000	0.0004687
21.67	0.0008714	0.000	0.0008714
21.21	0.0013485	0.021	0.0013485
19.28	0.0018826	0.110	0.0018826
16.21	0.0024614	0.252	0.0024614
12.23	0.0030759	0.436	0.0030759
7.51	0.0037192	0.654	0.0037192
2.17	0.0043863	0.900	0.0043863
Concrete tensile behavior		Concrete tension damage	
Yield Stress (MPa)	Cracking Strain	Damage parameter (d_t)	Cracking Strain
1.7	0	0	0
0.0017	0.0006123	0.99	0.0006123

4. f_{cu}=23.05 MPa, f_{cm}= 18.44 MPa, Concrete strength of BF 7, BF 8 and BF 9

Material parameter	f_{cu}= 23.05 Mpa	Plasticity Parameter	
		Dilation angle	31
		Eccentricity	0.1
Concrete Elasticity		f_{b0}/f_{co}	1.16
E (Gpa)	26.14	K	0.666
ν (Poisson Ratio)	0.2	Viscosity	0
Concrete Compressive Behavior		Concrete Compressive Damage	
Stress (MPa)	Inelastic Strain	Damage Parameter (d_c)	Inelastic Strain
7.38	0.0000000	0.000	0.0000000
14.20	0.0001847	0.000	0.0001847
17.48	0.0005161	0.000	0.0005161
18.44	0.0009441	0.000	0.0009441
17.79	0.0014388	0.035	0.0014388
15.98	0.0019817	0.134	0.0019817
13.30	0.0025605	0.279	0.0025605
9.96	0.0031668	0.460	0.0031668
6.11	0.0037945	0.669	0.0037945
1.84	0.0044393	0.900	0.0044393
Concrete tensile behavior		Concrete tension damage	
Yield Stress (MPa)	Cracking Strain	Damage parameter (d_t)	Cracking Strain
1.58	0	0	0
0.0158	0.000656	0.99	0.000656

5. f_{cu}=21.49 MPa, f_{cm}= 17.19 MPa, Concrete strength of BC 3, BF 5 and BF 6

Material parameter	f_{cu}= 21.49 Mpa	Plasticity Parameter	
		Dilation angle	31
		Eccentricity	0.1
Concrete Elasticity		f_{b0}/f_{co}	1.16
E (Gpa)	25.88	K	0.666
ν (Poisson Ratio)	0.2	Viscosity	0
Concrete Compressive Behavior		Concrete Compressive Damage	
Stress (MPa)	Inelastic Strain	Damage Parameter (d_c)	Inelastic Strain
6.88	0.0000000	0.000	0.0000000
13.40	0.0001931	0.000	0.0001931
16.41	0.0005364	0.000	0.0005364
17.19	0.0009743	0.000	0.0009743
16.48	0.0014757	0.041	0.0014757
14.73	0.0020217	0.143	0.0020217
12.22	0.0026003	0.289	0.0026003
9.13	0.0032033	0.469	0.0032033
5.60	0.0038252	0.674	0.0038252
1.72	0.0044620	0.900	0.0044620
Concrete tensile behavior		Concrete tension damage	
Yield Stress (MPa)	Cracking Strain	Damage parameter (d_t)	Cracking Strain
1.5	0	0	0
0.015	0.000656	0.99	0.000656

Annex- B
Section Analysis of Control Beam BC 1, BC 2 and BC 3 According to ES-EN 1992

1. BC 1, With Original Steel Yield Stress

Concrete

Cylindrical Compressive Strength, $f_c = 0.8 \times f_{cu} = 26.82$ MPa

Tensile Strength= 2.6 MPa

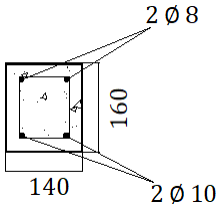

Steel

Phi 8

Yield Strength, f_y= 445.63 MPa

Ultimate Strength, f_u= 592.85 MPa

Ultimate Strain, ε_u= 0.3

Modulus of Elasticity, E_s=200 MPa

Phi 10

Yield Strength, f_y= 545.37 MPa

Ultimate Strength, f_u= 632.38 MPa

Ultimate Strain, ε_u= 0.24

Modulus of Elasticity, E_s=200 MPa

Section Property

Steel Reinforcement

Bottom Reinforcement, A_{s1}= 157.04 mm^2

Top Reinforcement, A_{s2} = 100.38 mm^2

Depth of the bottom reinforcement from the top (d_1) = 122 mm

Depth of the top reinforcement from the top (d') = 37 mm

Assumption of Concrete crush at 3.5‰=0.0035

Bottom reinforcement yield, $\varepsilon_{s1} > \varepsilon_y = \frac{f_y}{E_s} = \frac{545.37\ \text{MPa}}{200\ GPa} = 2.73‰ = 0.00273$

Top reinforcement does not yield, $\varepsilon_{s1} > \varepsilon_y = \frac{f_y}{E_s} = \frac{445.63\ \text{MPa}}{200\ GPa} = 2.23‰ = 0.00223$

Failure Strain Profile

A number of several strain profiles are tried to find the correct strain profile but in this annex only the final correct strain profile is presented for simplicity.

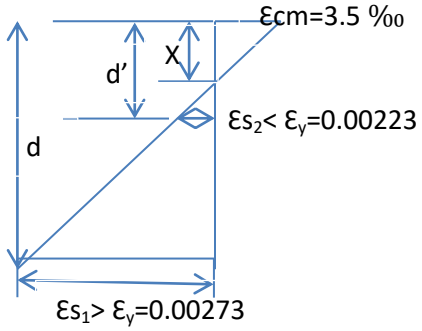

From similarity of Triangles

$$\frac{3.5+\varepsilon_{s1}}{d} = \frac{3.5+\varepsilon_{s2}}{d'}$$

$$\frac{3.5+\varepsilon_{s1}}{122} = \frac{3.5+\varepsilon_{s2}}{37}$$

$\varepsilon_{s2} = 0.303\varepsilon_{s1} - 2.438$ ….. (I)

$$\frac{\varepsilon_c+\varepsilon_{s1}}{d} = \frac{\varepsilon_c}{x} \quad k_x = \frac{x}{d} = \frac{\varepsilon_c}{\varepsilon_c+\varepsilon_{s1}} = \frac{3.5}{3.5+\varepsilon_{s1}}$$

,

From Equilibrium of Forces in the section of the beam;

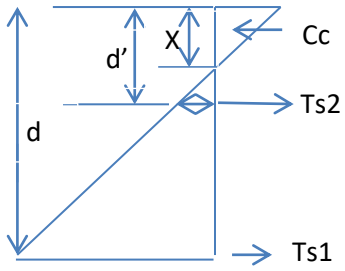

$Cc=T_{s1}+T_{s2}$

$\alpha_c f_c bd = f_y A_{s1} + \varepsilon_{s2} E_s A_{s2}$

$$\alpha_c = \frac{545.37N/mm^2 * (157.08mm^2) + 200{,}000N/mm^2 * (100.38mm^2) * \varepsilon_{s1}}{26.82N/mm^2 * 140mm * 122mm}$$

$\alpha_c = 0.187 + 0.044\,\varepsilon_{s2}$, but $\varepsilon_{s2} = 0.303\varepsilon_{s1} - 2.438$

$\rightarrow \quad \alpha_c = 0.08 + 0.0133\,\varepsilon_{s1}$ ……(II)

Using parabolic Stress Box if $\varepsilon c > \varepsilon_{c2}=0.002$,

$$\alpha_c = k_x \frac{(3\varepsilon_{cm} - 2)}{3\varepsilon_{cm}}, \qquad k_x = \frac{3.5}{3.5 + \varepsilon_{s1}}$$

$$\alpha_c = \frac{3.5}{3.5 + \varepsilon_{s1}} * \left(\frac{3(3.5) - 2}{3(3.5)}\right) = \frac{2.833}{3.5 + \varepsilon_{s1}} \quad \text{..... (III)}$$

By equating equation II and III, and solving for the simultaneous equation,

$\varepsilon_{s1} = 9.89$ ‰ $> \varepsilon_y = 2.73$ ‰…….. OK!!

$\varepsilon_{s2} = 0.303\varepsilon_{s1} - 2.438 = 0.303(9.89) - 2.438 = 0.56$ ‰ $< \varepsilon_y = 2.37$ ‰……..OK!!

Therefore the failure assumption is correct!!

Moment capacity calculation

$$M_{rd} = \alpha_c f_c bd^2(1-\beta_c) - A_{s2}\varepsilon_{s2}E(d-d_2)$$

$$\alpha_c = = \frac{2.833}{3.5 + 9.89} = 0.212 \quad k_x = = \frac{3.5}{3.5 + 9.89} = 0.26$$

if $\varepsilon c > \varepsilon_{c2}=0.002$, $\beta_c = k_x \frac{\varepsilon_{cm}(3\varepsilon_{cm} - 4) + 2}{2\varepsilon_{cm}(3\varepsilon_{cm} - 2)} = 0.109$

Mrd = 0.212*26.82 MPa*140*122^2(1-0.109) – 200,000 MPa*0.00056*100.38 mm^2*(122-37mm)

= 9.604 KN.m, for a mid-point concentrated load the ultimate load is, P= 4*Mrd /L

P= 4*9.604 KN. m/ 1.4 m = <u>27.38 KN</u>

<u>Neutral Axis Depth Calculation</u>

$X=K_x*d=0.26*122mm=$ **<u>31.89 m</u>**

2. BC 1, With Reduced Steel Yield Stress

<u>Concrete</u>

Cylindrical Compressive Strength, $f_c = 0.8\times f_{cu}= 26.82$ MPa

Tensile Strength= 2.6 MPa

<u>Steel</u>

<u>Phi 8</u>

Yield Strength, f_y= 445.63 MPa

Ultimate Strength, f_u= 592.85 MPa

Ultimate Strain, ε_u= 0.3

Modulus of Elasticity, E_s=200 MPa

<u>Phi 10</u>

Yield Strength, f_y= 468.23 MPa

Ultimate Strength, f_u= 632.38 MPa

Ultimate Strain, ε_u= 0.24

Modulus of Elasticity, E_s=200 MPa

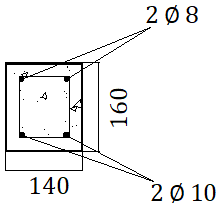

<u>Section Property</u>

<u>Steel Reinforcement</u>

Bottom Reinforcement, A_{s1}= 157.04 mm^2

Top Reinforcement, A_{s2} = 100.38 mm^2

Depth of the bottom reinforcement from the top (d_1) = 122 mm

Depth of the top reinforcement from the top (d') = 37 mm

Assumption of Concrete crush at 3.5‰=0.0035

Bottom reinforcement yield, $\varepsilon_{s1} > \varepsilon_y=\frac{f_y}{E_s} = \frac{468.23\ MPa}{200\ GPa} = 2.34‰=0.00234$

Top reinforcement does not yield, $\varepsilon_{s1} > \varepsilon_y=\frac{f_y}{E_s} = \frac{445.63\ MPa}{200\ GPa} = 2.23‰=0.00223$

<u>Failure Strain Profile</u>

A number of several strain profiles are tried to find the correct strain profile but in this annex only the final correct strain profile is presented for simplicity.

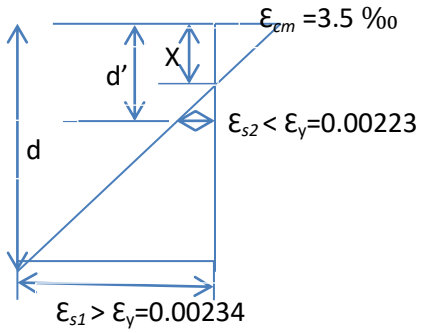

<u>From similarity of Triangles</u>

$$\frac{3.5+\varepsilon_{s1}}{d} = \frac{3.5+\varepsilon_{s2}}{d'}$$

$$\frac{3.5+\varepsilon_{s1}}{122} = \frac{3.5+\varepsilon_{s2}}{37}$$

$\varepsilon_{s2}=0.303\varepsilon_{s1}-2.438$….. (I)

$$\frac{\varepsilon_c+\varepsilon_{s1}}{d} = \frac{\varepsilon_c}{x} \quad k_x = \frac{x}{d} = \frac{\varepsilon_c}{\varepsilon_c+\varepsilon_{s1}} = \frac{3.5}{3.5+\varepsilon_{s1}}$$

,

From Equilibrium of Forces in the section of the beam;

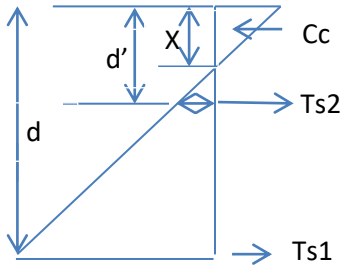

$$Cc = T_{s1} + T_{s2}$$

$$\alpha_c f_c bd = f_y A_{s1} + \varepsilon_{s2} E_s A_{s2}$$

$$\alpha_c = \frac{468.23N/mm^2 * (157.08mm^2) + 200{,}000N/mm^2 * (100.38mm^2) * \varepsilon_{s1}}{26.82N/mm^2 * 140mm * 122mm}$$

$$\alpha_c = 0.160 + 0.044\,\varepsilon_{s2}, \text{ but } \varepsilon_{s2} = 0.303\varepsilon_{s1} - 2.438$$

$$\rightarrow \quad \alpha_c = 0.053 + 0.0133\,\varepsilon_{s1} \ldots\ldots\ldots (II)$$

Using parabolic Stress Box if $\varepsilon c > \varepsilon_{c2} = 0.002$,

$$\alpha_c = k_x \frac{(3\varepsilon_{cm} - 2)}{3\varepsilon_{cm}}, \qquad k_x = \frac{3.5}{3.5 + \varepsilon_{s1}}$$

$$\alpha_c = \frac{3.5}{3.5 + \varepsilon_{s1}} * \left(\frac{3(3.5) - 2}{3(3.5)}\right) = \frac{2.833}{3.5 + \varepsilon_{s1}} \quad \ldots\ldots\ldots (III)$$

By equating equation II and III, and solving for the simultaneous equation,

$\varepsilon_{s1} = 10.83$ ‰ $> \varepsilon_y = 2.34$ ‰…….. OK!!

$\varepsilon_{s2} = 0.303\varepsilon_{s1} - 2.438 = 0.303(10.83) - 2.438 = 0.846$ ‰ $< \varepsilon_y = 2.37$ ‰……..OK!!

Therefore the failure assumption is correct!!

Moment capacity calculation

$$Mrd = \alpha_c f_c bd^2(1 - \beta_c) - A_{s2}\varepsilon_{s2} E(d - d_2)$$

$$\alpha_c = = \frac{2.833}{3.5 + 10.83} = 0.198, \qquad k_x = = \frac{3.5}{3.5 + 10.83} = 0.244$$

If $\varepsilon c > \varepsilon_{c2} = 0.002$, $\beta_c = k_x \frac{\varepsilon_{cm}(3\varepsilon_{cm} - 4) + 2}{2\varepsilon_{cm}(3\varepsilon_{cm} - 2)} = 0.102$

$Mrd = 0.198 * 26.82MPa * 140 * 122^2(1 - 0.102) - 100.38\ mm^2 * 0.00085 * 200{,}000\ MPa * (122 - 37\ mm)$

Mrd = 8.48 KN.m, for a mid-point concentrated load the ultimate load is, P= 4* Mrd /L

P= 4*8.48 KN. m/ 1.4 m = <u>24.23 KN</u>

Neutral Axis Depth Calculation

$X=K_x*d=0.244*122$ mm= **29.77 mm**

3. BC 2, With Original Steel Yield Stress

Concrete

Cylindrical Compressive Strength, $f_c = 0.8\times f_{cu}$= 21.71 MPa

Tensile Strength= 1.7 MPa

Steel

Phi 8

Yield Strength, f_y= 445.63 MPa

Ultimate Strength, f_u= 592.85 MPa

Ultimate Strain, ε_u= 0.3

Modulus of Elasticity, E_s=200 MPa

Phi 10

Yield Strength, f_y= 545.37 MPa

Ultimate Strength, f_u= 632.38 MPa

Ultimate Strain, ε_u= 0.24

Modulus of Elasticity, E_s=200 MPa

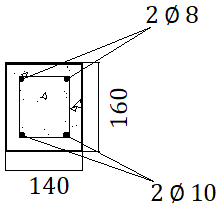

Section Property

Steel Reinforcement

Bottom Reinforcement, A_{s1}= 157.04 mm^2

Top Reinforcement, A_{s2} = 100.38 mm^2

Depth of the bottom reinforcement from the top (d_1) = 122 mm

Depth of the top reinforcement from the top (d') = 37 mm

Assumption of Concrete crush at 3.5‰=0.0035

Bottom reinforcement yield, $\varepsilon_{s1} > \varepsilon_y=\frac{f_y}{E_s} = \frac{545.37\ MPa}{200\ GPa}$ = 2.73‰=0.00273

Top reinforcement does not yield, $\varepsilon_{s1} > \varepsilon_y=\frac{f_y}{E_s} = \frac{445.63\ MPa}{200\ GPa}$ = 2.23‰=0.00223

Failure Strain Profile

A number of several strain profiles are tried to find the correct strain profile but in this annex only the final correct strain profile is presented for simplicity.

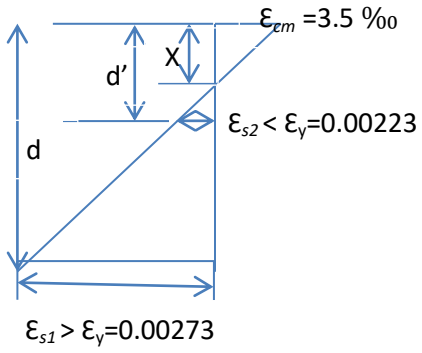

From similarity of Triangles

$$\frac{3.5+\varepsilon_{s1}}{d} = \frac{3.5+\varepsilon_{s2}}{d'}$$

$$\frac{3.5+\varepsilon_{s1}}{122} = \frac{3.5+\varepsilon_{s2}}{37}$$

$\varepsilon_{s2}=0.303\varepsilon_{s1}-2.438$….. (I)

$$\frac{\varepsilon_c+\varepsilon_{s1}}{d} = \frac{\varepsilon_c}{x} \quad k_x = \frac{x}{d} = \frac{\varepsilon_c}{\varepsilon_c+\varepsilon_{s1}} = \frac{3.5}{3.5+\varepsilon_{s1}}$$

,

From Equilibrium of Forces in the section of the beam;

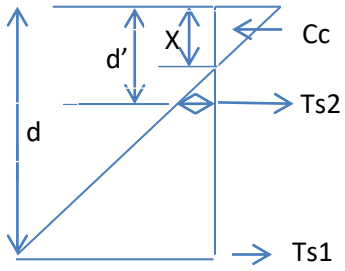

$Cc = T_{s1} + T_{s2}$

$\alpha_c f_c bd = f_y A_{s1} + \varepsilon_{s2} E_s A_{s2}$

$$\alpha_c = \frac{545.37N/mm^2 * (157.08mm^2) + 200{,}000N/mm^2 * (100.38mm^2) * \varepsilon_{s1}}{21.71N/mm^2 * 140mm * 122mm}$$

$\alpha_c = 0.231 + 0.054\ \varepsilon_{s2}$, but $\varepsilon_{s2} = 0.303\varepsilon_{s1} - 2.438$

→ $\alpha_c = 0.099 + 0.0164\ \varepsilon_{s1}$ ……..(II)

Using parabolic Stress Box if $\varepsilon c > \varepsilon_{c2} = 0.002$,

$$\alpha_c = k_x \frac{(3\varepsilon_{cm} - 2)}{3\varepsilon_{cm}}, \qquad k_x = \frac{3.5}{3.5 + \varepsilon_{s1}}$$

$$\alpha_c = \frac{3.5}{3.5 + \varepsilon_{s1}} * \left(\frac{3(3.5) - 2}{3(3.5)}\right) = \frac{2.833}{3.5 + \varepsilon_{s1}} \quad \text{..... (III)}$$

By equating equation II and III, and solving for the simultaneous equation,

$\varepsilon_{s1} = 8.433$ ‰ > $\varepsilon_y = 2.73$ ‰…….. OK!!

$\varepsilon_{s2} = 0.303\varepsilon_{s1} - 2.438 = 0.303(8.43) - 2.438 = 0.119$ ‰ < $\varepsilon_y = 2.37$ ‰……..OK!!

Therefore the failure assumption is correct!!

Moment capacity calculation

$Mrd = \alpha_c f_c bd^2(1-\beta_c) - A_{s2}\varepsilon_{s2}E(d-d_2)$

$$\alpha_c = = \frac{2.833}{3.5 + 8.433} = 0.237 \qquad k_x = = \frac{3.5}{3.5 + 8.433} = 0.293$$

If $\varepsilon c > \varepsilon_{c2} = 0.002$, $\beta_c = k_x \frac{\varepsilon_{cm}(3\varepsilon_{cm} - 4) + 2}{2\varepsilon_{cm}(3\varepsilon_{cm} - 2)} = 0.122$

$Mrd = 0.237 * 21.71MPa * 140 * 122^2(1 - 0.112) - 100.38\ mm^2 * 0.00012 * 200{,}000\ MPa * (122 - 37mm)$

Mrd = 9.23 KN.m, for a mid-point concentrated load the ultimate load is, P= 4* Mrd /L

P= 4*9.23 KN. m/ 1.4 m = <u>26.37 KN</u>

Neutral Axis Depth Calculation

$X=K_x*d=0.293*122$ mm= **35.79 mm**

4. BC 2, With reduced Steel Yield Stress

Concrete

Cylindrical Compressive Strength, $f_c = 0.8\times f_{cu}$= 21.71 MPa

Tensile Strength= 1.7 MPa

Steel

Phi 8

Yield Strength, f_y= 445.63 MPa

Ultimate Strength, f_u= 592.85 MPa

Ultimate Strain, ε_u= 0.3

Modulus of Elasticity, E_s=200 MPa

Phi 10

Yield Strength, f_y= 491.13 MPa

Ultimate Strength, f_u= 632.38 MPa

Ultimate Strain, ε_u= 0.24

Modulus of Elasticity, E_s=200 MPa

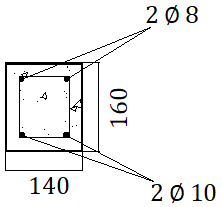

Section Property

Steel Reinforcement

Bottom Reinforcement, A_{s1}= 157.04 mm^2

Top Reinforcement, A_{s2} = 100.38 mm^2

Depth of the bottom reinforcement from the top (d_1) = 122 mm

Depth of the top reinforcement from the top (d') = 37 mm

Assumption of Concrete crush at 3.5‰=0.0035

Bottom reinforcement yield, $\varepsilon_{s1} > \varepsilon_y=\frac{f_y}{E_s} = \frac{491.13\ \text{MPa}}{200\ GPa}$ = 2.46‰=0.00246

Top reinforcement does not yield, $\varepsilon_{s1} > \varepsilon_y=\frac{f_y}{E_s} = \frac{445.63\ \text{MPa}}{200\ GPa}$ = 2.23‰=0.00223

Failure Strain Profile

A number of several strain profiles are tried to find the correct strain profile but in this annex only the final correct strain profile is presented for simplicity.

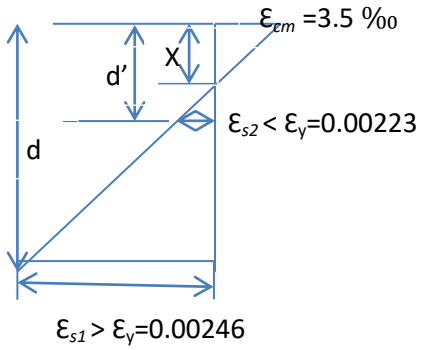

From similarity of Triangles

$$\frac{3.5+\varepsilon_{s1}}{d}=\frac{3.5+\varepsilon_{s2}}{d'}$$

$$\frac{3.5+\varepsilon_{s1}}{122}=\frac{3.5+\varepsilon_{s2}}{37}$$

$\varepsilon_{s2}=0.303\varepsilon_{s1}-2.438$….. (I)

$$\frac{\varepsilon_c+\varepsilon_{s1}}{d}=\frac{\varepsilon_c}{x}\quad k_x=\frac{x}{d}=\frac{\varepsilon_c}{\varepsilon_c+\varepsilon_{s1}}=\frac{3.5}{3.5+\varepsilon_{s1}}$$

,

From Equilibrium of Forces in the section of the beam;

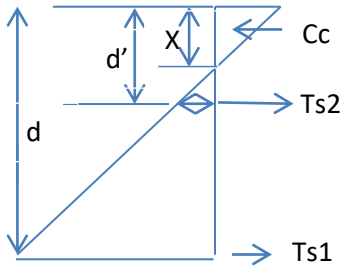

$$Cc = T_{s1} + T_{s2}$$

$$\alpha_c f_c b d = f_y A_{s1} + \varepsilon_{s2} E_s A_{s2}$$

$$\alpha_c = \frac{491.13N/mm^2 * (157.08mm^2) + 200{,}000N/mm^2 * (100.38mm^2) * \varepsilon_{s1}}{21.71N/mm^2 * 140mm * 122mm}$$

$$\alpha_c = 0.208 + 0.054\,\varepsilon_{s2}\text{, but } \varepsilon_{s2} = 0.303\varepsilon_{s1} - 2.438$$

$$\rightarrow \quad \alpha_c = 0.076 + 0.0164\,\varepsilon_{s1} \ldots\ldots\ldots (II)$$

Using parabolic Stress Box if $\varepsilon c > \varepsilon_{c2} = 0.002$,

$$\alpha_c = k_x \frac{(3\varepsilon_{cm} - 2)}{3\varepsilon_{cm}}, \qquad k_x = \frac{3.5}{3.5 + \varepsilon_{s1}}$$

$$\alpha_c = \frac{3.5}{3.5 + \varepsilon_{s1}} * \left(\frac{3(3.5) - 2}{3(3.5)}\right) = \frac{2.833}{3.5 + \varepsilon_{s1}} \quad \ldots\ldots\ldots (III)$$

By equating equation II and III, and solving for the simultaneous equation,

$\varepsilon_{s1} = 9.08$ ‰ $> \varepsilon_y = 2.73$ ‰…….. OK!!

$\varepsilon_{s2} = 0.303\varepsilon_{s1} - 2.438 = 0.303(9.08) - 2.438 = 0.317$ ‰ $< \varepsilon_y = 2.37$ ‰……..OK!!

Therefore the failure assumption is correct!!

Moment capacity calculation

$$Mrd = \alpha_c f_c b d^2 (1 - \beta_c) - A_{s2} \varepsilon_{s2} E (d - d_2)$$

$$\alpha_c = = \frac{2.833}{3.5 + 9.08} = 0.225, \qquad k_x = = \frac{3.5}{3.5 + 9.08} = 0.278$$

If $\varepsilon c > \varepsilon_{c2} = 0.002$, $\beta_c = k_x \frac{\varepsilon_{cm}(3\varepsilon_{cm} - 4) + 2}{2\varepsilon_{cm}(3\varepsilon_{cm} - 2)} = 0.116$

$Mrd = 0.225 * 21.71MPa * 140 * 122^2 (1 - 0.116) - 100.38\ mm^2 * 0.00032 * 200{,}000\ MPa * (122 - 37mm)$

Mrd = 8.47 KN.m, for a mid-point concentrated load the ultimate load is, P= 4* Mrd /L

P= 4*9.23 KN. m/ 1.4 m = <u>24.19 KN</u>

Neutral Axis Depth Calculation

$X=K_x*d=0.278*122$ mm= **33.55 mm**

5. BC 3, With Original Steel Yield Stress

Concrete

Cylindrical Compressive Strength, $f_c = 0.8\times f_{cu}$= 17.19 MPa

Tensile Strength= 1.5 MPa

Steel

Phi 8

Yield Strength, f_y= 445.63 MPa

Ultimate Strength, f_u= 592.85 MPa

Ultimate Strain, ε_u= 0.3

Modulus of Elasticity, E_s=200 MPa

Phi 10

Yield Strength, f_y= 545.37 MPa

Ultimate Strength, f_u= 632.38 MPa

Ultimate Strain, ε_u= 0.24

Modulus of Elasticity, E_s=200 MPa

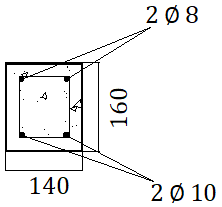

Section Property

Steel Reinforcement

Bottom Reinforcement, A_{s1}= 157.04 mm^2

Top Reinforcement, A_{s2} = 100.38 mm^2

Depth of the bottom reinforcement from the top (d_1) = 122 mm

Depth of the top reinforcement from the top (d') = 37 mm

Assumption of Concrete crush at 3.5‰=0.0035

Bottom reinforcement yield, $\varepsilon_{s1} > \varepsilon_y = \frac{f_y}{E_s} = \frac{545.37\ MPa}{200\ GPa}$ = 2.73‰=0.00273

Top reinforcement does not yield, $\varepsilon_{s1} > \varepsilon_y = \frac{f_y}{E_s} = \frac{445.63\ MPa}{200\ GPa}$ = 2.23‰=0.00223

Failure Strain Profile

A number of several strain profiles are tried to find the correct strain profile but in this annex only the final correct strain profile is presented for simplicity.

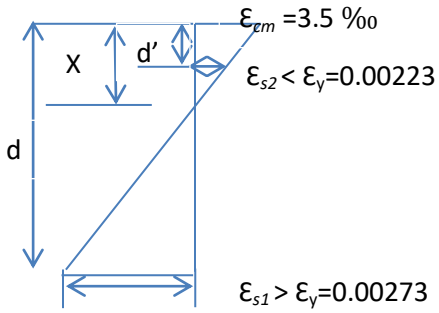

From similarity of Triangles

$$\frac{3.5+\varepsilon_{s1}}{d} = \frac{3.5-\varepsilon_{s2}}{d'}$$

$$\frac{3.5+\varepsilon_{s1}}{122} = \frac{3.5-\varepsilon_{s2}}{37}$$

ε_{s2}= 2.438 - 0.303ε_{s1}….. (I)

$$\frac{\varepsilon_c+\varepsilon_{s1}}{d} = \frac{\varepsilon_c}{x} \quad k_x = \frac{x}{d} = \frac{\varepsilon_c}{\varepsilon_c+\varepsilon_{s1}} = \frac{3.5}{3.5+\varepsilon_{s1}}$$

,

From Equilibrium of Forces in the section of the beam;

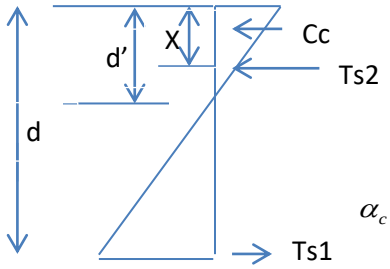

$Cc = T_{s1} - T_{s2}$

$\alpha_c f_c bd = f_y A_{s1} - \varepsilon_{s2} E_s A_{s2}$

$$\alpha_c = \frac{545.37N/mm^2 * (157.08mm^2) - 200{,}000N/mm^2 * (100.38mm^2) * \varepsilon_{s1}}{17.19N/mm^2 * 140mm * 122mm}$$

$\alpha_c = 0.292 - 0.068\,\varepsilon_{s2}$, but $\varepsilon_{s2} = 2.438 - 0.303\varepsilon_{s1}$

→ $\alpha_c = 0.126 + 0.0207\,\varepsilon_{s1}$ ……..(II)

Using parabolic Stress Box if $\varepsilon c > \varepsilon_{c2}=0.002$,

$$\alpha_c = k_x \frac{(3\varepsilon_{cm} - 2)}{3\varepsilon_{cm}}, \qquad k_x = \frac{3.5}{3.5 + \varepsilon_{s1}}$$

$$\alpha_c = \frac{3.5}{3.5 + \varepsilon_{s1}} * \left(\frac{3(3.5) - 2}{3(3.5)}\right) = \frac{2.833}{3.5 + \varepsilon_{s1}} \quad \text{..... (III)}$$

By equating equation II and III, and solving for the simultaneous equation,

$\varepsilon_{s1} = 6.993$ ‰ > $\varepsilon_y = 2.73$ ‰…….. OK!!

$\varepsilon_{s2} = 2.438 - 0.303\varepsilon_{s1} = 2.438 - 0.303(6.993) = 0.317$ ‰ < $\varepsilon_y = 2.37$ ‰……..OK!!

Therefore the failure assumption is correct!!

Moment capacity calculation

$Mrd = \alpha_c f_c bd^2(1-\beta_c) + A_{s2}\varepsilon_{s2}E(d-d_2)$

$$\alpha_c = = \frac{2.833}{3.5 + 6.993} = 0.27 \quad k_x = = \frac{3.5}{3.5 + 6.993} = 0.334$$

If $\varepsilon c > \varepsilon_{c2}=0.002$, $\beta_c = k_x \frac{\varepsilon_{cm}(3\varepsilon_{cm} - 4) + 2}{2\varepsilon_{cm}(3\varepsilon_{cm} - 2)} = 0.139$

$Mrd = 0.27 * 17.12MPa * 140 * 122^2(1 - 0.139) - 100.38\ mm^2 * 0.00032 * 200{,}000\ MPa * (122 - 37mm)$

Mrd = 8.87 KN.m, for a mid-point concentrated load the ultimate load is, P= 4* Mrd /L

P= 4*8.87 KN. m/ 1.4 m = 25.34 KN

Neutral Axis Depth Calculation

X=K_x*d=0.334*122 mm= **40.71 mm**

6. BC 3, With Reduced Steel Yield Stress

Concrete

Cylindrical Compressive Strength, f_c = 0.8×f_{cu}= 17.19 MPa

Tensile Strength= 1.5 MPa

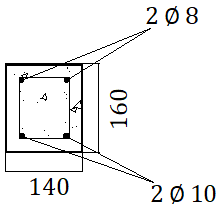

Steel

Phi 8

Yield Strength, f_y= 445.63 MPa

Ultimate Strength, f_u= 592.85 MPa

Ultimate Strain, ε_u= 0.3

Modulus of Elasticity, E_s=200 MPa

Phi 10

Yield Strength, f_y= 500.42 MPa

Ultimate Strength, f_u= 632.38 MPa

Ultimate Strain, ε_u= 0.24

Modulus of Elasticity, E_s=200 MPa

Section Property

Steel Reinforcement

Bottom Reinforcement, A_{s1}= 157.04 mm^2

Top Reinforcement, A_{s2} = 100.38 mm^2

Depth of the bottom reinforcement from the top (d_1) = 122 mm

Depth of the top reinforcement from the top (d') = 37 mm

Assumption of Concrete crush at 3.5‰=0.0035

Bottom reinforcement yield, $\varepsilon_{s1} > \varepsilon_y = \frac{f_y}{E_s} = \frac{500.42\ MPa}{200\ GPa}$ = 2.50‰=0.0025

Top reinforcement does not yield, $\varepsilon_{s1} > \varepsilon_y = \frac{f_y}{E_s} = \frac{445.63\ MPa}{200\ GPa}$ = 2.23‰=0.00223

Failure Strain Profile

A number of several strain profiles are tried to find the correct strain profile but in this annex only the final correct strain profile is presented for simplicity.

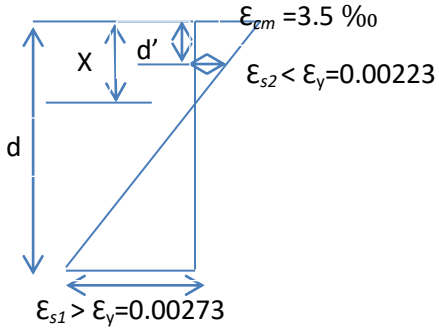

From similarity of Triangles

$$\frac{3.5+\varepsilon_{s1}}{d} = \frac{3.5-\varepsilon_{s2}}{d'}$$

$$\frac{3.5+\varepsilon_{s1}}{122} = \frac{3.5-\varepsilon_{s2}}{37}$$

ε_{s2}= 2.438 - 0.303ε_{s1}….. (I)

$$\frac{\varepsilon_c + \varepsilon_{s1}}{d} = \frac{\varepsilon_c}{x} \quad k_x = \frac{x}{d} = \frac{\varepsilon_c}{\varepsilon_c + \varepsilon_{s1}} = \frac{3.5}{3.5 + \varepsilon_{s1}}$$

From Equilibrium of Forces in the section of the beam;

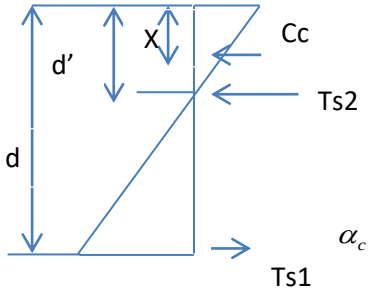

$Cc = T_{s1} - T_{s2}$

$\alpha_c f_c b d = f_y A_{s1} - \varepsilon_{s2} E_s A_{s2}$

$$\alpha_c = \frac{500.42N/mm^2 * (157.08mm^2) - 200{,}000N/mm^2 * (100.38mm^2) * \varepsilon_{s1}}{17.19N/mm^2 * 140mm * 122mm}$$

$\alpha_c = 0.268 - 0.068\ \varepsilon_{s2}$, but $\varepsilon_{s2} = 2.438 - 0.303\varepsilon_{s1}$

→ $\alpha_c = 0.102 + 0.0207\ \varepsilon_{s1}$ ……..(II)

Using parabolic Stress Box if $\varepsilon c > \varepsilon_{c2}=0.002$,

$$\alpha_c = k_x \frac{(3\varepsilon_{cm} - 2)}{3\varepsilon_{cm}} \quad , \quad k_x = \frac{3.5}{3.5 + \varepsilon_{s1}}$$

$$\alpha_c = \frac{3.5}{3.5 + \varepsilon_{s1}} * \left(\frac{3(3.5) - 2}{3(3.5)}\right) = \frac{2.833}{3.5 + \varepsilon_{s1}} \quad \text{..... (III)}$$

By equating equation II and III, and solving for the simultaneous equation,

$\varepsilon_{s1} = 7.525$ ‰ > $\varepsilon_y = 2.5$ ‰…….. OK!!

$\varepsilon_{s2} = 2.438 - 0.303\varepsilon_{s1} = 2.438 - 0.303(7.525) = 0.156$ ‰ < $\varepsilon_y = 2.37$ ‰……..OK!!

Therefore the failure assumption is correct!!

Moment capacity calculation

$$Mrd = \alpha_c f_c b d^2 (1 - \beta_c) + A_{s2}\varepsilon_{s2} E (d - d_2)$$

$$\alpha_c == \frac{2.833}{3.5 + 6.993} = 0.257 \quad k_x == \frac{3.5}{3.5 + 6.993} = 0.317$$

If $\varepsilon c > \varepsilon_{c2}=0.002$, $\beta_c = k_x \frac{\varepsilon_{cm}(3\varepsilon_{cm} - 4) + 2}{2\varepsilon_{cm}(3\varepsilon_{cm} - 2)} = 0.132$

$Mrd = 0.257 * 17.12MPa * 140 * 122^2 (1 - 0.132) - 100.38\ mm^2 * 0.00016 * 200{,}000\ MPa * (122 - 37mm)$

Mrd = 8.26 KN.m, for a mid-point concentrated load the ultimate load is, P= 4* Mrd /L

P= 4*8.26 KN. m/ 1.4 m = <u>23.59 KN</u>

<u>Neutral Axis Depth Calculation</u>

$X = K_x * d = 0.334 * 122$ mm= **<u>40.71 mm</u>**

Annex- C
Section Analysis of CFRP Strengthened Validation Beam

Material Property

Concrete

f_c=29 MPa

Steel

Yield Strength, f_y= 490 MPa

Modulus of Elasticity, E_s=209 MPa

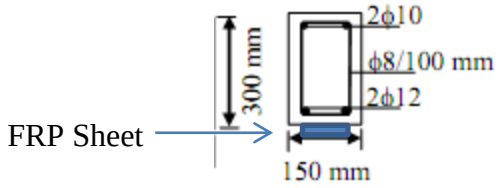

CFRP Sheet (1.2 mm×50mm)

CFRP

Tensile strength of FRP, (f_f) = 2640 N/mm^2

Modulus of Elasticity, E_f = 165 GPa

Section Property

Steel Reinforcement

Bottom Reinforcement, A_{s1}= 226.19 mm^2

Top Reinforcement, A_{s2} = 157.04 mm^2

FRP

Thickness (t_f) = 1.2 mm

Width (B_f) = 50 mm

Cross-sectional Area (A_f) = 60 mm^2

Section Analysis According to ACI-2R-08

The section analysis assumes perfect bonding and linear strain distribution along the section of a rectangular beam.

Depth of the FRP from the top (d_f)= 300+(1.2/2)=300.6 mm

Depth of the bottom reinforcement from the top (d_1) = 261 mm

Depth of the top reinforcement from the top (d') = 38 mm

Assumption Concrete crushes at 3.5‰=0.0035

Bottom reinforcement yield, $\varepsilon_{s1} > \varepsilon_y = \frac{f_y}{E_s} = \frac{495\ \text{MPa}}{209\ GPa}$ = 2.37‰=0.00237

Top reinforcement does not yield, $\varepsilon_{s'} < \varepsilon_y$=0.00237

The strain in the fiber is less than the ultimate strain, $\varepsilon_f < \varepsilon_{fu} = \frac{f_f}{E_f} = \frac{2640\text{MPa}}{165\ GPa}$ = 16‰=0.016

Neutral Axis depth (X) = 59.95 mm (This depth is taken as a trial depth and modified till the equilibrium equations are satisfied but for ease of the work the iteration is done on excel spread sheet and the final result is presented on this paper)

Strain in the FRP

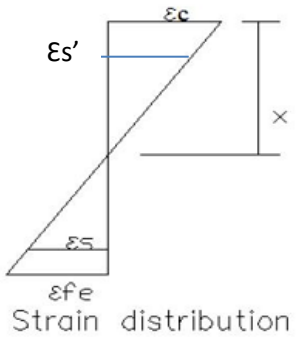

From similarity of Triangles

$$\frac{\varepsilon_{cm}}{x}=\frac{\varepsilon_{cm}+\varepsilon_f}{d_f}=\frac{\varepsilon_{cm}+\varepsilon_s}{d_1}$$

$$\frac{\varepsilon_{cm}}{x}=\frac{\varepsilon_{s'}}{x-d'} \qquad (4.32)$$

$$\varepsilon_f=\frac{3.5*d_f}{x}-3.5=14.01<\varepsilon_{fu}=16, \text{ OK!}$$

Strain at the bottom Reinforcement Steel

$$\varepsilon_s=\frac{3.5*d_s}{x}-3.5=11.79>\varepsilon_y=2.37 \ldots\ldots \text{ OK!}$$

Strain at the top Reinforcement Steel

$$\varepsilon_s'=\frac{3.5*(x-d')}{x}=1.28<\varepsilon_y=2.37 \ldots\ldots\ldots \text{OK!}$$

Stress in the FRP

$f_f = E_f * \varepsilon_f$ = 165000 MPa* 14.01‰= 2312.26 MPa

Stress in the Top Steel bar FRP

$f_{s'} = E_{s'} * \varepsilon_{s'}$ = 209000 MPa* 1.638‰= 267.85 MPa

Stress in the Bottom Steel bar FRP

$f_s = f_y$= 495 MPa

Stress In the concrete (Rectangular Stress Box)

$f_c = f_{cm}$ =29 MPa

Forces in the stress box of the section

Force= Stress*Area

Force in the Concrete (F_c) = 0.8* fc* x*B_c= 23.2 MPa* 59.95 mm*150 mm
= -208,636.44 N (Compression)

Force in the top bar ($F_{s'}$) = $f_{s'}$*$A_{s'}$ = 267.85 MPa * 157.04 mm^2 = -42, 063. 71 N (Compression)

Force in the bottom bar (F_s) = f_y * A_s = 495 MPa * 226.19 mm^2 = + 111, 964.06 N (Tension)

Force in the FRP (F_f) = f_f * A_f = 2312.26 MPa * 60 mm^2 = + 138735.8 N (Tension)

∑= 0 N (Equilibrium Maintained!!!)

Moment Capacity

$M_{rd} = (F_c)*0.4*x + F_{s'}*(x-d') + F_s*(d_1-x) + F_f*(d_f-x) =$ 61.85 KN.m

Failure Load (P)

$P = \frac{M_{max}}{0.26} =$ **237. 89 KN**

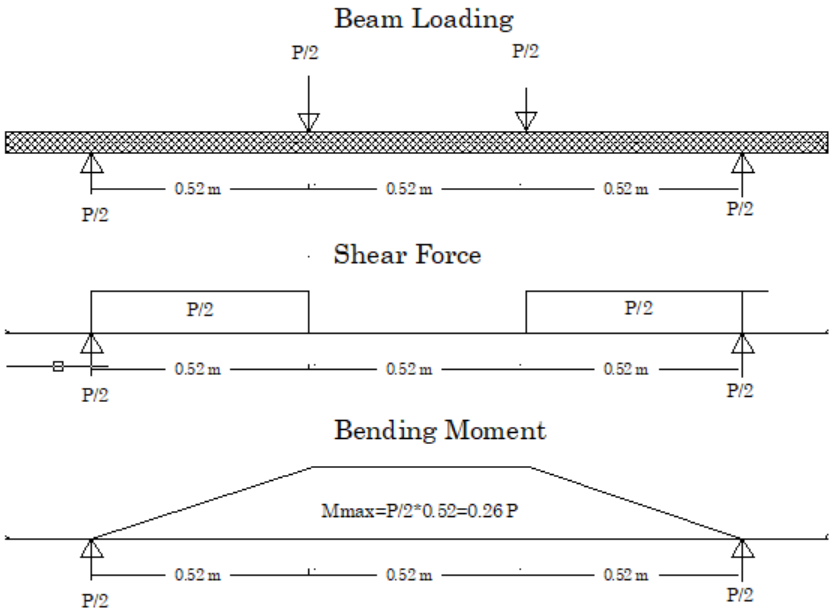

Annex- D
Deflection calculation of CFRP Strengthened unanchored Beams

Material Property

Concrete	Steel	CFRP
Ec=	Modulus of Elasticity, E_s= $n_s= E_s/E_c$	Modulus of Elasticity, E_f = $n_f=E_f/E_c$

Section Property

Concrete Beam

Width, B=

Depth, D=

Steel

Cross sectional area of the bottom Reinforcement, A_{s1}=

Cros sectional area of the top Reinforcement, A_{s2} =

FRP

Thickness (t_f) =

Width (B_f) = 50 mm

Cross-sectional Area (A_f) = $t_f \times B_f$

Deflection Calculation According to EC-2

In the calculation the CFRP laminate is simply assumed as additional bottom reinforcement at different depth. The mid span deflection, Δ, of a simply supported beam can be calculated as

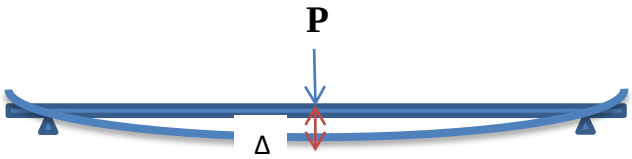

$$\Delta=\frac{Pl^3}{48\,EI_e}$$

Where, P= Point Load at mid span

L= Span length from support to support

E= Elastic modulus

I_e= Effective Moment of Inertia

$$I_e=\left(\frac{M_{cr}}{M_{\max}}\right)^3 I_g+\left[1-\left(\frac{M_{cr}}{M_{\max}}\right)^3\right]I_{cr}\le I_g$$

$$M_{cr}=\frac{f_{cm}I_g}{y_t}$$

I_{cr}= Transformed cracked section moment of inertia

y_t= Distance from N-A to tension face

I_g = Gross section moment of inertia

f_{cm}= Modulus of rupture =

Uncracked transformed Section

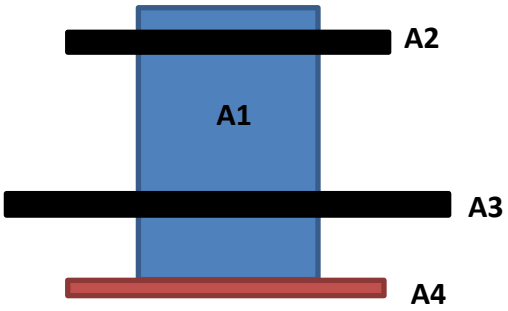

Area of the Concrete, A1= B×D
Area of the top reinforcement, A2= $(n_s-1) \times As_2$
Area of the bottom reinforcement, A3= $(n_s-1) \times As_2$
Area of the CFRP Laminate, A4= $n_f \times B_f \times t_f$

$I_g = \sum (I_i + A_i d^2)$, i=1,2,3 and 4
d= the vertical distance from the centroid of the local area to the centroid of the section,

The depth of the centroid of the section, $X = \frac{\sum(AiXi)}{\sum Ai}$

Cracked transformed Section

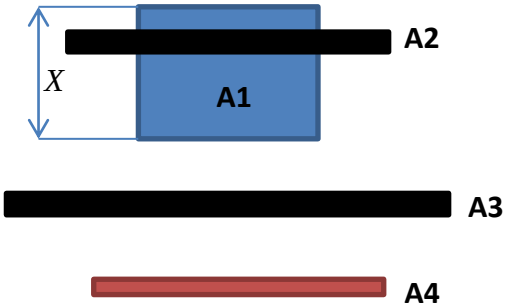

Area of the Concrete, A1= B×X
Area of the top reinforcement, A2= $(n_s-1) \times As_2$
Area of the bottom reinforcement, A3= $n_s \times As_2$
Area of the CFRP Laminate, A4= $n_f \times B_f \times t_f$

$I_g = \sum (I_i + A_i d^2)$, i=1,2,3 and 4
d= the vertical distance from the centroid of the local area to the centroid of the section,

The depth of the centroid of the section, $X = \frac{\sum(AiXi)}{\sum Ai}$